AD-A167 670   MODELING AND DLTS ANALYSIS OF IRRADIATED III-V   1/1
                MULTIJUNCTION SOLAR CELLS(U) FLORIDA UNIV GAINESVILLE
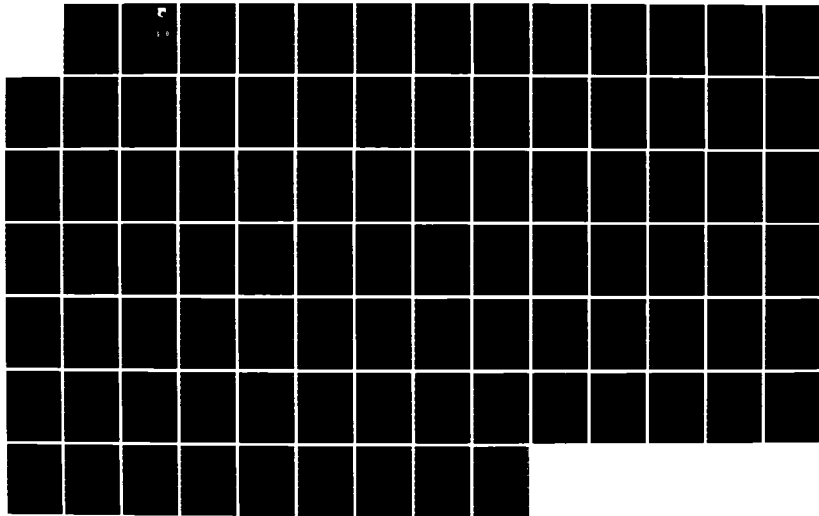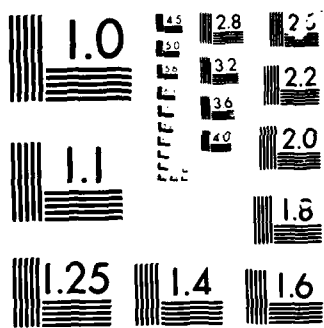   DEPT OF ELECTRICAL ENGINEERING S S LI FEB 86
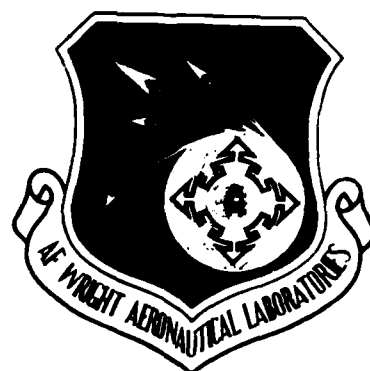UNCLASSIFIED   AFWAL-TR-85-2108 F33615-81-C-2058   F/G 20/12   NL

1.0 2.8 2.5

3.2 2.2

3.6

4.0 2.0

1.1 1.8

1.25 1.4 1.6

MICROCOPY CHART

AFWAL-TR-85-2108

MODELING AND DLTS ANALYSIS OF IRRADIATED III-V MULTIJUNCTION SOLAR CELLS

Sheng S. Li

University of Florida
Department of Electrical Engineering
Gainesville, FL 32611

February 1986

Final Report for Period November 1984 - October 1985

AERO PROPULSION LABORATORY
AIR FORCE WRIGHT AERONAUTICAL LABORATORIES
AIR FORCE SYSTEMS COMMAND
WRIGHT-PATTERSON AIR FORCE BASE, OHIO   45433
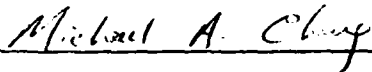
DTIC
ELECTE
MAY 1 6 1986
S   D
D

86 5 16 002

NOTICE

When Government drawings, specifications, or other data are used for any purpose other than in connection with a definitely related Government procurement operation, the United States Government thereby incurs no responsibility nor any obligation whatsoever, and the fact that the government may have formulated, furnished, or in any way supplied the said drawings, specifications, or other data, is not to be regarded by implication or otherwise as in any manner licensing the holder or any other person or corporation, or conveying any rights or permission to manufacture use, or sell any patented invention that may in any way be related thereto.

This report has been reviewed by the Office of Public Affiars (ASD/PA) and is releasable to the National Technical Information Service (NTIS). At NTIS, it will be available to the general public, including foreign nations.

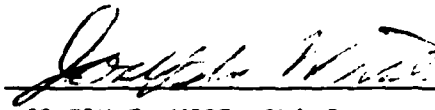This technical report has been reviewed and is approved for publication.

2Lt MICHAEL A. CHUNG
Project Engineer
Photovoltaics
Power Components Branch

JOSEPH F. WISE, Chief
Power Components Branch

FOR THE COMMANDER

JAMES D. REAMS
Chief, Aerospace Power Division
Aero Propulsion Laboratory

If your address has changed, if you wish to be removed from our mailing list, or if the addressee is no longer employed by your ogranization please nofity AFWAL/POOC, W-PAFB, OH 45433 to help us maintain a current mailing list.

Copies of this report should not be returned unless return is required by security considerations, contractual obligations, or notice on a specific document.

REPORT DOCUMENTATION PAGE

1a. REPORT SECURITY CLASSIFICATION	1b. RESTRICTIVE MARKINGS
UNCLASSIFIED	

2a. SECURITY CLASSIFICATION AUTHORITY	3 DISTRIBUTION/AVAILABILITY OF REPORT
	Approved for public release;
2b. DECLASSIFICATION/DOWNGRADING SCHEDULE	distribution is unlimited.

4. PERFORMING ORGANIZATION REPORT NUMBER(S)	5 MONITORING ORGANIZATION REPORT NUMBER(S)
	AFWAL TR-85-2108

6a. NAME OF PERFORMING ORGANIZATION	6b. OFFICE SYMBOL (If applicable)	7a. NAME OF MONITORING ORGANIZATION
University of Florida		Aero propulsion Laboratory (AFWAL/POOC) AF Wright Aeronautical Laboratories (AFSC)

6c. ADDRESS (City, State and ZIP Code)	7b. ADDRESS (City, State and ZIP Code)
Gainesville, Florida 32611	Wright-Patterson AFB OH 45433-6563

8a. NAME OF FUNDING/SPONSORING ORGANIZATION	8b. OFFICE SYMBOL (If applicable)	9 PROCUREMENT INSTRUMENT IDENTIFICATION NUMBER
		F33615-81-2058 Subcontract 72702, Task 006

8c. ADDRESS (City, State and ZIP Code)	10 SOURCE OF FUNDING NOS			
	PROGRAM ELEMENT NO.	PROJECT NO.	TASK NO.	WORK UNIT NO.
11. TITLE (Include Security Classification) Modeling and DLTS Analysis of Irradiated Multijunction Solar Cells (UNCLASSIFIED)	62203F	3145	19	10

12. PERSONAL AUTHOR(S)
Sheng Li

13a. TYPE OF REPORT	13b. TIME COVERED	14 DATE OF REPORT (Yr., Mo., Day)	15. PAGE COUNT
Final Report	FROM Nov. 84 TO Oct. 85	February 1986	91

16. SUPPLEMENTARY NOTATION

This effort was accomplished under the AFWAL/POO Scholarly Research Program.

17.	COSATI CODES		18 SUBJECT TERMS (Continue on reverse if necessary and identify by block number)
FIELD	GROUP	SUB GR.	DLTS, III-V Multibandgap Solar Cells Radiation Effects
1001	2202	2012	

19. ABSTRACT (Continue on reverse if necessary and identify by block number)

The objective of this research project was to develop a simple theoretical model based on Wilson's model (Reference 1) to calculate the displacement damages introduced by either protron or electron irradiation in AlGaAs, GaAs, InGaAs and Ge. These calculations would then be applied to obtain an optimized triple junction solar cell structure using these materials with a specified end of life conversion efficiency.

As presented in this report, empirical formulae and theoretical expressions were derived for calculating the displacement cross section, penetration depth, path length, total number of defects formed by an incident electron or proton, and the fractional loss of electron-hole pairs due to recombination loss. Additionally, formulae to calcualte the degradation of short-circuit current under different electron and proton fluences and energies in AlGaAs, GaAs, InGaAs, Ge single junction solar cells and the triple junction cells formed from these materials were developed. The results of our calculations indicate that the

20. DISTRIBUTION/AVAILABILITY OF ABSTRACT	21 ABSTRACT SECURITY CLASSIFICATION
UNCLASSIFIED/UNLIMITED ☒ SAME AS RPT ☐ DTIC USERS ☐	UNCLASSIFIED

22a. NAME OF RESPONSIBLE INDIVIDUAL	22b. TELEPHONE NUMBER (Include Area Code)	22c. OFFICE SYMBOL
JOSEPH F. WISE	(513) 255-6235	AFWAL/POOC

DD FORM 1473, 83 APR   EDITION OF 1 JAN 73 IS OBSOLETE

ITEM 19 - Abstract - Cont'd:

degradation rate in each cell varies greatly, and depends critically not only the energy, fluence and the direction of the incident electrons and protons but also on the thickness of each cell in the triple junction cells. The calculations were carried out for both single and triple junction cells using AlGaAs as the top cell, GaAs as the middle cell, and InGaAs or Ge as the bottom cell for electron energies ranging from 200 KeV to 5 MeV and fluences from 10^{14} to 10^{17} e/cm^2, and for proton energies from 200 KeV to 10 MeV and fluences from 10^{10} to 10^{12} p/cm^2. In addition to the above criteria, calculations of a given space environment have been made for 3-year, 7-year, and 10-year durations.

Major difficulties encountered in performing the theoretical calculations using the model developed in this report included many unknown parameters and the lack of experimental data on electron and proton damages in the AlGaAs and InGaAs solar cells for comparison with theoretical calculations. These uncertainties can be removed once the actual cell structures for the proposed triple junction cells are fabricated and measurements of radiation damage are made in these cells. This may be realized with the actual cells are fabricated for our study.

Table of Contents

Section II DLTS Analysis of Radiation Induced Defects In Proton-Irradiated AlGaAs Solar Cells

Section I

Displacement Damage Calculations

1.1. Introduction

A simple model for computing the space radiation damage in GaAs solar cells was first introduced by Wilson [Reference 1] in 1982. Yaung [Reference 2] proposed some modifications of this model. But until very recently, there have been no reports published on the studies of electron and proton radiation damage in multijunction solar cells such as AlGaAs/GaAs/InGaAs and AlGaAs/GaAs/Ge systems.

The objective of this research project was to develop a simple theoretical model based on Wilson's model [Reference 1] to calculate the displacement damages introduced by either proton or electron irradiation in AlGaAs, GaAs, InGaAs and Ge. These calculations would then be applied to obtain an optimized triple-junction solar cell structure using these materials with a specified end of life conversion efficiency.

As presented in this report, empirical formulae and theoretical expressions were derived for calculating the displacement cross section, penetration depth, path length, total number of defects formed by an incident electron or proton, and the fractional loss of electron-hole pairs due to recombination loss. Additionally, formulae to calculate the degradation of short-circuit current under different electron and proton fluences and energies in AlGaAs, GaAs, InGaAs and Ge single junction solar cells and the triple-junction cells formed from these materials were developed. The results of our calculations indicate that the degradation rate in each cell varies greatly and depends critically not only on the energy, fluence and direction of the incident electrons and protons, but also on the thickness of each cell in the triple-junction cells. The calculations were carried out for both single and triple-junction cells using

1

AlGaAs as the top cell, GaAs as the middle cell and InGaAs or Ge as the bottom cell for electron energies ranging from 200 KeV to 5 MeV and fluences from 10^{14} to 10^{17} e/cm^2, and for proton energies from 200 KeV to 10 MeV and fluences from 10^{10} to 10^{12} p/cm^2. In addition to the above criteria, calculations for a given space environment have been made for 3-year, 7-year, and 10-year durations.

Major difficulties encountered in performing the theoretical calculations using the model developed in this report included many unknown parameters and the lack of experimental data on electron and proton damages in the AlGaAs and InGaAs solar cells for comparison with theoretical calculations. These uncertainties can be removed once the actual cell structures for the proposed triple-junction cells are fabricated and measurements of radiation damage are made in these cells. This may be realized when the actual cells are fabricated for our study.

1.2. Design of A Triple Junction Solar Cell

In order to design a triple-junction solar cell with AMO conversion efficiency greater than or equal to 30 percent, the selection of materials for a triple-junction solar cell is guided by the following criteria: [Reference 3-5]

(a) Favorable bandgap energies for the triple-junction solar cell,

(b) Lattice matching between each cell,

(c) Direct optical transitions,

(d) Compatible metallurgical system,

(e) An available compatible substrate and

(f) Environmental stability.

1.2.1. Design Criteria:

The most critical factor in desiging a multijunction solar cell is the bandgap energy of each cell. [Reference 5] Because of the series connection of the three cells, the optimum design requires the short-circuit currents of three

cells to be equal. Therefore, a combination of three bandgaps such as 1.95 eV/ 1.40 eV/1.0 eV could be used to achieve the optimum triple junction cell structure. [Reference 6] Since the bandgap of GaAs (1.43 eV) falls within the optimum bandgap between 1.4 and 1.6 eV and it also satisfies the above design criteria of (c),(d) and (e), the middle cell must be GaAs [Reference 4, 9].

In addition to the bandgap energy, the lattice match is also an important factor in designing a multijunction solar cell. According to References 3 and 7, AlGaAs is the best selection for the top cell due to its highest AMO efficiency to date obtained with GaAs and its lattice match over the complete ternary alloy range. As for the bottom cell, InGaAs can be chosen to have a direct bandgap, however the lattice mismatch with GaAs requiring the grading for a monolithic cell can negate any advantage due to the graded region which can result in a considerable optical loss penalty. Thus, it requires a good tunnel junction in GaAs.[Reference 4]

Based on the above analysis, it is obvious that the AlGaAs/GaAs/InGaAs triple-junction solar cell shows the potential to offer the optimum triple-junction structure. Since the Ge cell is known to have good radiation resistance, it is worthy to include the AlGaAs/GaAs/Ge triple-junction cell in our calculations.

1.2.2. AMO Efficiency of Selected Design

(a) AlGaAs/GaAs/InGaAs [Reference 4]

	Bandgap	AMO Efficiency
Top cell	1.90eV	19.20%
Middle cell	1.43eV	12.70%
Bottom cell	1.03eV	7.44%

Total = 39.34%

3

(b) AlGaAs/GaAs/Ge [Reference 4]

		Bandgap	AMO Efficiency
Top	cell	1.90eV	18.20%
Middle cell		1.43eV	12.20%
Bottom cell		0.70eV	3.00%

Total = 33.40%

1.3. A Simple Model for Calculating Displacement Damage in A Solar Cell

1.3.1. Atomic Displacements

A solid may be affected in two ways by energetic particle bombardment as follows: [Reference 10]

(1) Lattice atoms are removed from their regular lattice sites, producing displacement damage, and

(2) The irradiating particle causes change in the chemical properties of the solid via ion implantation or transmutation.

In our model, it is assumed that the dominant defect produced by the incident electrons or protons is due to lattice displacement. Under this assumption, an atom will be invariably displaced from its lattice site during collisions if its kinetic energy exceeds the threshold energy (T_d) for the atomic displacement to take place, and conversely will not be displaced if its kinetic energy is less than T_d. [Reference 11]

1.3.1.1. Defect Formation by Proton Bombardment

When energetic protons collide with atoms, the energy transferred to the struck atoms is the most important consideration in evaluating irradiation damage. [Reference 11] The number of defects formed by an energetic proton coming to rest in a solar cell is related to the energy of the proton, the transferred energy, and the threshold energy, T_d, of the solar cell. Given the conservation of energy and momentum, it follows that the maximum energy which

4

can be transferred to the struck atom in a primary headon collision with energy, E, is given by

$$T_M = 4 \ M_1 \ M_2 \ E/(M_1+M_2)^2 \qquad (1.3.1)$$

where E is the initial energy of the proton, M_1 is the mass of the proton and M_2 is the mass of the struck atom. This transferred energy may range from zero in a glacing collision to a maximum T_M in a head-on collision. As for a proton, the energy transfer in a collision can be calculated by ignoring the screening effect. Therefore, the scattering in proton collision obeys the Rutherford differential cross section $d\sigma_p$ given by

$$d\sigma_p = C(dT/T^2) \qquad (1.3.2)$$

where $C=4\pi a_o^2 \ (M_1/M_2) \ Z_1^2 \ Z_2^2(E_r^2/E)$

and where T is the transferred energy. M_1 and M_2 are the same as those in equation 1.3.1, Z_1, Z_2 are the atomic number of the proton and struck atom, E_r is the Rydberg constant and a_o is the Bohr radius. Since the defects occur when the energy transfer is greater than T_d, the displacement cross section σ_p is given by

$$\sigma_p = \int_{T_d}^{T_M} d\sigma_p = \int_{T_d}^{T_M} C(dT/T^2) = C(1/T_d - 1/T_M) \qquad (1.3.3)$$

The average energy transfer, $\bar{T}$, in Rutherford collisions which displace atoms can be calculated as follows:

$$\bar{T} = \int_{T_d}^{T_M} T \ \sigma_p \ / \int_{T_d}^{T_M} d\sigma_p$$

$$= [T_d \ T_M/(T_M - T_d)]\ln(T_M/T_d) \qquad (1.3.4)$$

If the transferred energy is sufficiently large $(T \gg T_d)$, additional displacement can be produced by the recoiling nucleus before it comes to rest at an interstitial site. The average number of recoil displacements, v, produced by one initiating proton collision event is given as a function of T_M based on the assumption that half of the recoil energy produces further displacement, and the other half is dissipated in other processes, such as [References 1, 11]

$$\overline{V}_p(E) = \begin{cases} 1.0 & \text{for} \quad T_d < T_M < 2T_d \\ 1 + T_M/2(T_M - T_d) \ln(T_M/T_d) & \text{for} \quad 2T_d \leqq T_M \end{cases} \tag{1.3.5}$$

Since the mass of a proton is heavier than that of an electron, the velocity of an energetic proton is slower than an electron with the same energy. Thus, a proton has the potential of multiple scattering before coming to rest. Here we assume that the density of scattering centers in three cells are the same (i.e., $N = 4.42 \times 10^{22}/cm^3$). Thus, the average number of defects per unit length formed by an incident proton with energy E is

$$\overline{D}(E) = N \, \sigma_p \, \overline{V}_p \tag{1.3.6}$$

where σ_p is the displacement cross section and $\overline{V}_p$ is given by equation 1.3.5. The total number of defects formed by an incident proton is obtained by integrating equation 1.3.6 along the path length traveled by a proton, which can be expressed by

$$D(E_o) = \int_0^{E_0} N \, \sigma_p \, \overline{V}_p \, dP \tag{1.3.7}$$

where dp is the first derivative of path length traveled by a proton in coming to rest. The path length is a function of proton energy, and is obtained by fitting the data of Janni.[Reference 12]

6

1.3.1.2. Defect Formation by Electron Bombardment

Because of the small mass of an electron, the electron must travel at a relativistic velocity in order to produce displacements. The maximum energy which can be transferred in a collision by an electron with mass m and kinetic energy E is

$$T_M = 2(E + 2 m c^2) E / M_2 c^2 \qquad (1.3.8)$$

where C is the velocity of light, M_2 is the mass of struck atom and $m \ll M_2 c^2$. Consequently, the nonrelativistic Rutherford scattering is inadequate for the electron. Relativistic Coulomb scattering is treated by Mckinley-Feshbach as follows: [Reference 13]

$$d\sigma_e = \frac{4\pi (a_0 Z_2 {}^* E_r)^2 (1-B^2)}{m^2 c^4 B^4} \{1 - B^2 T/T_M + Z_2 B[(T/T_M)^{1/2} - T/T_M]/137\} T_M dT/T^2 \qquad (1.3.9)$$

where a_o is the Bohr's radius, Z_2 is the struck atom's atomic number, E_r is the Rydberg constant, B is the electron velocity ratio to the velocity of light, C , and M is the electron mass. T is the energy transferred to the struck atom during collision. This is given by equation 1.3.8. Integrating equation 1.3.9 yields the displacement cross section for an incident electron.

$$\sigma_e = [4\pi a_o^2 Z_2^2 E_R^2 (1-B^2)/m^2 c^4 B^4]\{(T_M/T_d) - 1 - B^2 \ln(T_M/T_d) +$$

$$2\pi aB[T_M/T_d)^{1/2} - 1] - \pi aB\ln(T_M/T_d)\} \qquad (1.3.10)$$

where a equals $Z_2/137$, T_d is the threshold energy of the struck atom and all other parameters are the same as in equation 1.3.9. The average energy transfer during a collision is

7

$$\bar{T} = \int_{T_d}^{T_M} T \, d\sigma_e \bigg/ \int_{T_d}^{T_M} d\sigma_e$$

$$= \frac{T_M \ln(T_M/T_d) - B^2(T_M - T_d) + 2\pi \, aB[T_M - (T_M - T_d)^{1/2}] - \pi aB(T_M - T_d)}{(T_M/T_d) - 1 - B^2 \ln(T_M/T_d) + 2\pi aB[(T_M/T_d)^{1/2} - 1] - \pi aB \ln(T_M/T_d)} \qquad (1.3.11)$$

Thus, if the energy transfer is large enough (i.e., $T \gg T_d$), additional displacement can be produced by the initial recoiling nucleus before it comes to rest at an interstitial or replacement site. The average number of recoil displacements produced by one initial electron collision event is given as a function of T by the assumption that half the recoil energy produces further displacement and the other half is dissipated in other processes. [References 1, 11]

$$\bar{V}_e(E) = \begin{cases} 0 & \bar{T}(E) < T_d \\ 1 & T_d \leq \bar{T} \leq 2T_d \\ 1 + \bar{T}(E)/2T_d & 2\,T_d < \bar{T}(E) \end{cases} \qquad (1.3.12)$$

The average number of defects per unit penetration depth formed by an incident electron with initial energy, E, is

$$\bar{D}(E) = N \, \sigma_e \, \bar{V}_e \qquad (1.3.13)$$

where N is the density of scattering centers in a solar cell, σ_e is the displacement cross section and $\bar{V}_e$ is given by equation 1.3.12. The total number of defects integrated along the penetration depth is

$$D(E_o) = \int_o^{E_o} N \, \sigma_e \, \bar{V}_e \, dR \qquad (1.3.14)$$

where R is the penetration depth of an electron before coming to rest. Since the electron mass is small, we can neglect the effects of multiple scattering. The

8

empirical formula of penetration depth is given by fitting the data in [Reference 14].

1.3.2. Short-circuit Current (I_{sc}) Degradation

To derive an expression for the I_{sc} in an irradiated cell, the following simplified assumptions were made : [References 1, 15-16]

(1) Radiation-induced defects do not greatly alter the internal cell electric field

(2) Radiation defects alter the cell operation mainly through change in minority carrier lifetimes in the bulk, and

(3) Radiation-induced displacements within the solar cell form recombination centers for minority carriers of electron-hole pairs produced by photon absorption.

According to Wilson's model, a minority carrier, once formed, undergoes thermal diffusion until it is trapped and recombined or is separated at the junction. The root mean square distance traveled in coming to a position a distance L away from the source point is given by [Reference 17]

$$r = (6)^{1/2} L \qquad\qquad (1.3.15)$$

The fractional loss of pairs due to recombination in reaching the junction along a fixed direction is given by

$$f(u) = \begin{cases} 1 - \exp[-\int_{x_j}^{x} \sigma_r D_v(x)(6)^{1/2} dx/u] & (x > x_j) \\ \\ 1 - \exp[-\int_{x}^{x_j} \sigma_r D_v(x)(6)^{1/2} dx/u) & (x < x_j) \end{cases} \qquad (1.3.16)$$

where u is the cosine of the direction to the junction, $D_v(x)$ is the displacement density, x_j is the junction depth and σ_r is the recombination cross section. Averaging f(u) over the entire direction towards the junction

9

yields

$$F(x) = \int_o^1 f(u) \, du$$

$$= 1 - E_2[(6)^{1/2} \delta_r \phi (D_c(E_x) - D_c(E_{xj}))] \qquad (1.3.17)$$

where E_2 is the second order of exponential integral, E_x is the energy reduced after traveling a distance x, Ex_j is the energy reduced after traveling to the junction depth x_j and $D_c(x)$ is the defect density after penetrating a depth x. It also follows that

$$D_c(x) = [D(E_o) - D(E(x))] \phi(E_o) \qquad (1.3.18)$$

where ϕ is the fluence of the incident electrons or protons and $D(E_o)$ is the total number of defects produced by one incident electron or proton with initial energy E_o.

The density of the photon absorption rate at a depth x within the solar cell is given by

$$p(x) = K \, r \, \exp(-rx) \qquad (1.3.19)$$

where K is the integrated flux in the absorption band and r is the photon absorption coefficient averaged over the solar spectrum. Thus, the photo-current collected under a short circuit condition is given by

$$I_{sco} = \int_o^t \eta_c p(x) dx \qquad (1.3.20)$$

where η_c is the normal collection efficiency and t is the depth of active region. The degraded short-circuit current after irradiation is given by

$$I_{sc} = \int_o^t \eta_c [1 - F(x)] \, p(x) dx \qquad (1.3.21)$$

10

Thus, the fraction of remaining current is given as

$$I_{sc}/I_{sco} = 1 - [\int_{o}^{t} \eta_c(x)F(x)p(x)dx / \int_{o}^{t} \eta_c(x)p(x)dx \qquad (1.3.22)$$

If we assume $n_c = 1$, then the normalized short-circuit current degradation is given by

$$I_{sc}/I_{sco} = 1 - \int_{o}^{t} p(x)F(x)dx / \int_{o}^{t} p(x)dx \qquad (1.3.23)$$

1.4. Input Parameters and Empirical Formulae for Simulation

1.4.1. Input Parameters

The input parameters for this simulation program are given as follows:

T_d --- threshold energy of each cell

Z_2 --- average charge number of each cell

M_2 --- average mass of each cell

σ_r --- electron-hole recombination cross section

N --- density of scattering centers of each cell

a --- absorption coefficient of each cell

η_c --- cell charge collection efficiency

X_j --- junction depth of each cell

T_j --- depth of each region

ϕ --- fluence of the proton or electron

E_o --- initial electron or proton energy

X_c --- thickness of coverglass

$Plen(E_o)$ --- function for calculating path length

$Rlen(E_o)$ --- function for calculating penetration length

$Eleft(x)$ --- function for calculating reduced energy

$D_{cx}(E_o)$ --- function for calculating total number of defects

1.4.2. Empirical Formulae

1.4.2.1. Material Selection

The materials selected for this simulation include $Al_xGa_{1-x}As$, GaAs and $In_{1-x}Ga_x$ As or germanium as the top, middle and the bottom junction solar cells respectively for the triple junction solar cell structure. In order to achieve a 30 percent AMO efficiency, the optimum bandgaps for the triple junction solar cell formed by these three materials should be 1.90 eV for the top cell, 1.43 eV for the middle cell and 0.75 eV for the bottom cell. Values of x for the Al_xGa_xAs and $In_{1-x}Ga_xAs$ were calculated by using the empirical formulae given by [Reference 18]

$$1.90 = 1.424 + 1.266\ x + 0.266x^2 \qquad eV \qquad\qquad (1.4.1)$$

for $Al_xGa_{1-x}As$. With Eg = 1.90 eV, x = 0.35.

$$0.75 = 0.35 + 0.63\ x + 0.45x^2 \qquad\qquad (1.4.2)$$

for $In_{1-x}Ga_xAs$. With Eg = 0.75 eV, x = 0.47.

1.4.2.2. Threshold Energy

The threshold energies for GaAs and Ge are given respectively by 9.5 eV and 27.5 eV [Reference 19, 22], while those of InGaAs and AlGaAs are still unknown. Since we know the threshold energies of Al (16 eV) [Reference 20], InAs (7.6 eV) [Reference 19] and GaAs (9.5 eV), the threshold energy for $Al_{0.35}Ga_{0.65}As$ is calculated from the known values of the threshold energy for each element of this material, which is given by

$$T_d = (\ Al^*0.35 + Ga^*0.65 + As\ )/2.0 = 10.7\ eV \qquad (1.4.3)$$

For $In_{0.53}Ga_{0.47}As$, the value of T_d is calculated by

$$T_d = (InGa)_{0.53} + (GaAs)_{0.47} = 8.49\ eV \qquad\qquad (1.4.4)$$

1.4.2.3. Path Length and Penetration Depth

In addition to the threshold energy, the path length or penetration depth (range) for an electron or proton before coming to rest is unknown. Thus, we adopt the path length and the penetration depth from the data given recently by Janni. [Reference 12]. Since all the data for path length or penetration depth are for elements, approximations were made in calculating the path length and range for $Al_{0.35}Ga_{0.65}As$, GaAS and $In_{0.53}Ga_{0.47}As$ based on the following assumptions: [Reference 21]

$$1/P_c = \sum (W_i/P_i) \qquad (1.4.5)$$

$$1/R_c = \sum (W_i/R_i) \qquad (1.4.6)$$

where P_c and R_c are the path length and range of the compound materials respectively, P_i and R_i are path length and range for each element and W_i is the weighting function of each element. The least square method was employed in fitting the data to obtain the expressions for P_c and R_c for these three cells, (see Appendix A).

1.4.2.4. Reduced Energy

To calculate the reduced energy for a proton with initial energy E_0 after travelinga distance x, we must consider the multiple scattering effect of a proton. Therefore, the value for reduced energy is obtained by averaging the reduced energy for traveling a distance x with and without multiple scattering. As stated, the multiple scattering effect for electrons is negligible. The empirical formulae of reduced energy for protons and electrons are presented in Appendix B.

1.4.2.5. Total Number of Displacement Damage

Since the empirical formulae of path length and penetration length are given in Section1.4.2.3, we can apply equations 1.3.7and1.3.14 to obtain the empirical formulae of the total number of displacements for protons and electrons. These are presented in Appendix C.

13

1.5. Results of Computer Simulation For A Single Junction Cell

The following results for four single junction cells are obtained under the input values given in Table 1.5.1.

1.5.1. Results of Proton Radiation Damage

The results of simulation for the displacement cross section, average energy transferred to recoil nucleus and total number of displacements due to proton bombardment are shown in Figures 1.5.1 through 1.5.3 respectively. Figure 1.5.1 shows that the Ge solar cell creates much less displacement damage than the other cells due to the high threshold energy of the Ge cell. This higher threshold energy also explains why the average energy transferred for the Ge cell is much higher than that in the other three cells shown in Figure 1.5.2. Figure 1.5.3 shows that the Ge cell again creates much less displacements than the other cells, especially for high energy protons. For this reason, we included the Ge cell in addition to the InGaAs cell for the bottom cell in this simulation.

Figures 1.5.4 through 1.5.7 show the short-circuit current degradations compared to different fluences and energies of protons. According to these figures, we find that the maximum degradation occurred near 100 KeV. The reason for these results is that high energy protons will penetrate through the cell and not create much degradation. These figures also show that high fluences of protons will degrade cells much more rapidly than cells irradiated by low fluences of protons.

1.5.2. Results of Electron Radiation Damage

Figure 1.5.8 through 1.5.14 are the results of displacement cross section, average energy transferred to recoil nucleus, total number of displacements and short-circuit current degradation due to electron bombardment. The explanations of the different results obtained for each cell are similar to those of proton damaged cells. The main difference is that the mass of an electron is much

smaller than that of a proton. Therefore, the degradation of each cell after electrons irradiation is more uniformly due to the absence of multiple scattering. This also explains why the number of displacements for each cell is much less than that of protons. Thus, it needs higher fluences of electrons than those of protons to create short-circuit current degradation in electron irradiated cells.

1.6. Results Of Computer Simulation For the Triple Junction Solar Cells

The structures of a triple-junction solar cell used in our simulation consist of the top cell -- $Al_{0.35}Ga_{0.65}As$ with X_j = 0.3 um, T_j = 20 um, the middle cell -- GaAs with X_j = 0.5 um , T_j = 300 um and the bottom cell -- $In_{0.53}Ga_{0.47}As$ with X_j =0.5 um, T_j = 15 um or Ge with X_j = 0.5 um , T_j = 15 um. The cover glass has a thickness of 0.1 um.

According to the results of the simulation obtained in subsection 1.5, we find that the I_{sc} degradation rate for each cell is related to the energy and fluence of the incident electron and proton. The algorithm and results of simulation for these triple-junction cells are given as follows:

1.6.1. Algorithm for Calculating I_{sc} degradation for a triple junction cell:

Step 1 : Calculate the penetration depth R1 of the top cell using the initial energy E_o of an incident electron or proton.

Step 2 : If R1 < 20 um ,hen go to step 11.

Step 3 : Calculate I_{sc} degradation rate of the top cell.

Step 4 : Calculate the reduced energy E1 with initial energy E_o after traveling a distance of 20 um of the top cell.

Step 5 : Calculate the penetration depth R2 of the middle cell using the energy E1 in step 4.

Step 6 : If R2 < 300 um then go to step 12.

Step 7 : Calculate the I_{sc} degradation rate of the middle cell.

Step 8 : Calculate the reduced energy E2 with initial energy E1 after

15

traveling a distance of 300 um of the middle cell.

Step 9 : Calculate the penetration depth R3 of the bottom cell using the energy E2 in step 8.

Step 10 : Calculate the I_{sc} degradation rate of the bottom cell and then go to step 13.

Step 11 : Set I_{sc} degradation rates of the middle and bottom cells to be 1, go to step 13.

Step 12 : Set I_{sc} degradation rate of the bottom cell to be 1.

Step 13 : If the I_{sc} degradation rate of each cell is not optimum then adjust the active region of each cell and go to step 1 else go to step 14.

Step 14 : Optimum structure is found. Stop.

1.6.2. Results of simulation for proton

Figures 1.6.1 through 1.6.5 show the results of the penetration depth, total number of displacements and the short circuit-current degradation rate of each cell in the triple-junction solar cell such as AlGaAs/GaAs/InGaAs or AlGaAs/GaAs/Ge due to protons irradiation. To estimate the effect of the proton irradiation on three cells we refer to Table 1.6.1. According to Figure 1.6.1, we find that the 0.5 MeV proton can only penetrate about 4.5 um into the top cell (AlGaAs), therefore there is no damage to the middle cell and the bottom cell. At the specified fluence of 10^{12} p/cm^2 only 6% of the short circuit current is lost in the top cell. For 10 MeV proton, the penetration depths are about to 355 um and 353 um depending on the different bottom cells (Figures 1.6.1 and 1.6.2) which are greater than the thickness of triple-junction cells studied here. Table 1.6.1 shows that under these conditions, the damage caused by 10 MeV proton irradiation is relatively small, leading to a short-circuit current loss for the top cell of only 4% at 3×10^{11} p/cm^2. Our calculations thus show that for the specified energies and fluences, the proton damage in the

16

triple-junction cells is negligible when compared to 1 MeV electron.

Figures 1.6.3 and 1.6.4 show that the proton energy which is greater than 9.4 MeV will create displacements in the bottom cell. In both Figures, we found again that the Ge cell creates less displacements than that of InGaAs cell. However, the reduced energy after traveling through the top and middle cells is so small that there is no obvious damage on the Ge or InGaAs cell (Figure 1.6.5).

1.6.3. Results of Simulation for Electron

Figures 1.6.6 through 1.6.11 show the penetration depth, total number of displacements and the short-circuit current degradation rate of each cell in a triple-junction cell due to electrons irradiation. Since the electron produces uniform damage in the solar cell, thus the electron damage in the triple-junction cell is higher than the proton damage. According to Figures 1.6.6 and 1.6.7, we found that the penetration depth of a 1 MeV electron is about 1000 um which is far beyond the thickness of the triple junction cells proposed in this study. Thus, it is obvious that short-circuit current degradations occurred in these triple junction cells, as shown in Table 1.6.2.

1.7. Simulation of Space Radiation Environment

The simulation of space radiation environment was performed by using the data provided by Hughes Research Lab (see Table 1.7.1). In this simulation, we limited the maximum proton energy to 10 MeV due to the precision of the empirical formulae presented in Appendices A-C. The results are shown in Figures 1.7.1 through 1.7.4. Figure 1.7.1 shows the I_{sc} degradation vs ϕ and E for 3, 7 and 10 years of protons exposure for the AlGaAs solar cell. Figure 1.7.2 shows the I_{sc} degradation vs ϕ and E with 3, 7 and 10 years of protons exposure for the GaAs solar cell. Figure 1.7.3 shows the I_{sc} degradation vs ϕ and E with 3, 7 and 10 years of protons exposure for the InGaAs or Ge solar cell. Figures 1.7.4 through 1.7.7 are for AlGaAs, GaAs, and InGaAs or Ge cells subjected to 3,

17

7, 10 years of the electron exposure, respectively.

1.8. Summary and Conclusions

In this report a simple model for computing the displacement damage for a single and triple-junction solar cell has been developed and applied to the proton and electron irradiated AlGaAs/GaAs/InGaAs or Ge triple junction solar cell under different fluences, energies and space environmental conditions. In this study it is shown that in order to obtain an optimized triple junction solar cell structure with specified end of life conversion efficiency, various physical parameters for each cell should be determined. It is pointed out that major difficulties encountered in carrying out the theoretical calculations using the model developed in this work include many unknown input parameters and the lack of experimental data to facilitate comparison with our calculations. These uncertainties can be removed once the actual cell structures for the proposed triple junction cells are fabricated and characterized. This may be realized when the AlGaAs/GaAs/InGaAs or Ge triple junction solar cells are fabricated for our study. Methods for improving our theoretical model and calculations are summarized as follows:

1. Since the threshold energy T_d plays a major role in this displacement damage model, it is important that an accurate value of T_d is needed for each material used in the triple junction cell. Except for GaAs and Ge, values of T_d for other materials used in the present model are still not wellknown and new data are needed in order to obtain a more accurate calculation of the displacement damages in the AlGaAs/GaAs/InGaAs or Ge triple junction cell.

2. The path length and penetration depth are based on Janni's data. Further experimental data for AlGaAs and InGaAs are needed for further improvement of our calculations.

3. The recombination cross section used in the calculations of short circuit

18

current is assumed to be the same for AlGaAs, GaAs, InGaAs and Ge, which may not be valid and need further improvement. This can be achieved by using the DLTS technique to determine the recombination cross section in each cell.

4. The use of an average optical absorption coefficient in our calculations of the short-circuit current need to be revised; this is due to the fact that the absorption coefficient is a function of the wavelength. Therefore, future calculation of short-circuit current due to the proton and electron damage should be modified so that a more accurate model can be obtained.

5. In our calculation of displacement damage, we assumed that the probability of multiple scattering for protons is 50 percentand therefore, we averaged the effect of the multiple scattering and non-multiple scattering. This may have to be modified in the calculation of multijunction cells.

6. In order to calculate the damage constant, we need the knowledge of diffusion length for each cell. This is not known at present for AlGaAs and InGaAs materials. Measurements of diffusion length for both of these materials before and after protons or electrons damage should be performed in order to improve our calculations of the short-circuit current in the triple-junction cells.

7. In our calculations of the short-circuit current degradation we did not consider the difference between the p-emitter and n-base region separately, and hence the electron and hole are treated equally. This should be modified in our future calculations.

In short, the simple model presented in this report may be considered as a first order approximation for calculating the displacement damage due to protons or electrons bombardment. For further improvement in our model, factors cited above should be included in the present model so that more accurate results can be deduced from this model.

Section II

DLTS Analysis of Radiation Induced Defects in 200 KeV Proton Irradiated

$Al_xGa_{1-x}As$ and Germanium P-N Junction Solar Cells

2.1. Introduction

Studies of native defects and radiation –induced defects in $Al_xGa_{1-x}As$ and germanium have received considerable attention in recent years due to the increasing interest in the development of high efficiency AlGaAs/GaAs/Ge (or InGaAs) tripl-junction solar cells for space power generation. It is well known that prolonged operation of solar cells in space environment will result in degradation of solar cell efficiency as a result of the radiation damage produced in the semiconductor materials. However, recent advances in the III-V compound semiconductor growth technology have greatly improved the quality of epitaxial films with very low defect density. This is particularly attractive for the fabrication of multijunction solar cells using III-V compound semiconductors prepared by MOCVD growth technique. In order to assess the quality of the epitaxial films and the effects of radiation damage created by electron and proton bombardment, it is important to conduct a systematic study of the grown-in deep-level defects and the radiation induced defects in these solar cell materials so that improvement of the conversion efficiency and performance characteristics of the multijunction solar cells fabricated by the MOCVD growth technique can be achieved.

In this report, we present the results of our DLTS analysis of the deep-level defects induced by 200 keV proton irradiation (using H^+ implantation) in $Al_xGa_{1-x}As$ p-n junction solar cells, and compare the results with the grown-in defects observed in the unirradiated samples. DLTS analyses of grown-in defects in germanium samples with different background dopant densities were also being carried out in this study. Defect parameters such as defect energy level,

20

defect density and capture cross section were determined from the C-V and DLTS measurements, and the results are presented in this report.

2.2. Experimental

Sn-doped $Al_xGa_{1-x}As$ (x = 0.2 and 0.3) p-n junction cells fabricated at Hughes Research Laboratories using the liquid-phase epitaxy (LPE) technique on n-GaAs substrates were used in this study. 200 keV protons were irradiated on the $Al_xGa_{1-x}As$ samples at room temperature by hydrogen implantation at proton fluences of 10^{10} cm^{-2} and 10^{11} cm^{-2}. I-V, C-V, and DLTS measurements were performed on these irradiated cells as well as on the controlled cells.

Four germanium p-n junction diodes with dopant densities of N_D= 1.2 x 10^{15}, 2.26 x 10^{16}, 93 x 10^{16}, and 1.86 x 10^{17} cm^{-3} , supplied by General Diode Corporation, were analyzed by our DLTS measurements. The results of this study are also included in this report. Studies of proton radiation -induced defects in germanium p-n junction cells have not been made due to the delay of shipment by General diode Corp., of the specially ordered germanium wafers which are to be used for our C-V and DLTS studies of proton and neutron- irradiation induced- defects in these samples. This work has to be postponed until the next phase of the contract is renewed.

2.3. Results and Discussion

Figure 2.3.1 shows the DLTS spectrum of the electron traps observed in the unirradiated $Al_{0.3}Ga_{0.7}As$ cell with a carrier concentration of 7.01 x 10^{16} cm^{-3}. Two electron traps (i.e., the so- called donor-vacancy complex or the DX-center) were observed in this sample. The E_c- 0.18 eV level is attributed to the Sn-related DX- center, and the E_c- 0.28 eV level is attributed to the Te-related DX- center [Reference 1]. The E_c- 0.28 eV level was also observed in the undoped $Al_{0.3}Ga_{0.7}As$ sample [Reference 2]. The DLTS spectra of the electron traps observed in the proton irradiated $Al_{0.3}Ga_{0.7}As$ cell are shown in Figure 2.3.2 and Figure 2.3.3, which reveal two electron traps identical to those

observed in the unirradiated samples.

C-V measurements showed that carrier densities in the proton-irradiated $Al_{0.3}Ga_{0.7}As$ cells decrease with increasing proton fluences, indicating some carrier removable occured in these proton irradiated samples.. The background dopant densities for both unirradiated and proton irradiated $Al_{0.3}Ga_{0.7}As$ and $Al_{0.2}Ga_{0.8}As$ p-n junction cells are shown in Figure 2.3.7 and Figure 2.3.8 respectively.

The trap densities of $Al_{0.3}Ga_{0.7}As$ cells determined by the combined C-V and DLTS measurements were found to closely be proportional to the background dopant densities. The ratio N_t/N_D is almost constant from cell to cell. Both the unirradiated and the proton irradiated $Al_{0.3}Ga_{0.7}As$ cells have nearly the same doping densities and trap densities. Therefore, from the results of our C-V and DLTS measurements on these proton- irradiated and unirradiated AlGaAs cells, it is clearly shown that little or no damage was created by the low energy bombardment in the $Al_{0.3}Ga_{0.7}As$ cell at fluences of 10^{10} cm^{-3} and 10^{11} cm^{-3}. This result is consistent with our forward I-V measurements shown in Figure 2.3.9, in which all the I-V curves of the $Al_{0.3}Ga_{0.7}As$ cells nearly coincide for both proton-irradiated and unirradiated cells. However, it is noted that in the $Al_{0.2}Ga_{0.8}As$ p-n junction cells, the effect of proton damage is more prominent. Both the defect density and dark current are found to increase with increasing proton fluences, as evidenced by Figures 2.3.5, 2.3.6 and 2.3.10. This result shows that increasing the aluminum concentration in the AlGaAs p-n junction cells may be beneficial for reducing the radiation damage in these cells.

Figure 2.3.4, Figure 2.3.5 and Figure 2.3.6 show the DLTS spectra of electron traps for both the unirradiated and the proton irradiated $Al_{0.2}Ga_{0.8}As$ cells, respectively. In contrast to the $Al_{0.3}Ga_{0.7}As$ cells, the trap densities in these cells tend to increase with increasing proton fluence, with the exception that the trap density for the E_c- 0.20 eV level was found to decrease

slightly at a fluence of 10^{10} cm^{-2} and then increase again at higher fluence. The C-V and DLTS measurements on the $Al_{0.2}Ga_{0.8}As$ cells indicate that $Al_{0.2}Ga_{0.8}As$ cells are more heavily damaged by proton irradiation than that of $Al_{0.3}Ga_{0.7}As$ cell. This can be explained by the fact that forward I-V curves show significantly higher recombination current component for the $Al_{0.2}Ga_{0.8}As$ cell at a proton fluence of 10^{11} cm^{-2} as shown in Figure 2.3.10. For $Al_{0.2}Ga_{0.8}As$ with the fluence 10^{10} cm^{-2}, the total defect concentration compared to the unirradiated $Al_{0.2}Ga_{0.8}As$ cell was not increased, but the density of the deeper DX center, the $E_c- 0.31$ eV, did increase at a proton fluence of 10^{11} cm^{-2}. Since the deeper DX center is the more efficient recombination center and the recombination current is proportional to its density, the forward I-V curves shown in Figure 2.3.10 are in agreement with the result of the DLTS measurement. The reverse I-V measurement of $Al_{0.2}Ga_{0.8}As$ cells also supports this conclusion, which shows a significant increase in reverse dark current at a proton fluence of 10^{11} cm^{-2}. The defect parameters of $Al_{0.2}Ga_{0.8}As$ and $Al_{0.3}Ga_{0.7}As$ cells are summarized in Table 2.3.1. A comparison of the DLTS data in both $Al_{0.2}Ga_{0.8}As$ with $Al_{0.3}Ga_{0.7}As$ cells, reveals that the former is more ·susceptible than the latter samples to proton irradiation. This result is in agreement with the report by Polimdei et al.[Reference 3] They showed that an increase in Al content increases the radiation hardness of $Al_xGa_{1-x}As$ for both gamma and neutron irradiation.

I-V, C-V, and DLTS measurements were made on four germanium diodes of different background doping densities. The DLTS scans of the electron trap ($E_c- 0.20$ eV) and hole trap ($E_v+ 0.15$ eV) in the unirradiated germanium cells are shown in Figure 2.3.11 and Figure 2.3.12, respectively. These levels coincide with the gold levels ($E_v+ 0.04$ eV, $E_v+ 0.15$ eV, $E_c- 0.20$ eV, and $E_c- 0.04$ eV)(4) reported in the literature. The results of DLTS measurements on the unirradiated germanium samples are summarized in Table 2.3.2. In GE1 the

23

densities of the $E_c - 0.20$ eV and $E_v + 0.15$ eV are almost identical. It suggests that both levels are due to the gold impurity. The reason why the $E_v + 0.15$ eV level could not be observed except for GE1 is that it is hard to inject holes into the highly doped n-type base in DLTS measurement by forward biasing. The possibility that the $E_c - 0.20$ eV level is due to oxygen impurity cannot be refuted. Oxygen has the $E_c - 0.04$ eV and $E_c - 0.20$ eV level and is known as a fast contaminant in germanium(4). Copper impurity, which is usually a contaminated impurity in germanium, could not be observed. Probably germanium cells underwent a special process to reduce copper impurity contamination into germanium [Reference 4]. The forward I-V curves for the unirradiated germanium cell are also shown in Figure 2.3.13, and the C-V data are shown in Figure 2.3.14 for these samples. The results of C-V and DLTS measurements are listed in Table 2.3.2.

2.4. Summary and Conclusions

Detailed characterization of deep level defects in the unirradiated, proton-irradiated LPE $Al_x Ga_{1-x} As$ (x = 0.2 & 0.3) cells, and the unirradiated germanium has been made using DLTS, C-V, and I-V measurements. 200 KeV proton with fluences of 10^{10} cm^{-2} and 10^{11} cm^{-2} were used in this study. DLTS analyses of the proton irradiated AlGaAs cells showed no extra deep levels are produced by low energy proton irradiation in the $Al_x Ga_{1-x} As$ (x = 0.2 & 0.3) cells. However, results of DLTS measurements showed that $Al_{0.3} Ga_{0.7} As$ cells are less damaged by radiation than the $Al_{0.2} Ga_{0.8} As$ cells. Increasing Al contents in AlGaAs cells appears beneficial for increasing radiation tolerance in these high bandgap solar cells.

As for the unirradiated germanium cells, the $E_c - 0.20$ eV and $E_v + 0.15$ eV were observed. Both levels are ascribed to gold impurity related defects.

24

References

[1] Wilson, J. J., Stith, J. J., and Stock, L. V., A Simple Model of Space Radiation Damage in GaAs Solar Cell, NASA Technical Paper 2242, 1983.

[2] Yaung, J. Y., Model of Solar Cell Proton Damage, NASA Space Photovoltaic Research and Technology Conference, 1983.

[3] Lamorte, M. L., and Abbott, D. H., Computer Modeling of a Two Junction Monolithic Cascade Solar cells, IEEE Transaction on Electron Devices , Vol. ED-27 Jan. 1980.

[4] Loo, R. Y., private communication.

[5] Bedair, S. M., Phatak S. B., and Hauser, J. R., Materials and Device Consideration for Cascade Solar Cell, IEEE Transaction on Electron Devices, Vol. ED-27 No. 4, April 1980.

[6] Lewis, C. R., Dietze, W. T., and Ludowise, M. J., Development of a 30% efficiency 3-junction Monolithic Cascade Solar cell , NASA Conference Publication 2314, 1982.

[7] Knechtli, R. C., Loo, R. Y., and Kamath, G. S., High efficiency GaAs Solar Cells, IEEE Transaction on Electron Devices, Vol. 31, No.5,May 1984.

[8] Dalal, V. L., Realistic Design of Monolithic Multiple junction Amorphous Solar cell, the 18th IEEE Photovoltaic Specialists Conference, 1984.

[9] Hovel, H. J., Solar cells, in Semiconductors and Semimetals, Vol. 11, pp.74-75, 1975.

[10] Peterson, N. L, and Harkness, S. D, eds., Radiation Damage in Metals, American Soc. for Metals, C. pp. 59, 1976.

[11] Dienes, G. J., and Vineyard, G. H., Radiation Effects in Solids, Interscience Publishers Inc., New York, 1957.

[12] Janni, J. F., Proton Range-Energy Tables, 1Kev- 10 GeV,. Atomic Data and Nuclear Data Tables 27, pp. 147-339, 1982.

[13] Mckinley, W. A. Jr., and Feshbach, H, <u>The Coulomb Scattering of Relativistic Electrons,</u> by Nuclei. Phys. Rev. Vol 74, NO. 12, 1948.

[14] Pages, L., Bertel, E., Joffre, H. and Sklavenitis, L., <u>Energy Loss, Range and Bremsstrahling Yield for 10 keV to 100 Mev Electron in Various Elements and Chemical Compounds,</u> Atomic Data, Vol.4, pp. 1-127, 1972.

[15] Walker, G. H and Conway, E. J, <u>Short Circuit Current Changes in Electron Irradiated AlGaAs/GaAs solar Cells,</u> Thirteenth IEEE Photovoltaic Specialist Conference, 1978.

[16] Walker, G. H. and Conway, E. J., <u>Recovery of Shallow Junction GaAs Solar Cells Damaged by Electron Irradiation,</u> J. ElectroChem Soc. Oct. 1978.

[17] Liverhant, S. E., <u>Nuclear Reactor Physics,</u> John Wiley & Sons Inc., 1960.

[18] Kressel, H. and Butter, J. K., <u>Semiconductor Lasers and Heterojunction LEDs,.</u> Academic Press., pp. 357-393, 1977.

[19] Bauerlein, R., <u>Messung Der Energie Zur Verlagerung eines Gitteratoms durch Elektronenstoss A^{III}B^{V}-Verbindugen,</u> Z Phys., 1963.

[20] Peterson, N. L. and Harkness S. D. eds., <u>Radiation Damage in Metals,</u> American Soc. for Metals. C. pp. 65, 1976.

[21] Janni, J. F., <u>Calculations of Energy Loss, Range, Pathlength, Straggling, Multiple Scattering and the Probability of Inelastic Nuclear Collisions for 0.1 to 1000 MeV Protons,</u> AFWL-TR-65-150, Sept. 1966.

[22] Lang, D. V. and Logan, R. A., Inst. Phys. Conf. Ser. No. 59, pp. 305, 1981.

[23] Li, S. S., Schoenfeld, S. W., Chiu, T. T. and Lin, C. Y., Inst. Phys. Conf. Ser. No. 59, pp. 305, 1981.

[24] Polimadei, P., Epstein, A., Lynch, R. and Sullivan, D., IEEE Transaction on Nuclear Science, NS-21, pp. 96, 1974.

[25] Milnes, A. G.,<u>Deep Impurities in Semiconductors,</u> pp. 44, Wiley, 1973.

[26] Hiraki, A., Cleveland, J. W. and Crawford, Jr., J. H., Journal of Applied Physics, Vol. 38, No.9, pp.3519, 1967.

Table 1.5.1 Input parameters for each cell

Cell	X_j	T_j	T_d	Z_2	M_2	a	σ_{rn} (cm^2)	σ_{rp} (cm^2)
Top:								
AlGaAs	.3 um	20 µm	10.7 eV	28.85	64.84	2.0	4×10^{-14}	6×10^{-14}
Middle:								
GaAs	.5 um	300 µm	9.5 eV	32	72.5	1.4	4×10^{-14}	6×10^{-14}
Bottom:								
InGaAs	.5 um	15 µm	8.49 eV	36.77	84.27	1.1	4×10^{-14}	6×10^{-14}
Ge	.5 um	15 µm	27.5 eV	32	72.59	0.3	4×10^{-14}	6×10^{-14}

Table 1.6.1 I_{sc} degradation for each cell of a AlGaAs/GaAs/InGaAs or Ge
triple-junction solar cell for two different proton energies
and fluences.

Cell	E = 0.5 MeV, $\phi=10^{10}$ p/cm^2	E = 10 MeV $\phi = 3\times10^{11}$ p/cm^2
	(I_{sc}/I_{sco})	
Top: AlGaAs	0.939	0.969
Middle: GaAs	1.0	0.961
Bottom: InGaAs	1.0	0.999
Ge	1.0	0.999

Table 1.6.2 I_{sc}/I_{sco} for each cell in a AlGaAs/GaAs/InGaAs
or Ge triple junction solar cell irradiated
by 1 MeV electron with 10^{15} e/cm^2.

Top cell (AlGaAs)	Middle cell (GaAs)	Bottom cell InGaAs	Ge
0.924	0.886	0.904	0.999

Table 1.7.1 Flux Spectrum per Year of Space Radiation Environment

Particles	Energy (MeV)	Integral Flux / year
Proton	0.1	1.2×10^{14} p/cm^2
	0.2	6.2×10^{13} p/cm^2
	0.4	2.0×10^{13} p/cm^2
	1.0	2.2×10^{12} p/cm^2
	2.0	3.7×10^{13} p/cm^2
	3.0	1.1×10^{13} p/cm^2
	4.0	7.5×10^{12} p/cm^2
	6.0	6.7×10^{11} p/cm^2
	10.	9.2×10^{10} p/cm^2
Electron	0.1	7.4×10^{14} e/cm^2
	0.5	6.4×10^{13} e/cm^2
	1.0	1.8×10^{13} e/cm^2
	2.0	3.4×10^{12} e/cm^2
	3.0	6.1×10^{11} e/cm^2
	4.0	8.5×10^{10} e/cm^2
	5.0	8.5×10^{9} e/cm^2

Table 2.3.1 Defect parameters in 200 keV proton irradiated $Al_xGa_{1-x}As$

(x = 0.2 & 0.3)

	Fluence (cm^{-2})	N_D (cm^{-3})	E_T (eV)	N_T (cm^{-3})	σ_n (cm^2)
$Al_{0.2}Ga_{0.8}As$	0	2.92×10^{17}	$E_c - 0.20$	3.10×10^{16}	3.47×10^{-14}
	10^{10}	1.67×10^{17}	$E_c - 0.20$	1.37×10^{16}	3.47×10^{-14}
			$E_c - 0.31$	1.55×10^{16}	8.22×10^{-14}
	10^{11}	1.10×10^{17}	$E_c - 0.20$	7.50×10^{16}	3.47×10^{-14}
			$E_c - 0.31$	3.70×10^{16}	8.22×10^{-14}
$Al_{0.3}Ga_{0.7}As$	0	7.01×10^{16}	$E_c - 0.18$	5.70×10^{16}	6.89×10^{-15}
			$E_c - 0.28$	7.92×10^{15}	8.00×10^{-15}
	10^{10}	5.81×10^{16}	$E_c - 0.18$	4.24×10^{16}	6.89×10^{-15}
			$E_c - 0.28$	5.81×10^{15}	8.00×10^{-15}
	10^{11}	4.36×10^{16}	$E_c - 0.18$	3.16×10^{16}	6.89×10^{-15}
			$E_c - 0.28$	4.15×10^{15}	8.00×10^{-15}

Table 2.3.2 Defect parameters of Ge as determined by DLTS measurements.

Diodes	N_D (cm^{-3})	E_T (eV)	N_T (cm^{-3})	σ_n (cm^2)	σ_p (cm^2)
GE4	1.20×10^{15}	$E_c - 0.20$	5.09×10^{14}	2.68×10^{-17}	
		$E_v + 0.15$	5.03×10^{14}		2.36×10^{-17}
GE3	2.22×10^{16}	$E_c - 0.20$	8.76×10^{15}	2.68×10^{-17}	
GE2	9.30×10^{16}	$E_c - 0.20$	2.37×10^{16}	2.68×10^{-17}	
GE1	1.86×10^{17}	$E_c - 0.20$		2.68×10^{-17}	
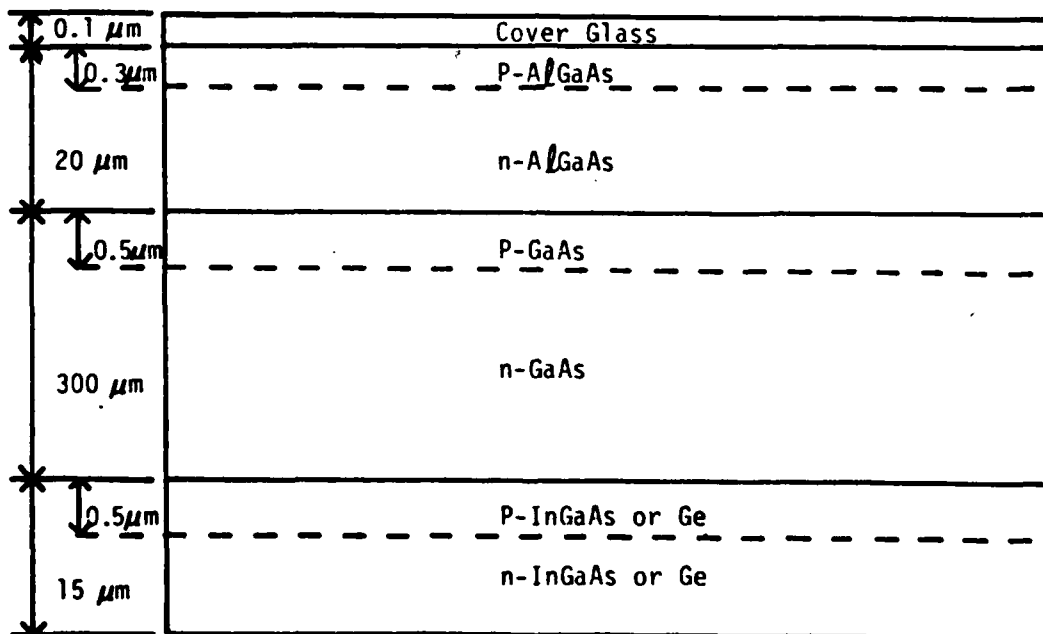
Figure 1.1.1 Schematic diagram of a AℓGaAs/GaAs/InGaAs or Ge triple junction solar cell.
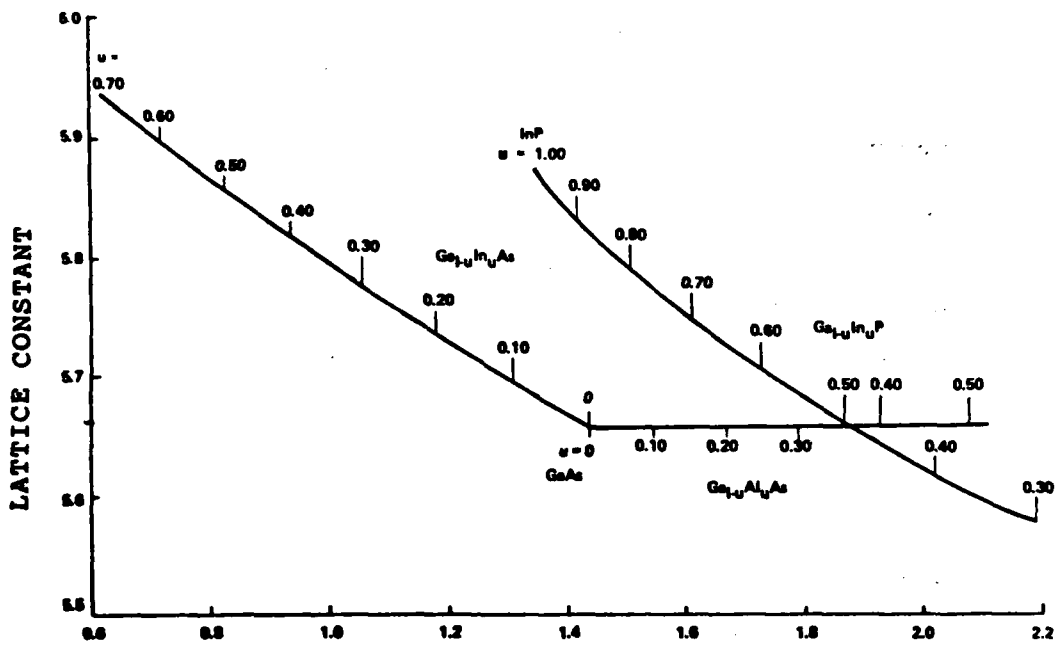
Fig. 1.2.1 Lattice constant vs. energy bandgap at room temperature
for the GaInAs, AlGaAs, and GaInP ternary alloys
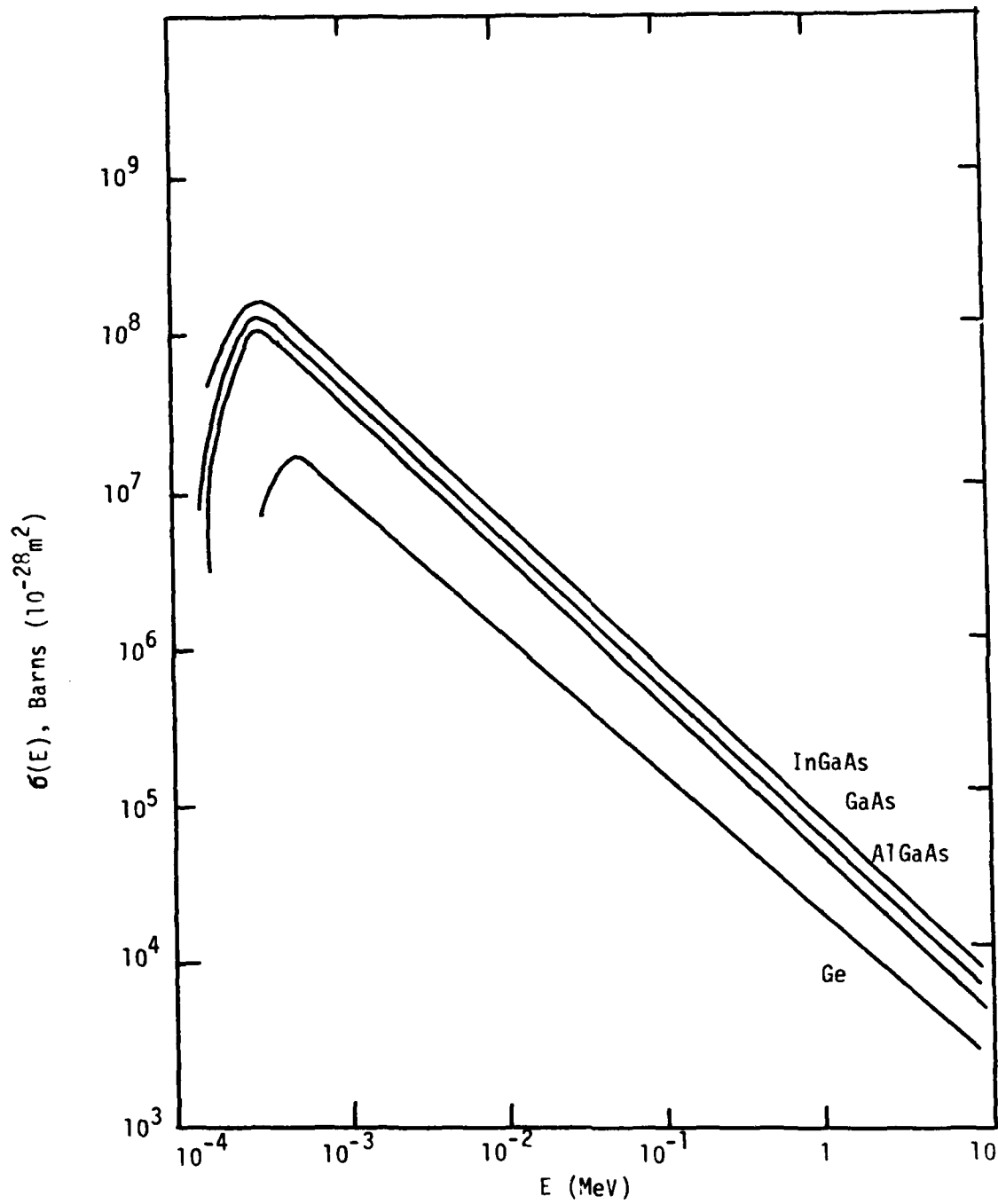
Figure 1.5.1 Displacement Cross Section vs. Proton Energy for
InGaAs, GaAs, AlGaAs, and Ge Single Junction Cell
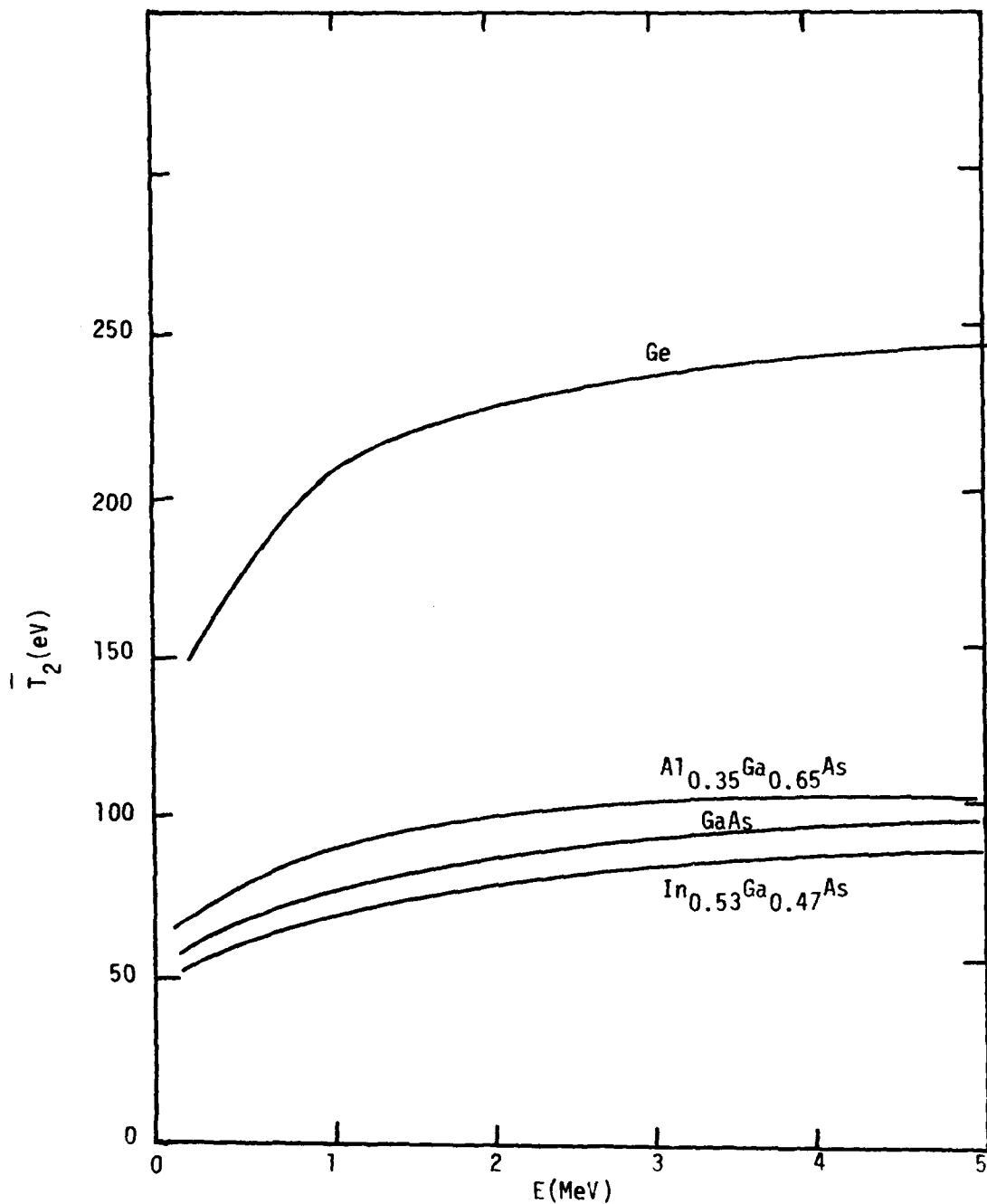
Figure 1.5.2   Average Energy Transferred to Recoil Nucleus by
Proton in Ge, AlGaAs, GaAs and InGaAs single junction
solar cell.
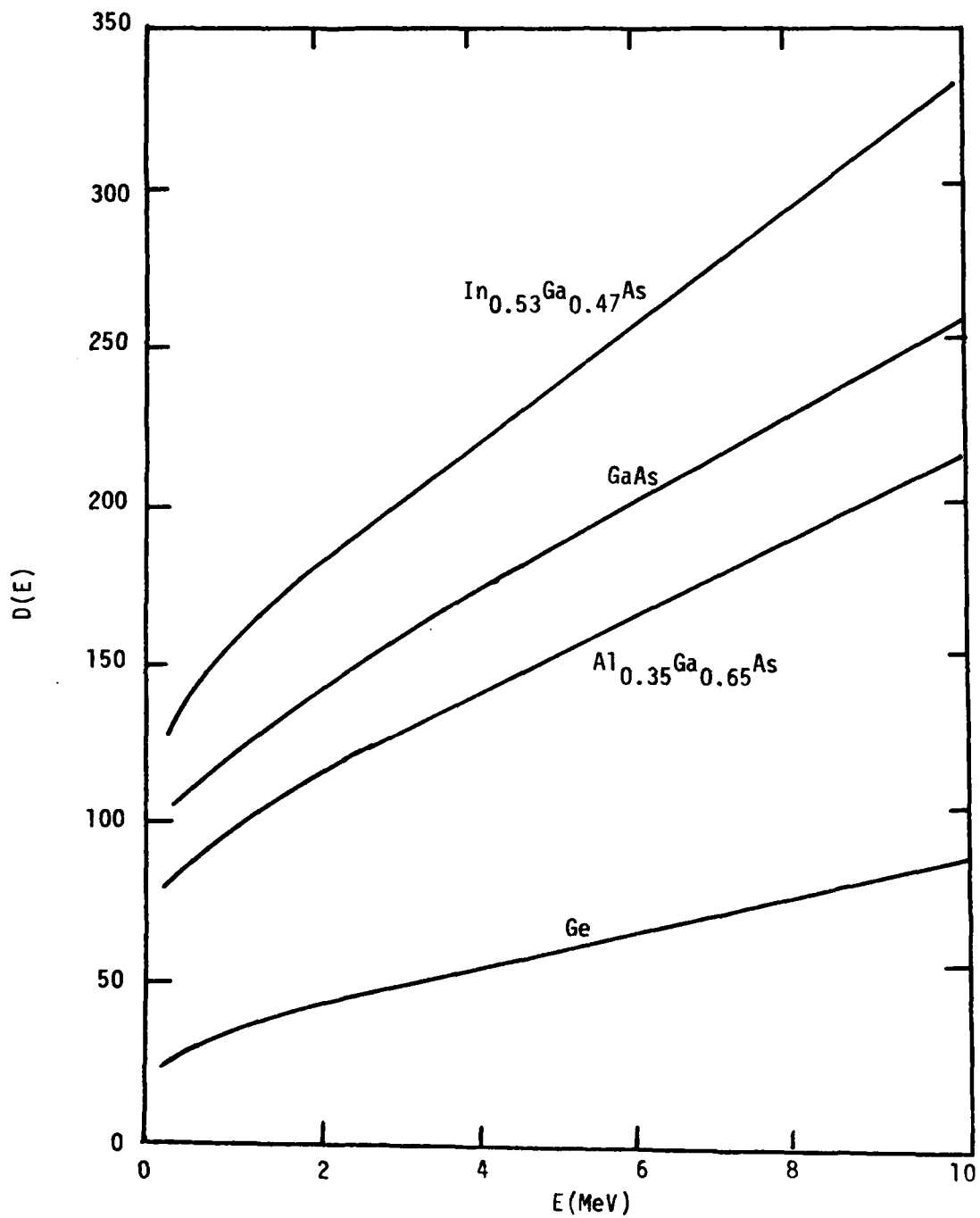
Figure 1.5.3   Total Number of Displace vs. Proton Energy E for InGaAs, GaAs, AℓGaAs and Ge P/N Junction Solar Cell.
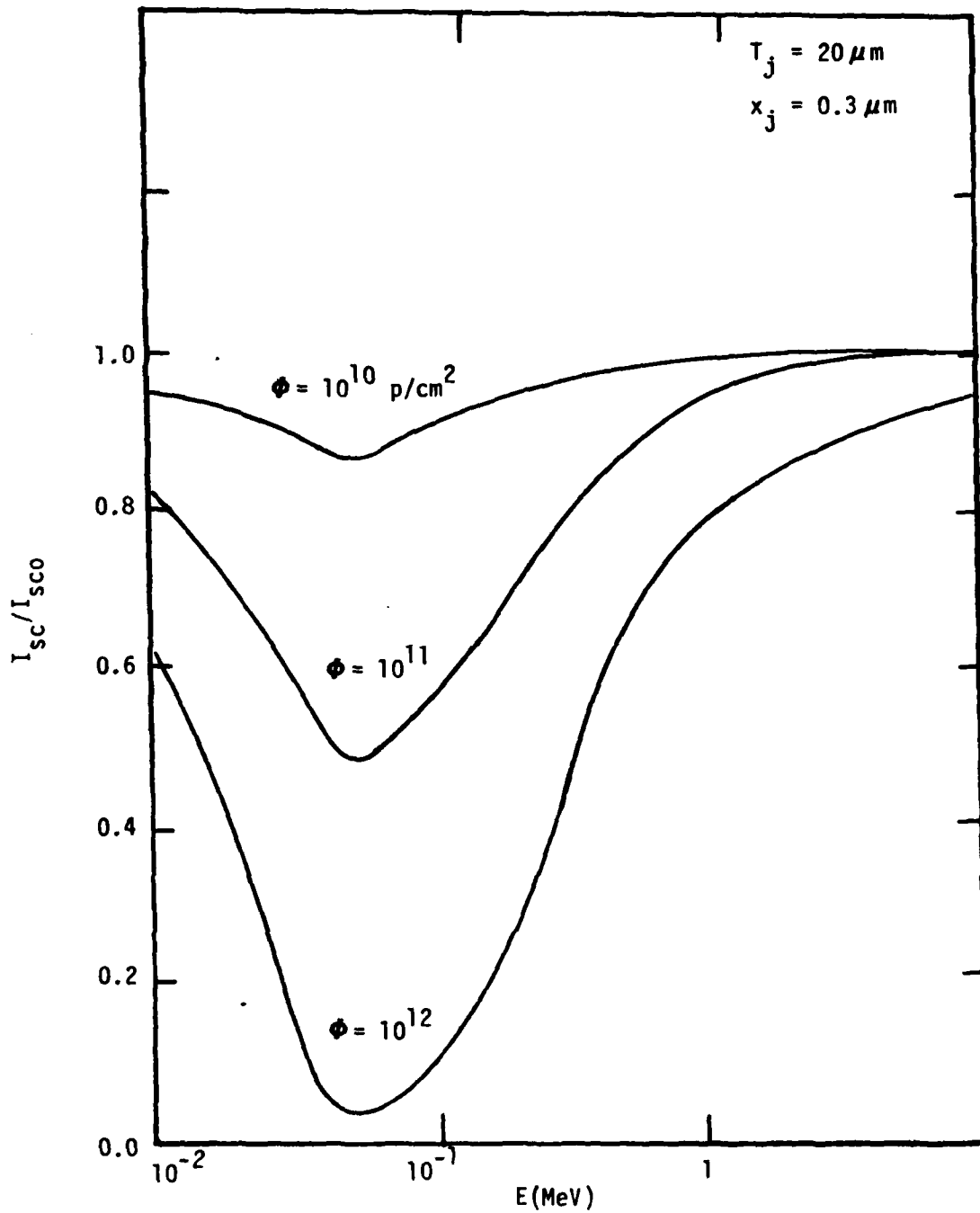
Figure 1.5.4   Normalized short-circuit current vs. proton energy
for $Al_{0.35}Ga_{0.65}As$ p-n junction cell with different
proton fluences.

36
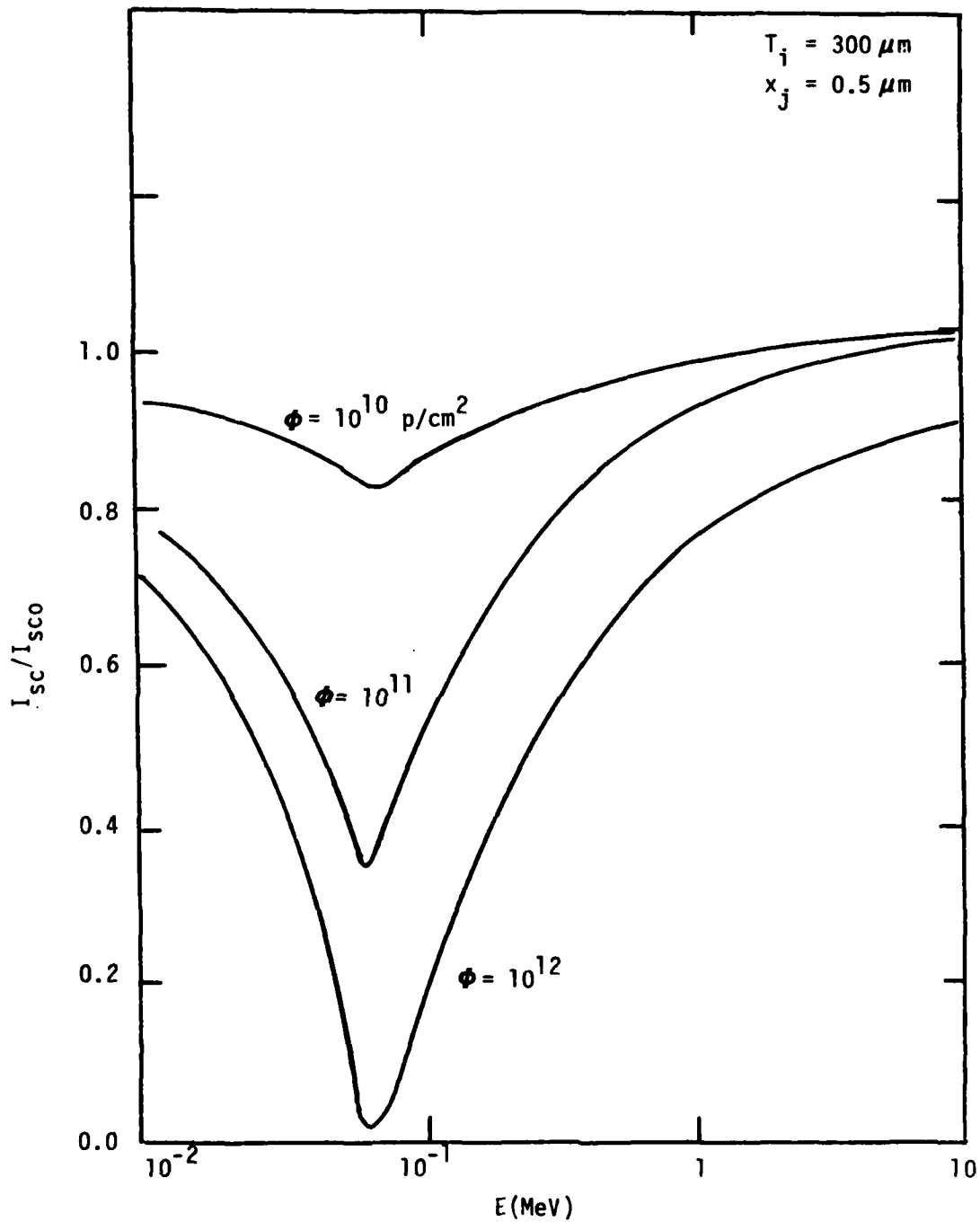
Figure 1.5.5   Normalized short-circuit current vs. proton
energy for GaAs p-n junction cell for different
proton fluences.
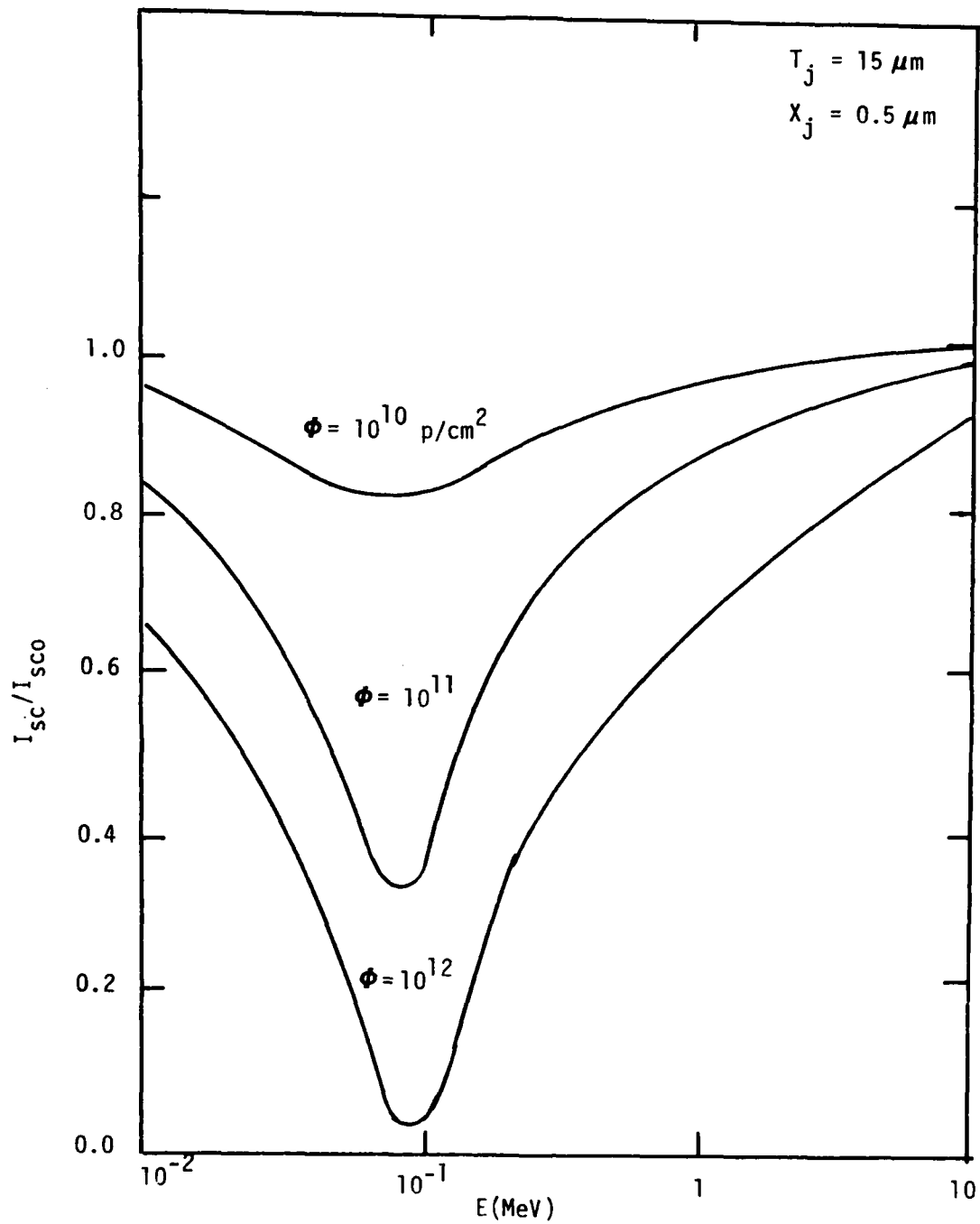
Figure 1.5.6   Normalized short circuit current vs. Proton Energy
for $In_{0.53}Ga_{0.47}As$ p-n junction solar cell for
different proton   fluences.
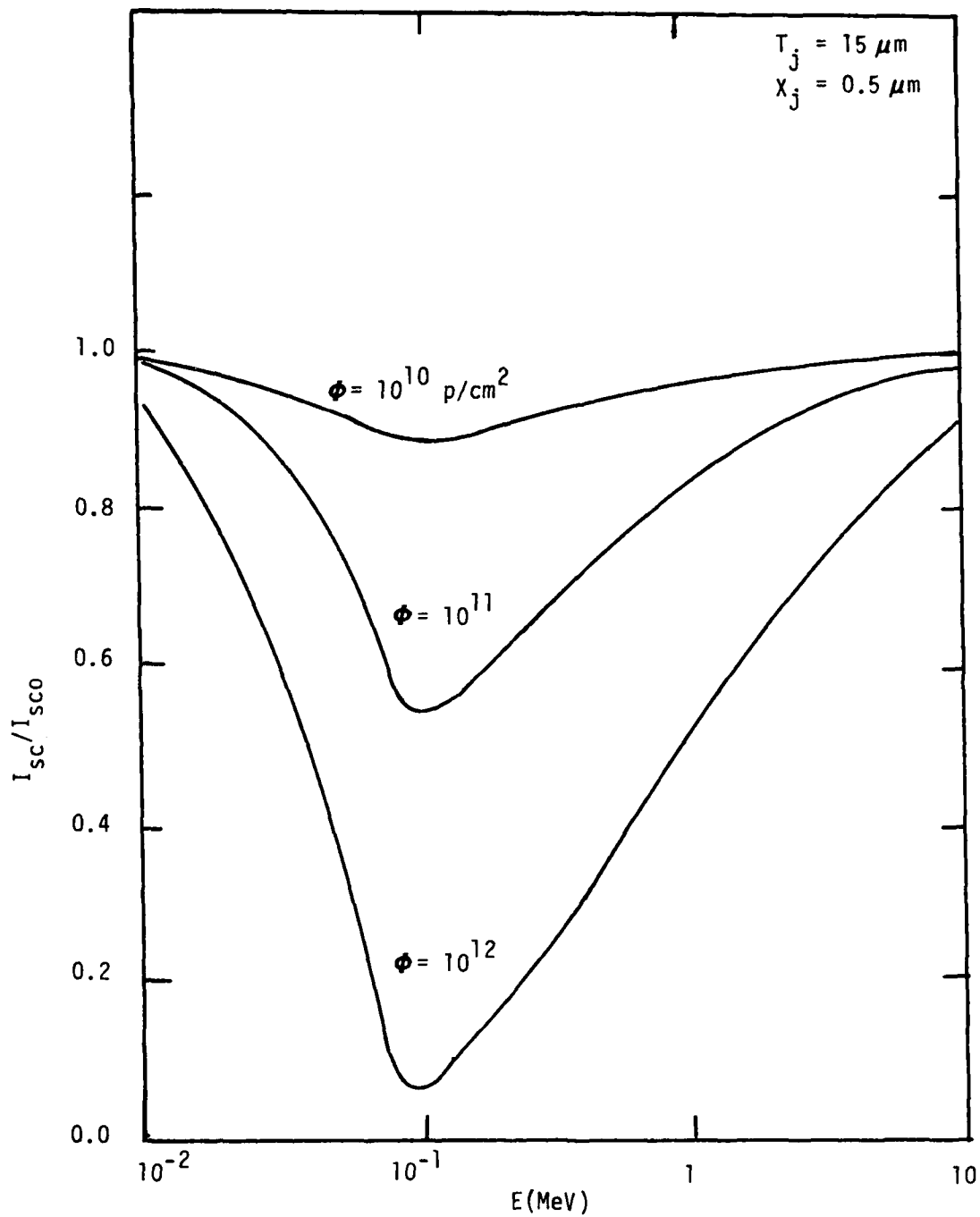
Figure 1.5.7   Normalized short circuit current vs. Proton Energy
for Ge p-n junction cell for different proton
fluences.
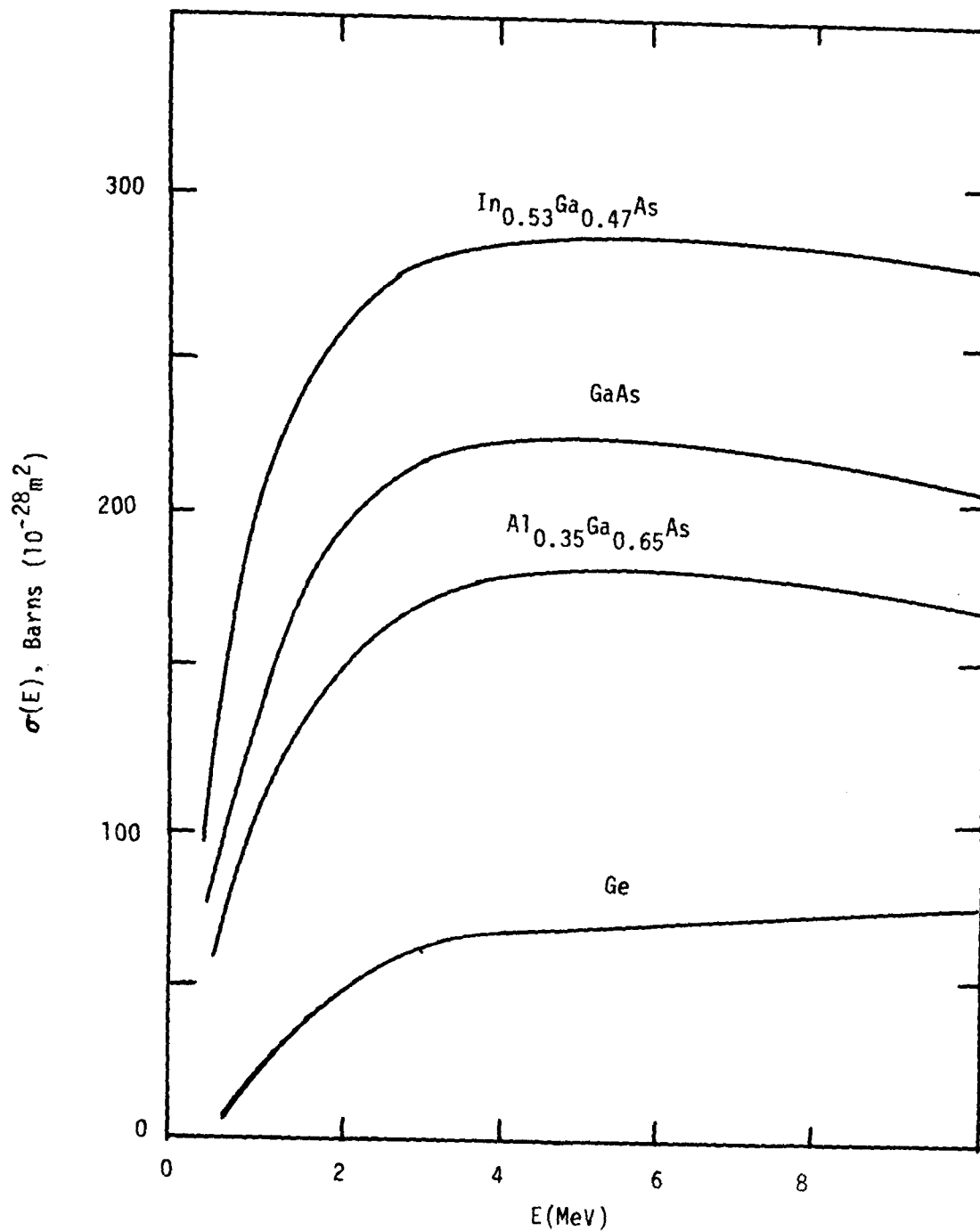
Figure 1.5.8   Displacement Cross Section vs. Electron Energy
for Single Junction Solar Cell.

40
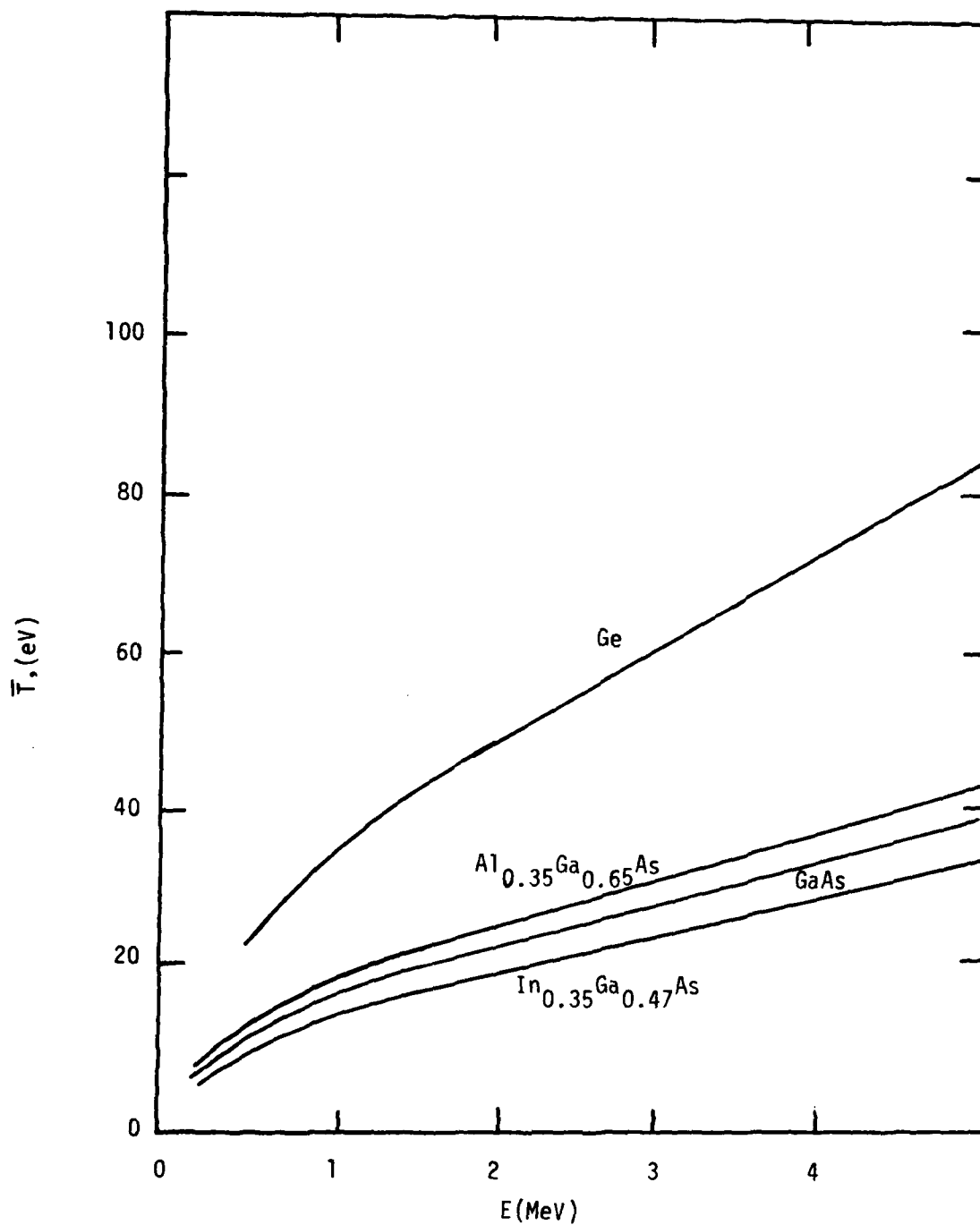
Figure 1.5.9   Average Energy Transferred to Recoil Nucleus by
Electron

41
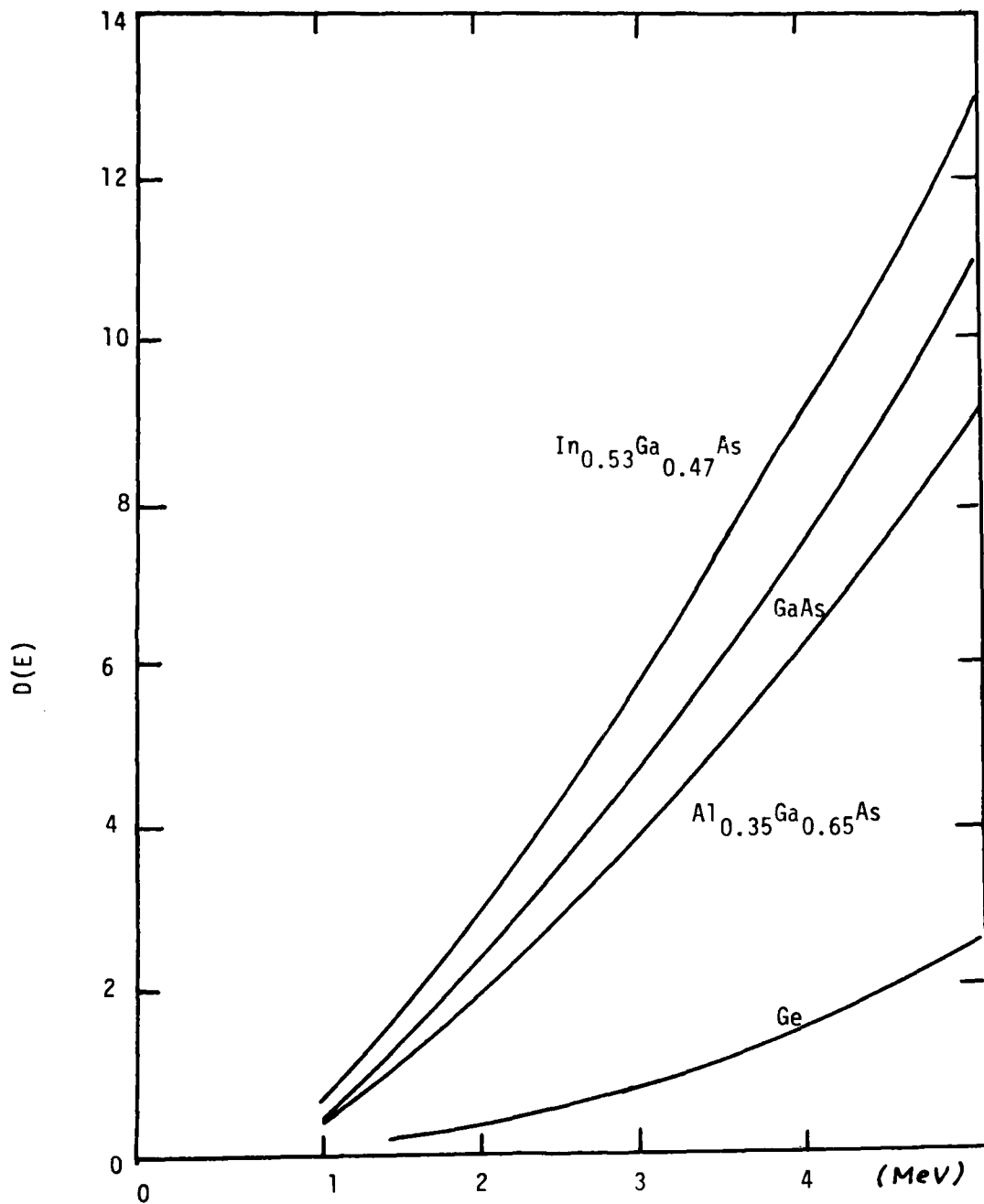
Figure 1.5.10   Total Number of Displacement vs. Electron Energy
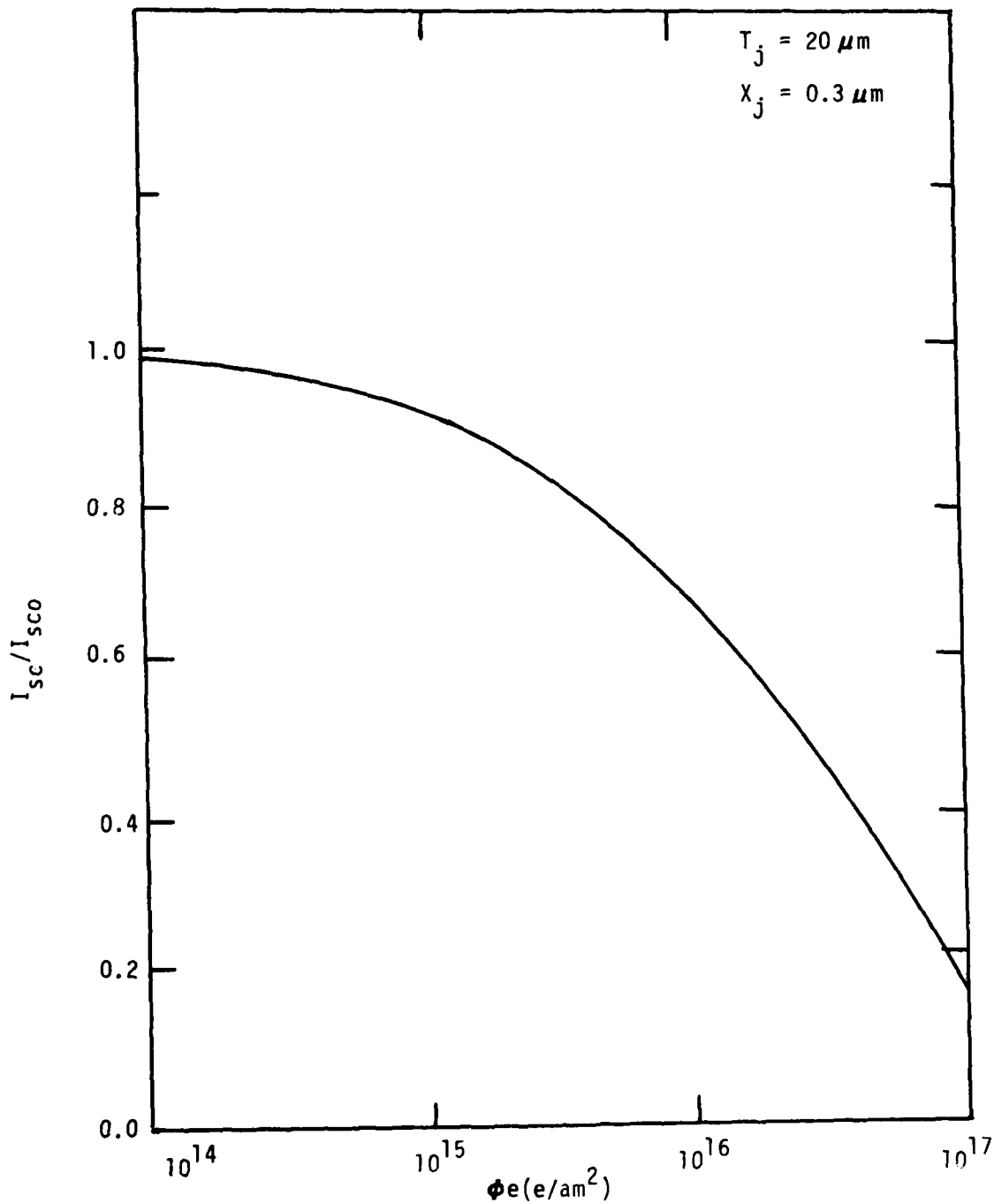
Figure 1.5.11   Normalized I_{sc} vs. Electron Fluence for
$Al_{0.35}Ga_{0.65}As$ Single Junction cell.
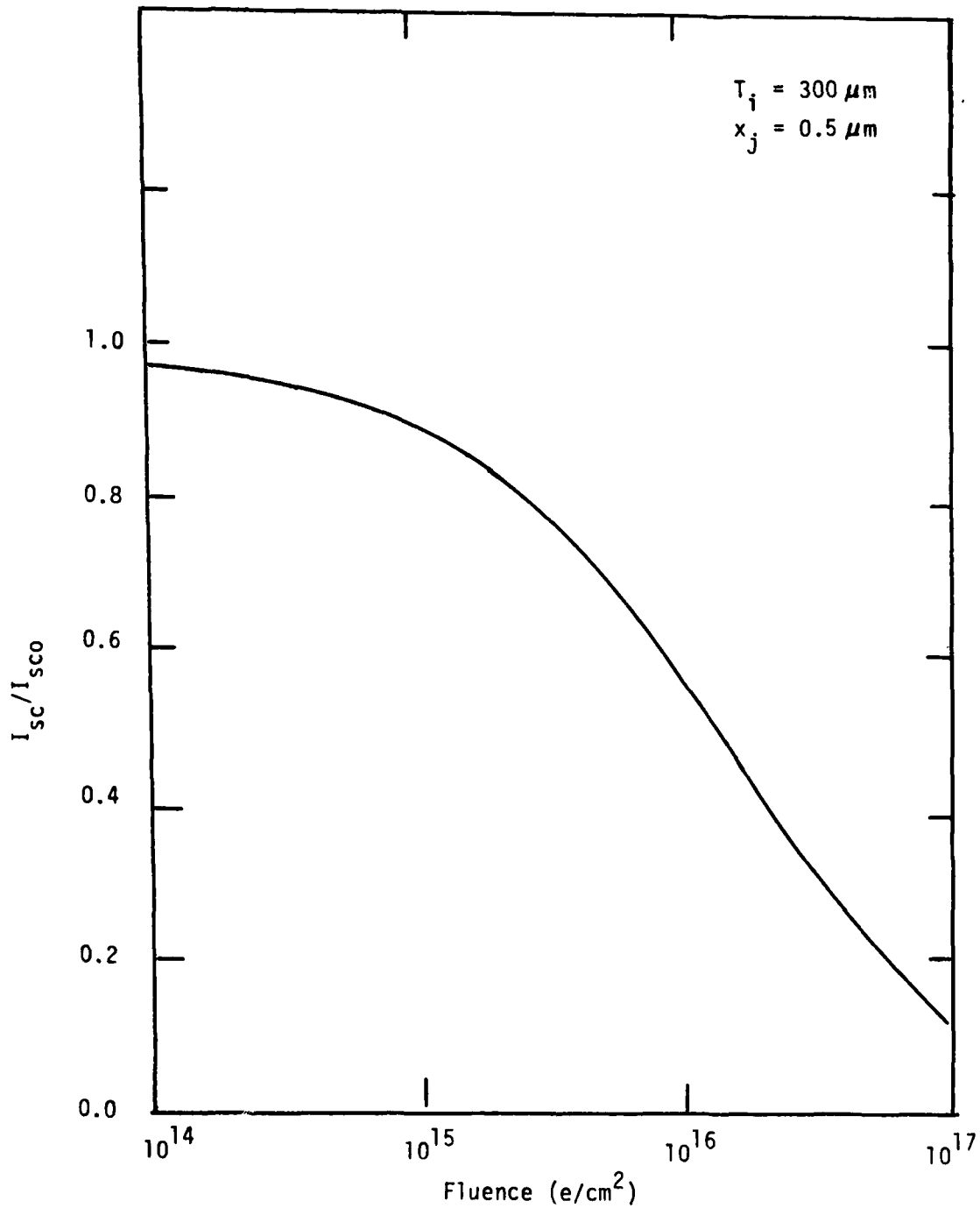
Figure 1.5.12 I_{sc} Degradation vs. Electron Fluence for GaAs
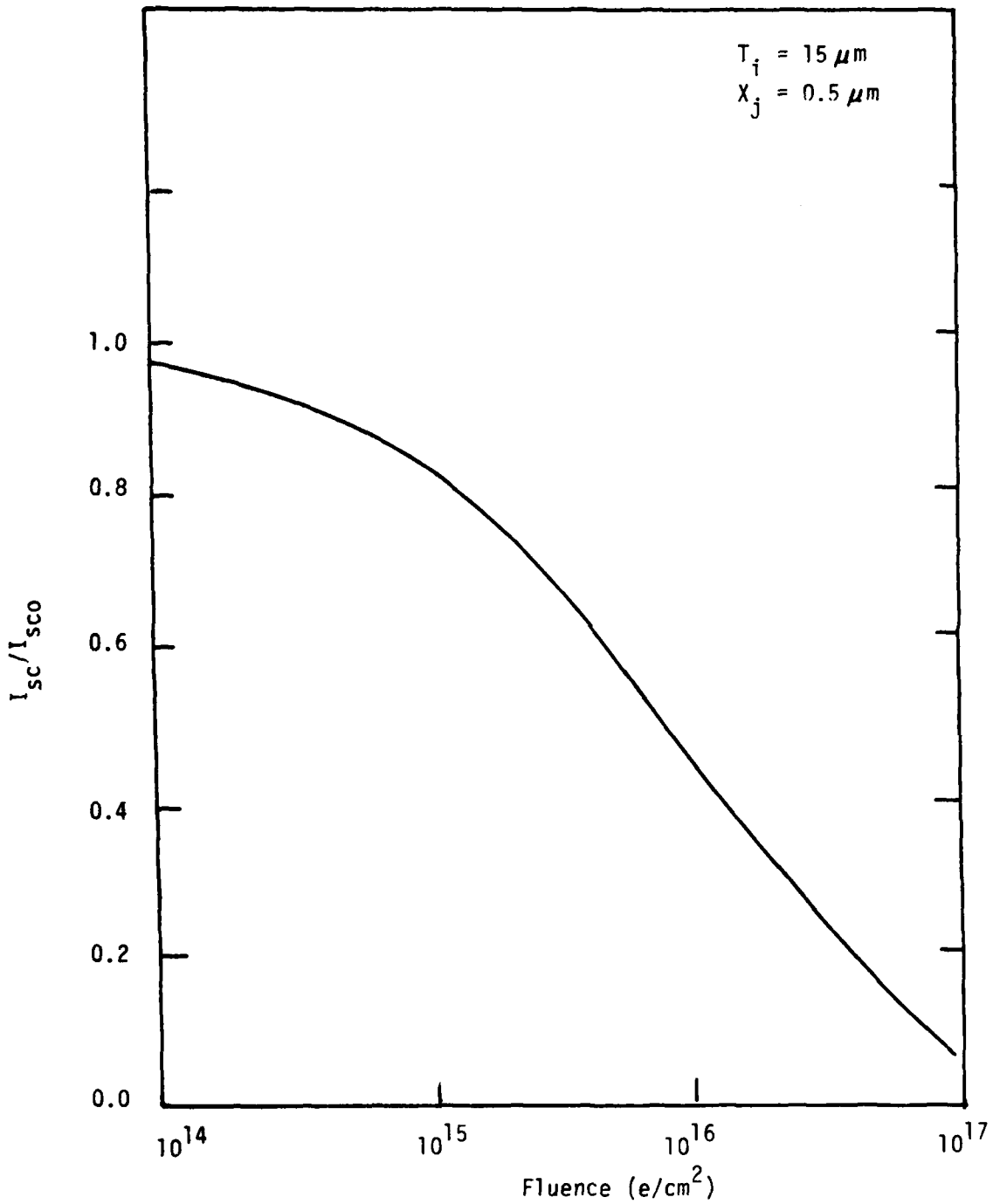
Figure 1.5.13 I_{sc} Degradation vs. Electron Fluence for $In_{0.53}Ga_{0.47}As$

45
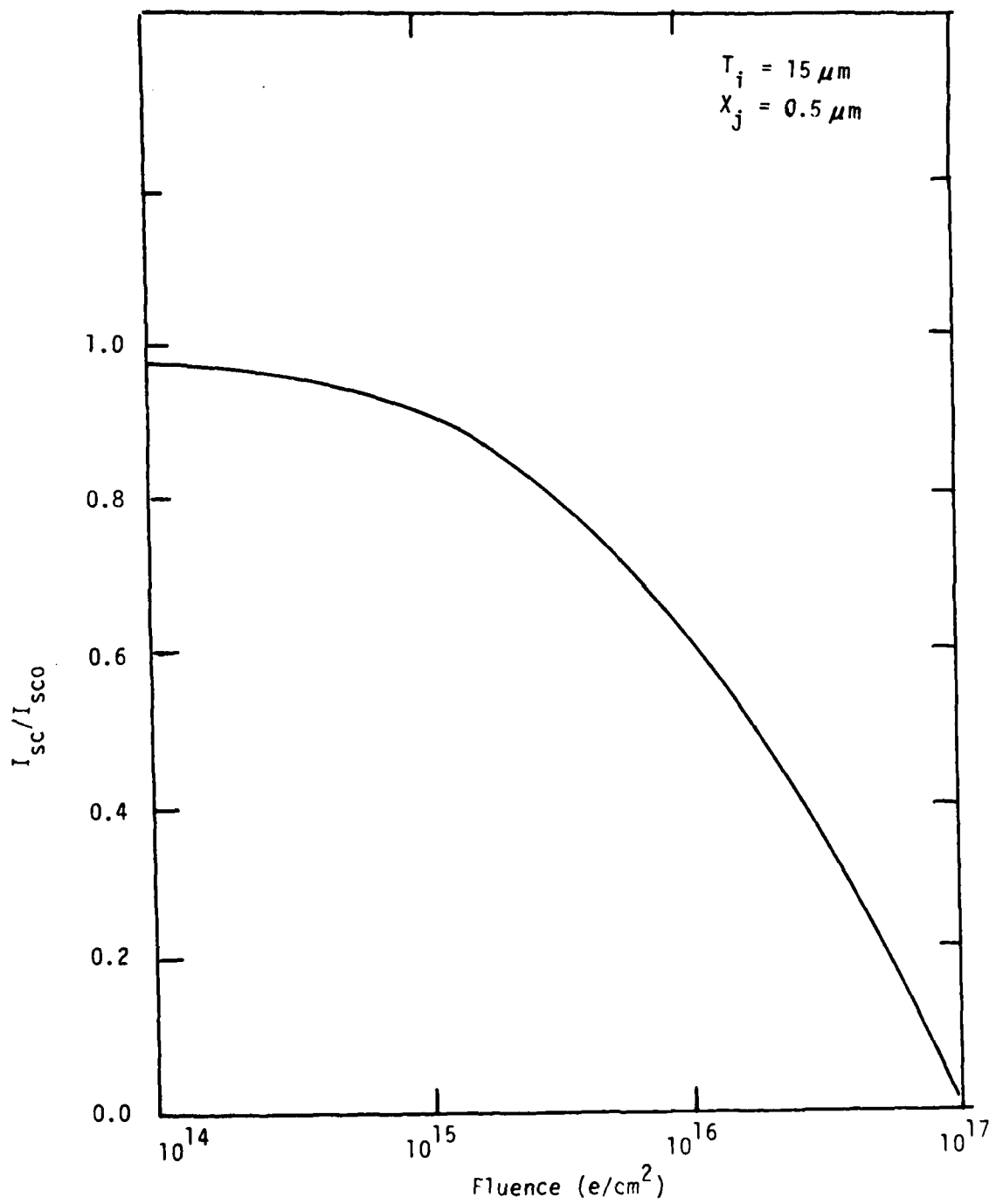
Figure 1.5.14 I_{sc} Degradation vs. Electron Fluence for Ge
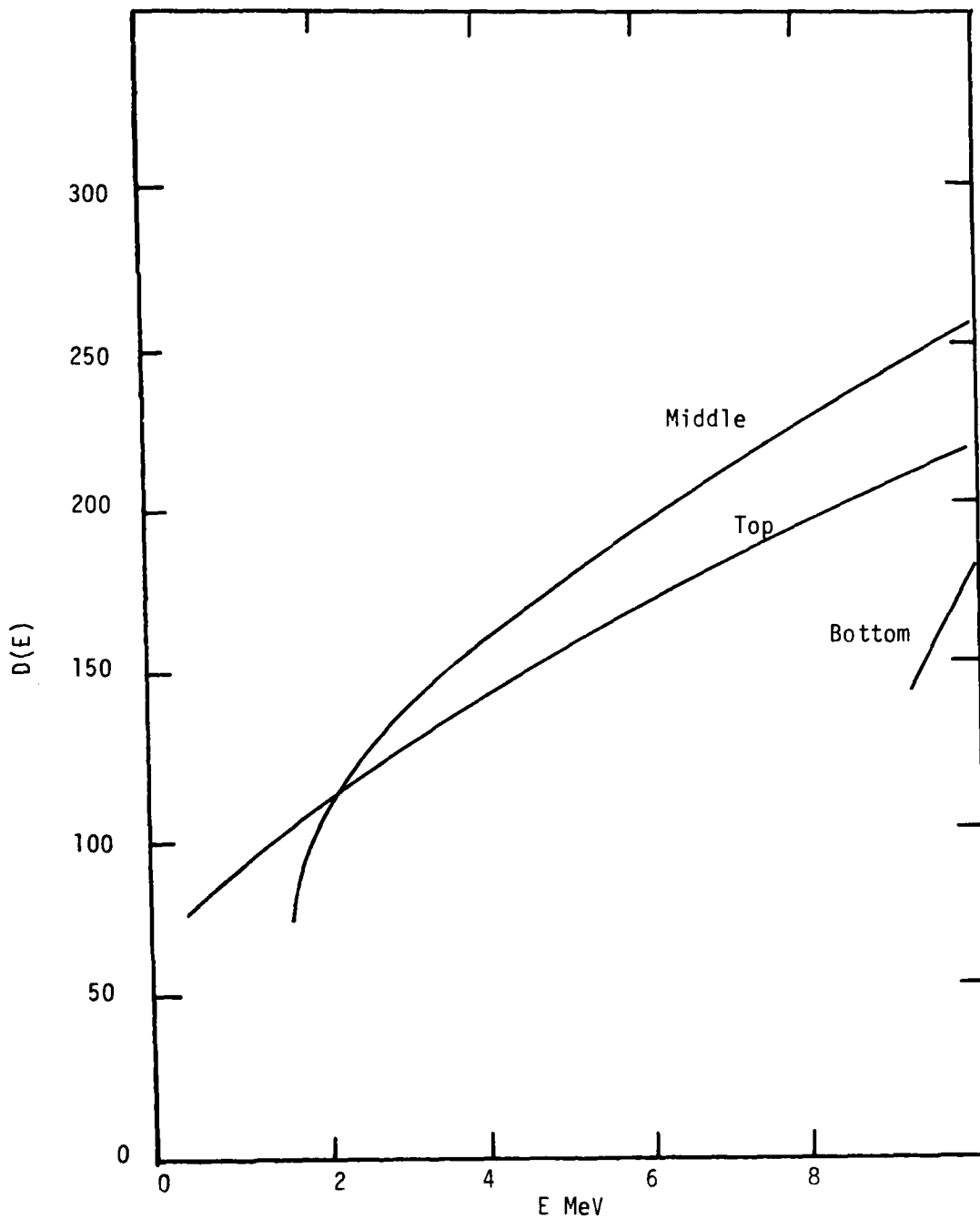
Figure 1.6.1   D(E) in Each Cell vs. Proton Energy for a
AlGaAs/GaAs/InGaAs Triple Junction Cell

47
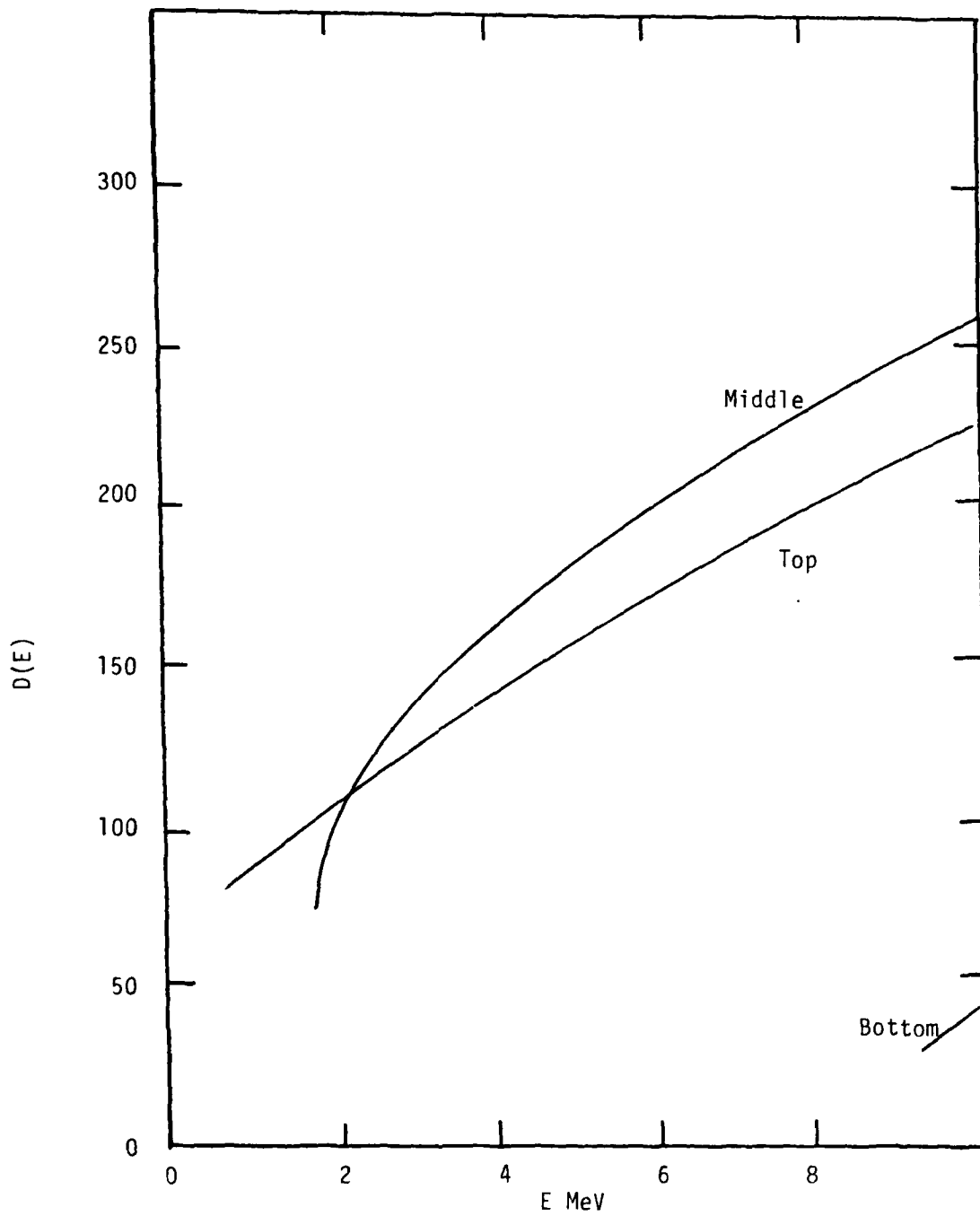
Figure 1.6.2 D(E) in Each Cell vs. Proton Energy for a
AlGaAs/GaAs/Ge Triple Junction Cell

48
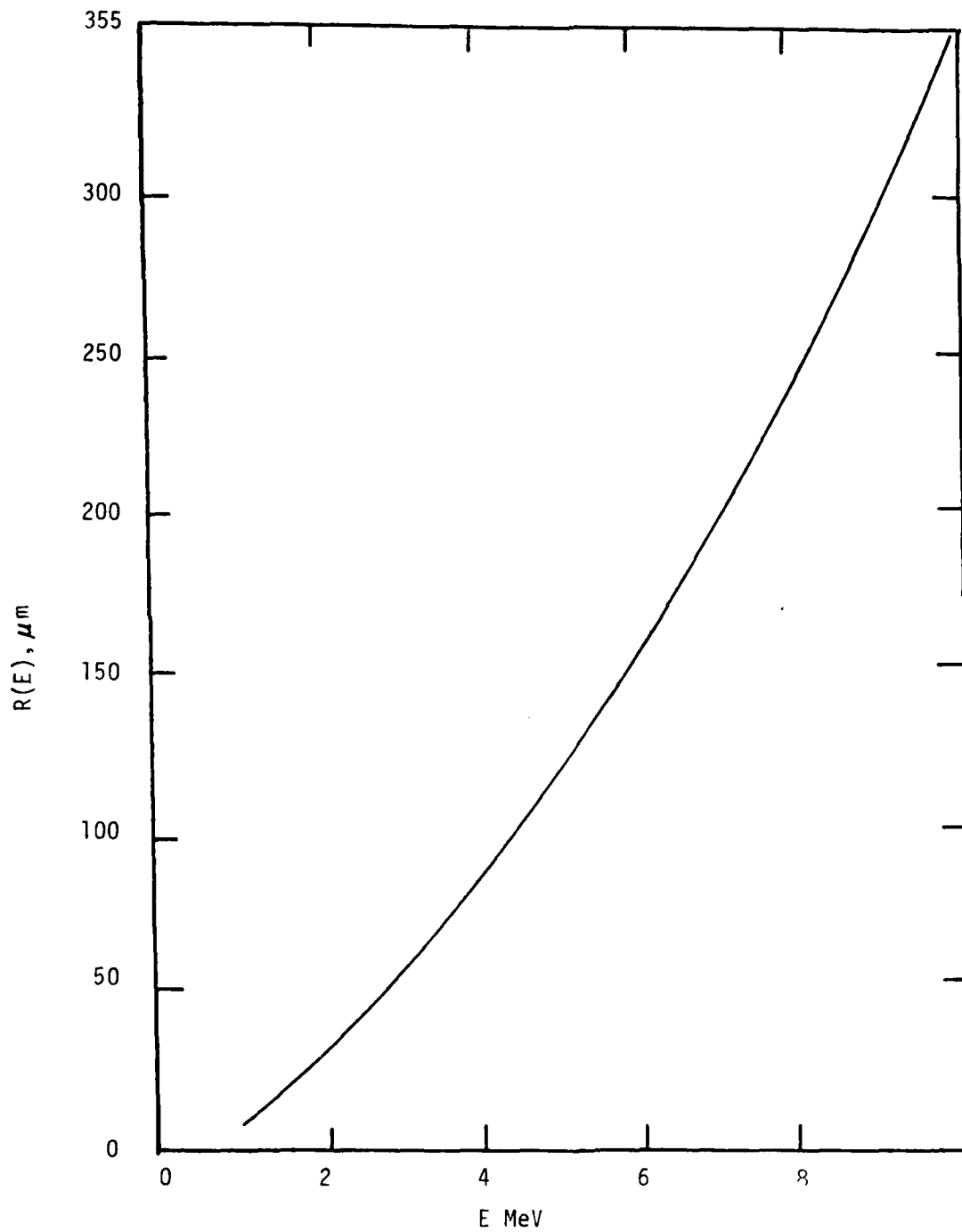
Figure 1.6.3   Penetration Depth vs. Proton Energy for a
AlGaAs/GaAs/InGaAs Triple Junction Cell
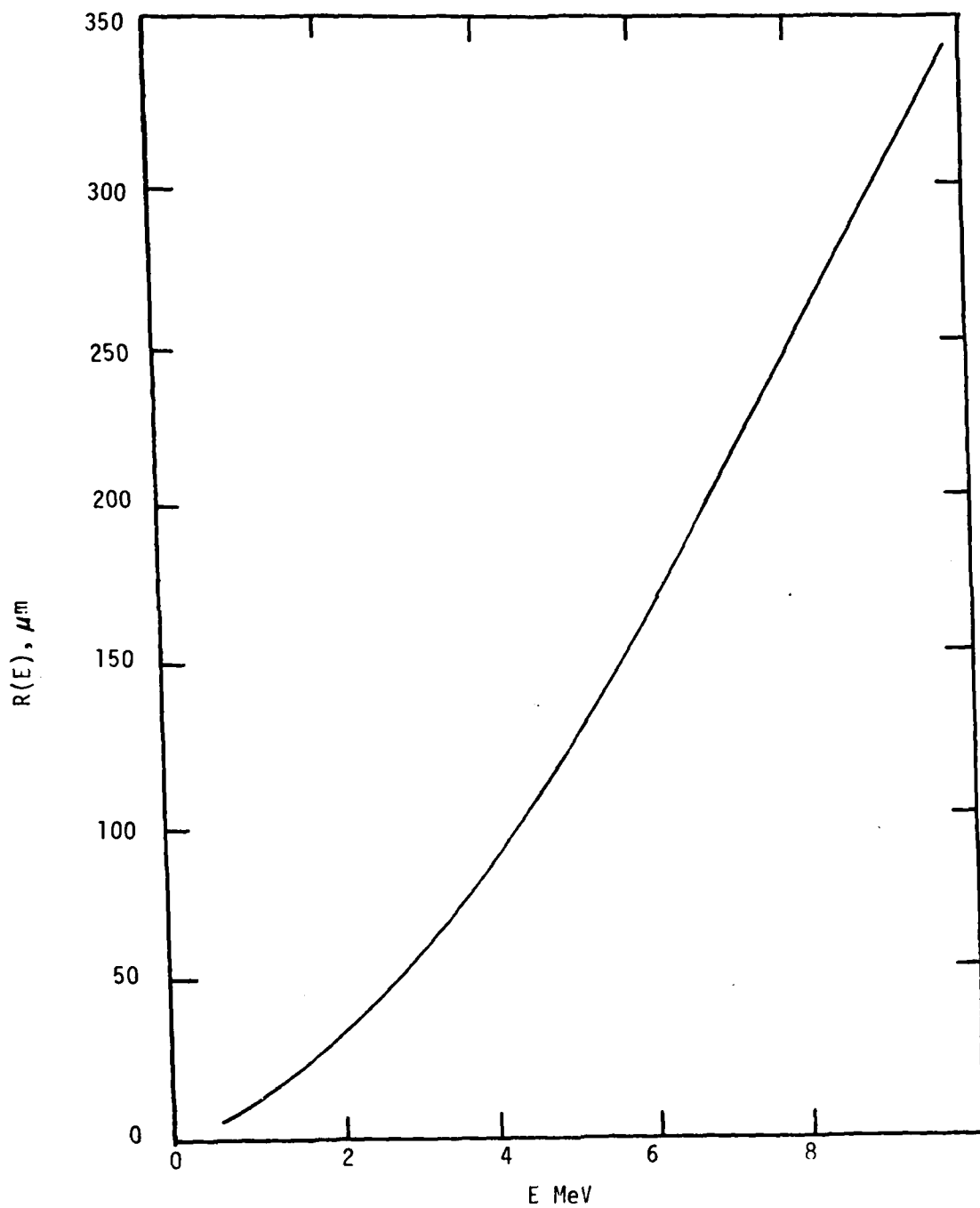
Figure 1.6.4   Penetration Depth vs. Proton energy for a
AlGaAs/GaAs/Ge Triple Junction Cell
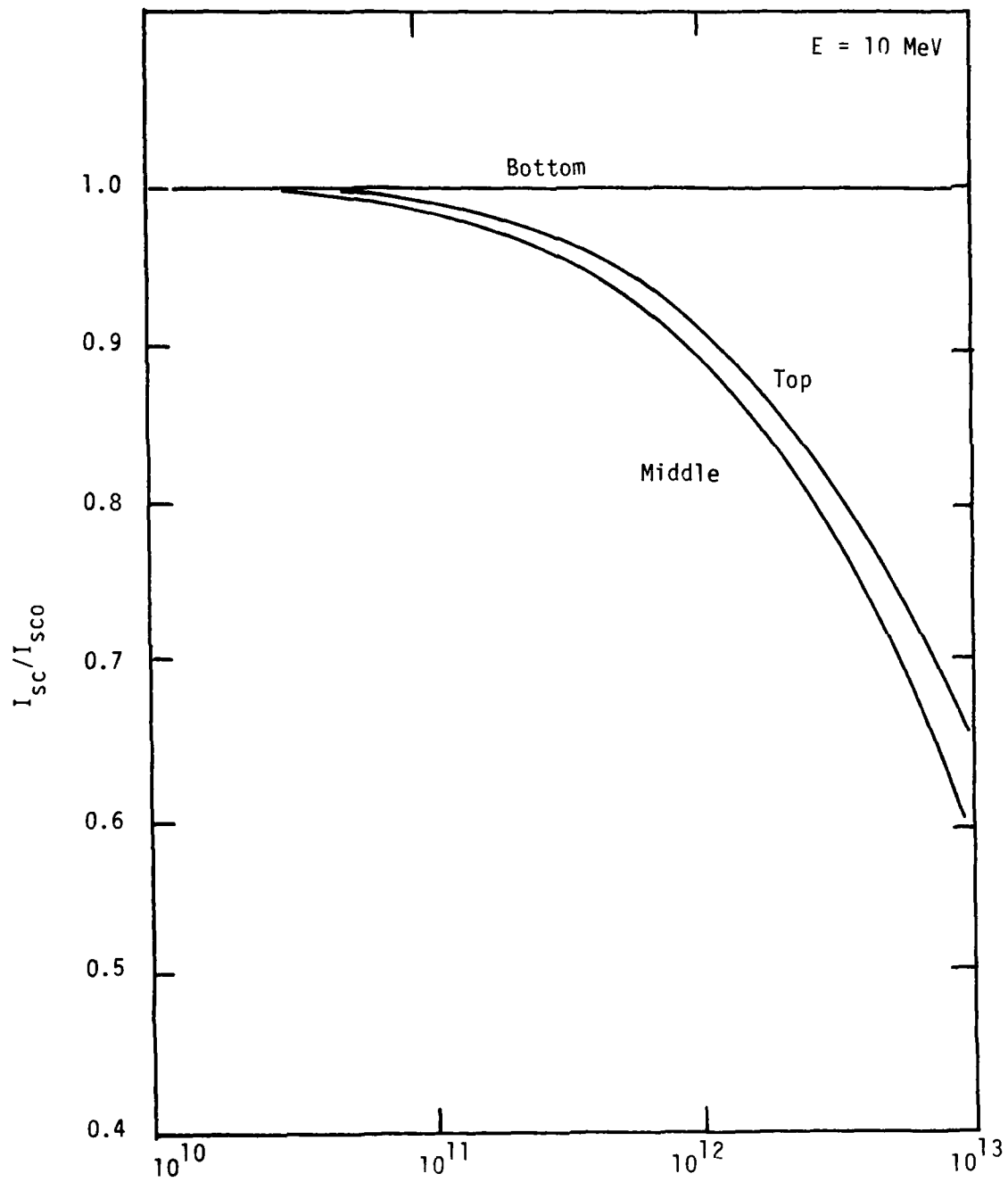
Figure 1.6.5 I_{sc} Degradation vs. Proton Fluences for a

AlGaAs/GaAs/InGaAs for Ge Triple Junction Cell
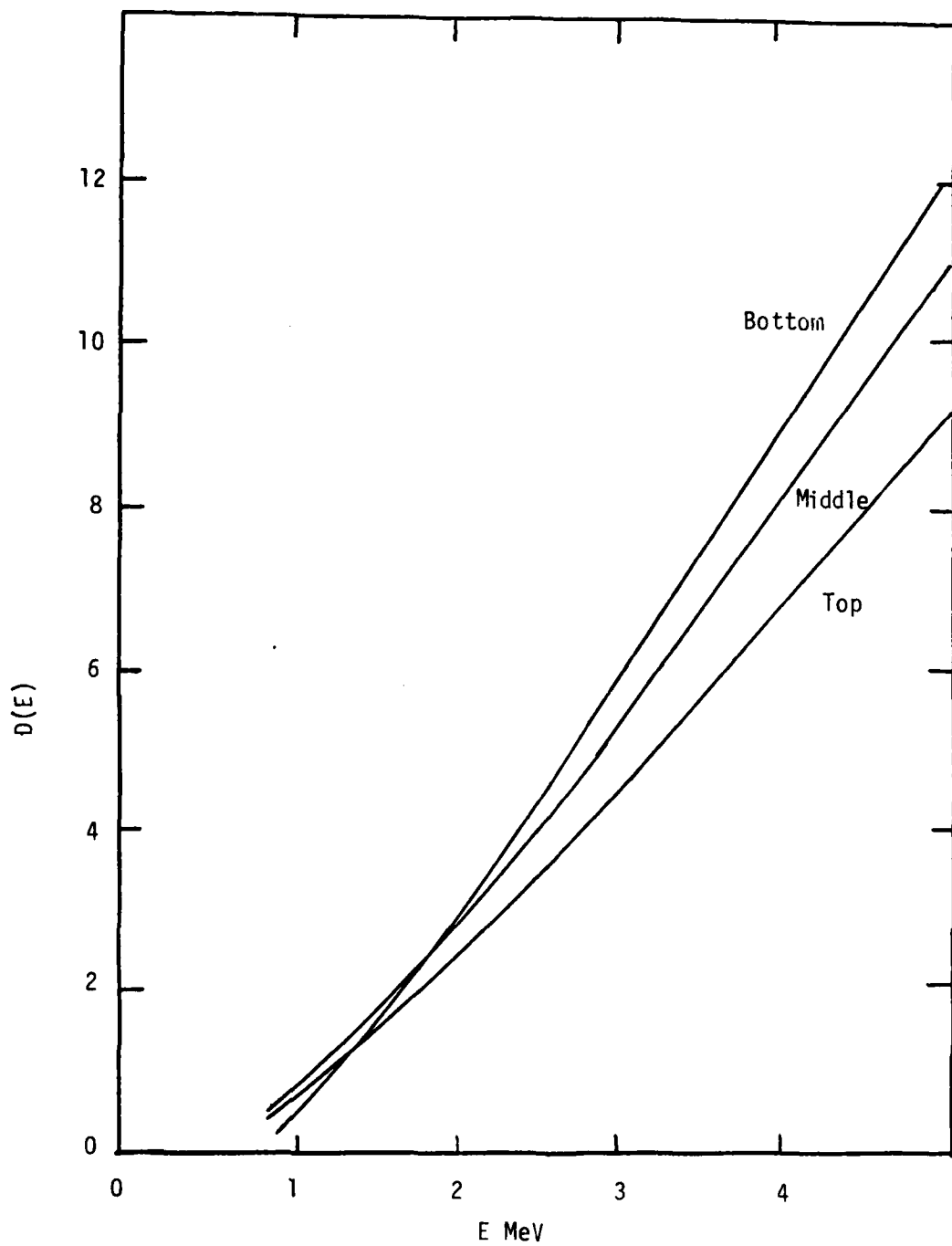
Figure 1.6.6   D(E) in Each Cell vs, Electron Energy for a
AlGaAs/GaAs/InGaAs Triple JunctionCell

52
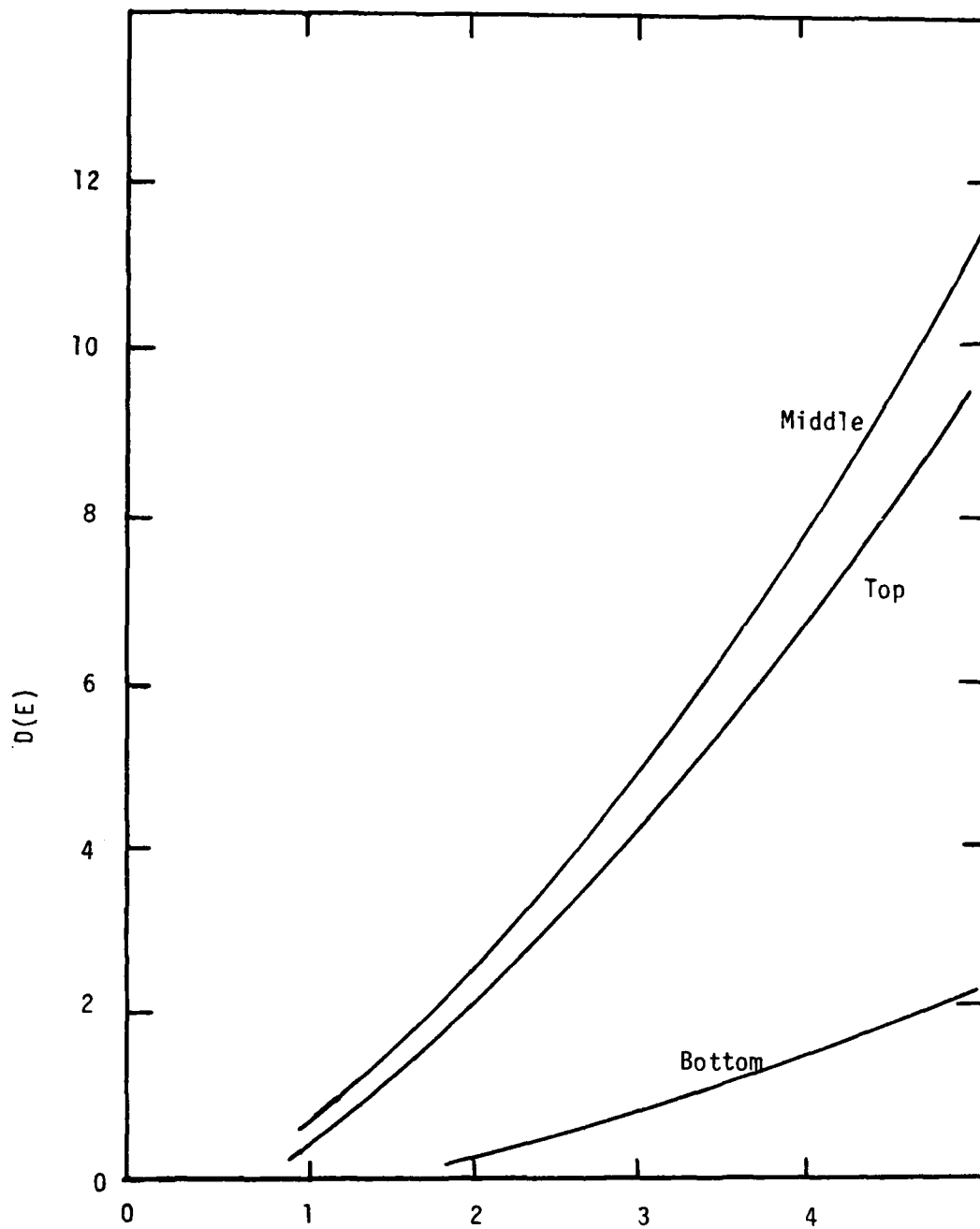
Figure 1.6.7 D(E) in Each Cell vs. Electron Energy for a
AlGaAs/GaAs/Ge Triple Junction Cell
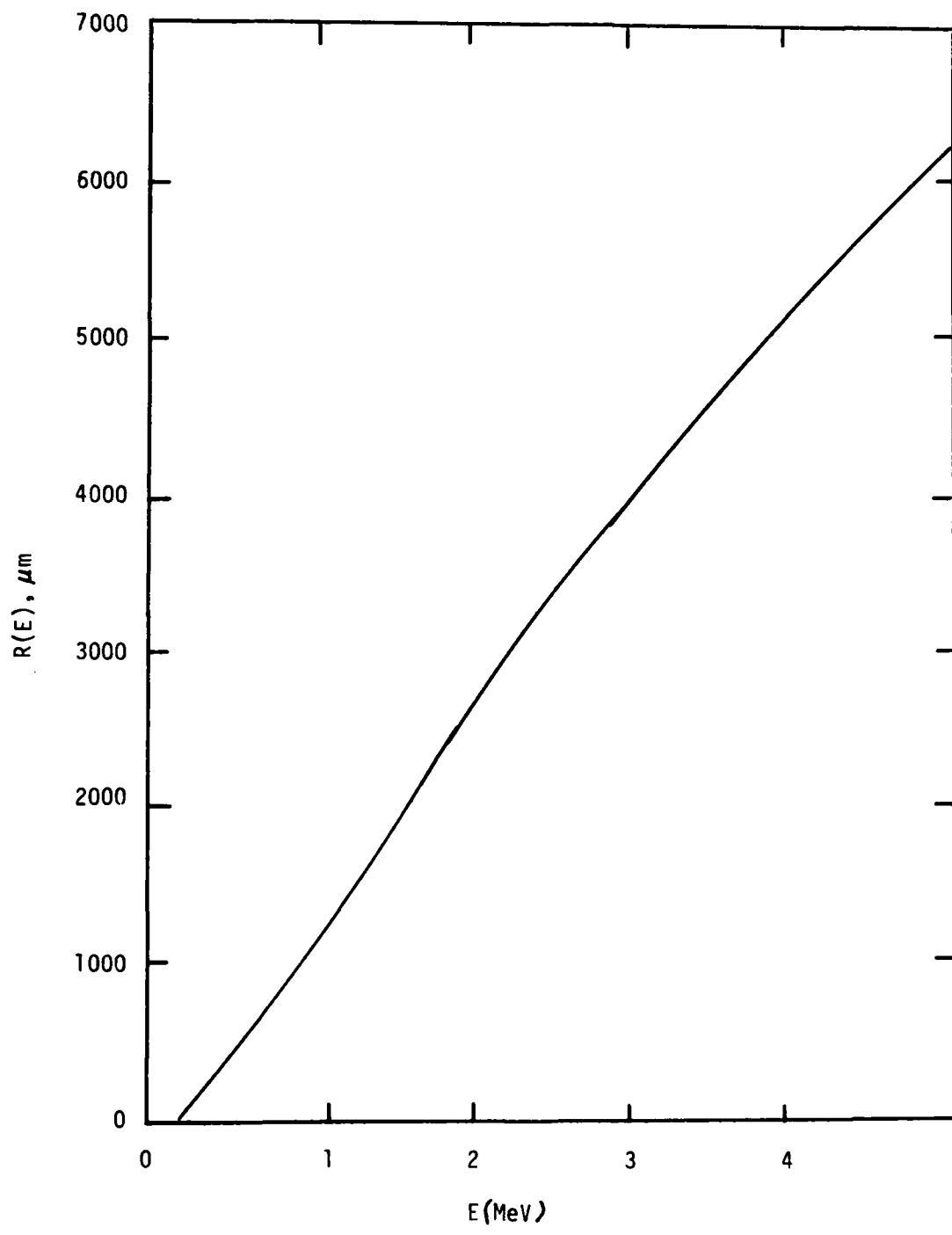
Figure 1.6.8 Penetration Depth vs. Electron Energy for a
AlGaAs/GaAs/InGaAs Triple Junction Cell

54
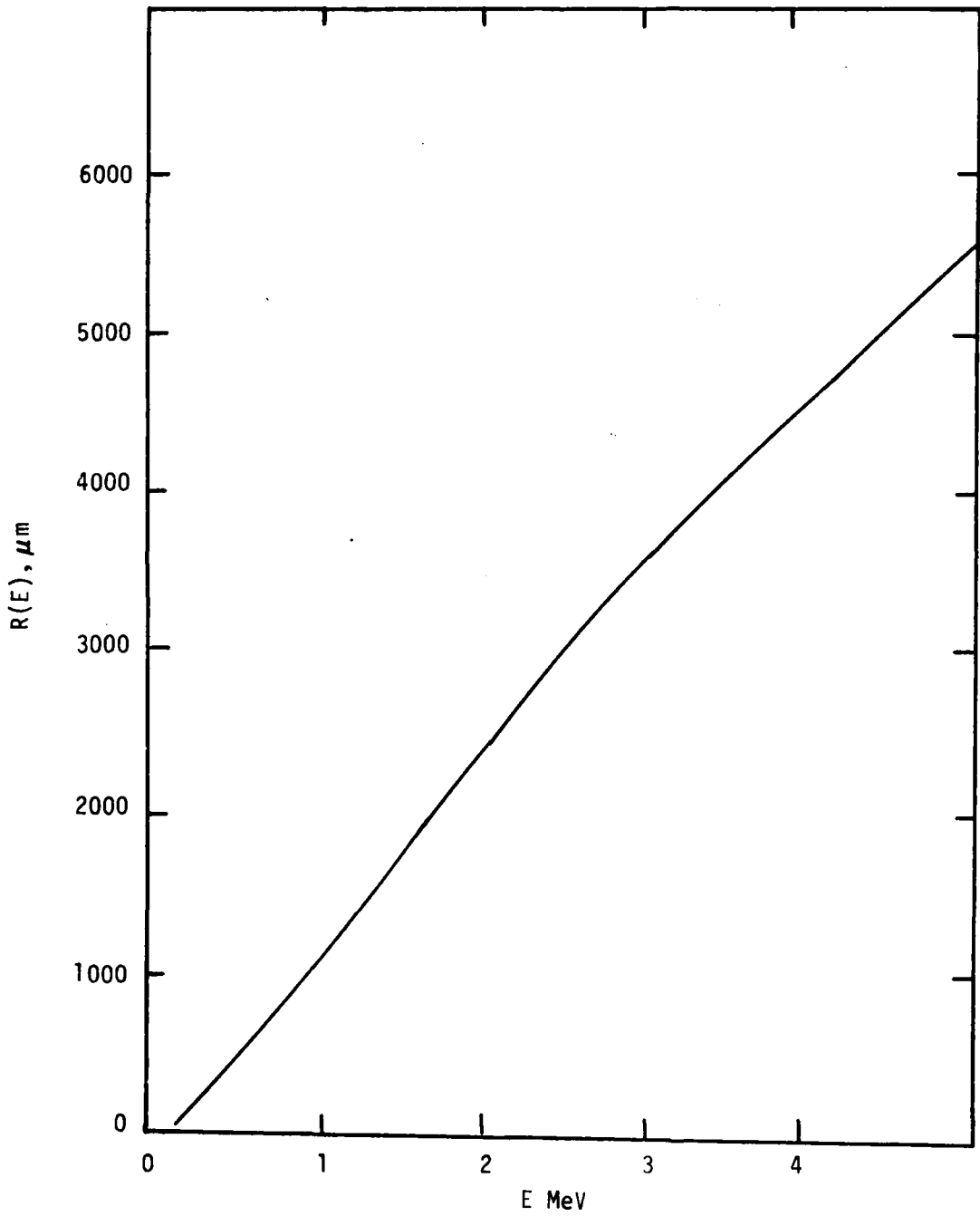
Figure 1.6.9   Penetration Depth vs. Electron Energy for a
AlGaAs/GaAs/Ge Triple Junction Cell
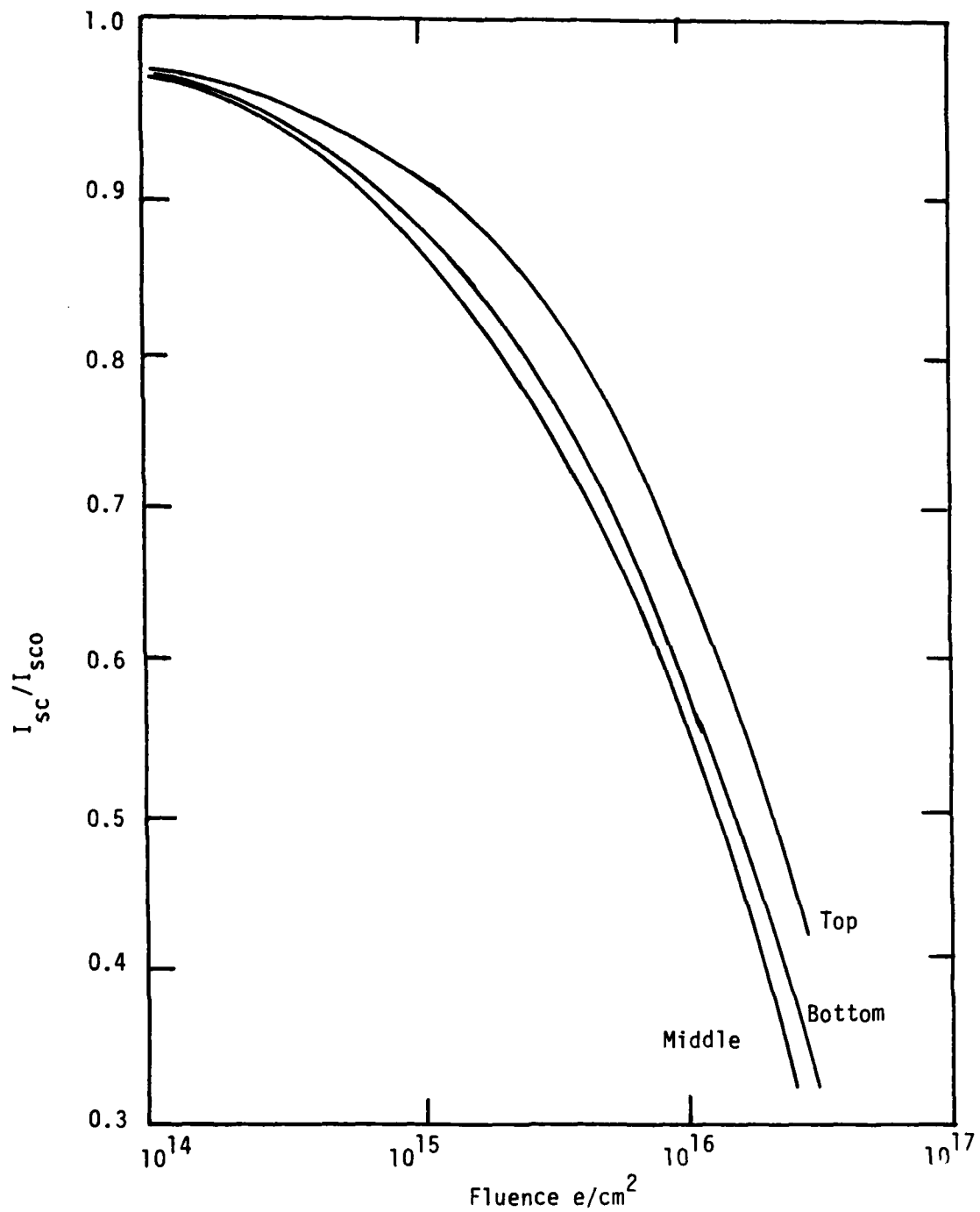
Figure 1.6.10 I_{sc} Degradation vs. Electron and 1 MeV Energy for a
AlGaAs/GaAs/InGaAs Triple Junction Cell

56
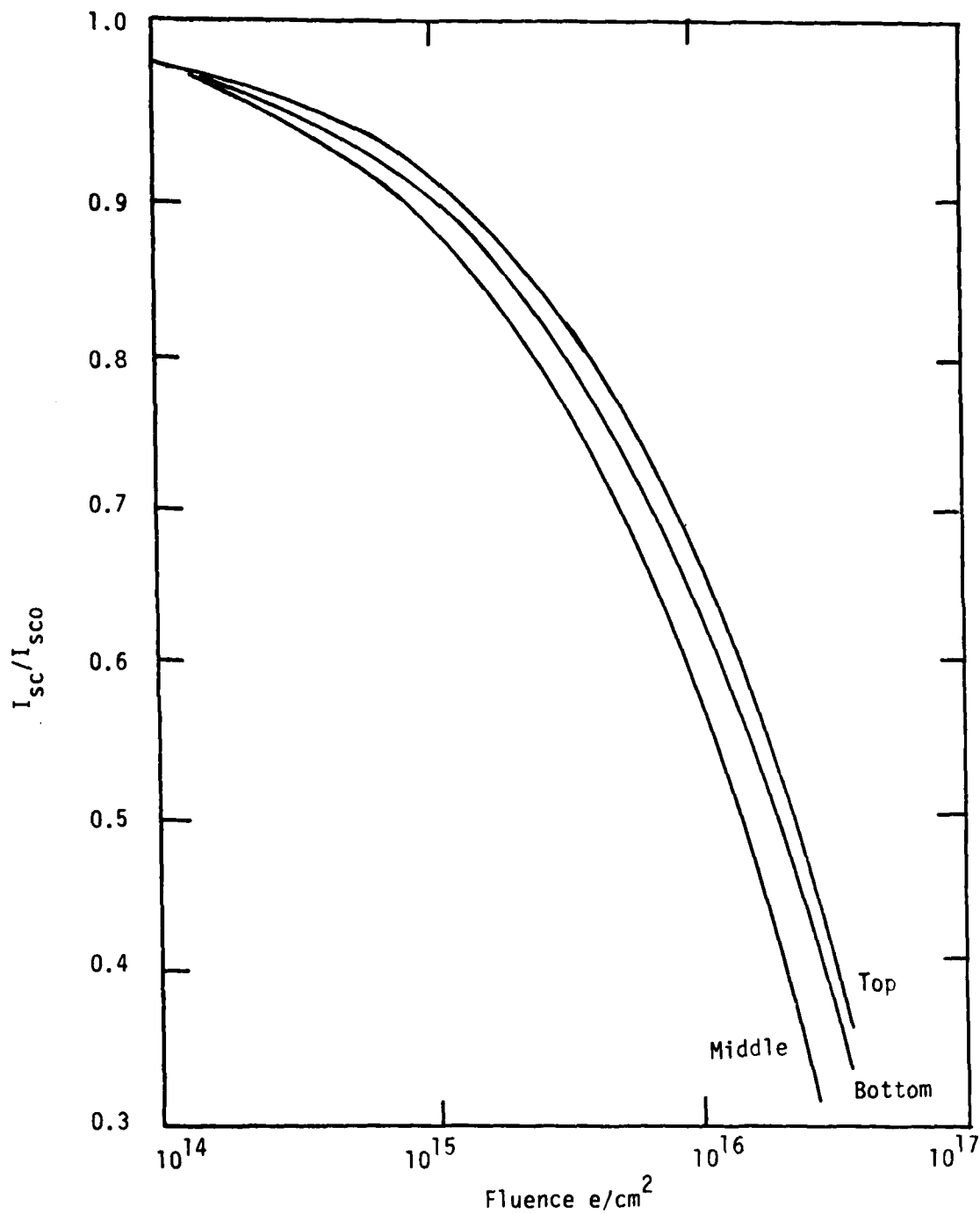
Figure 1.6.11 I_{sc} Degradation vs. electron fluence and 1 MeV energy
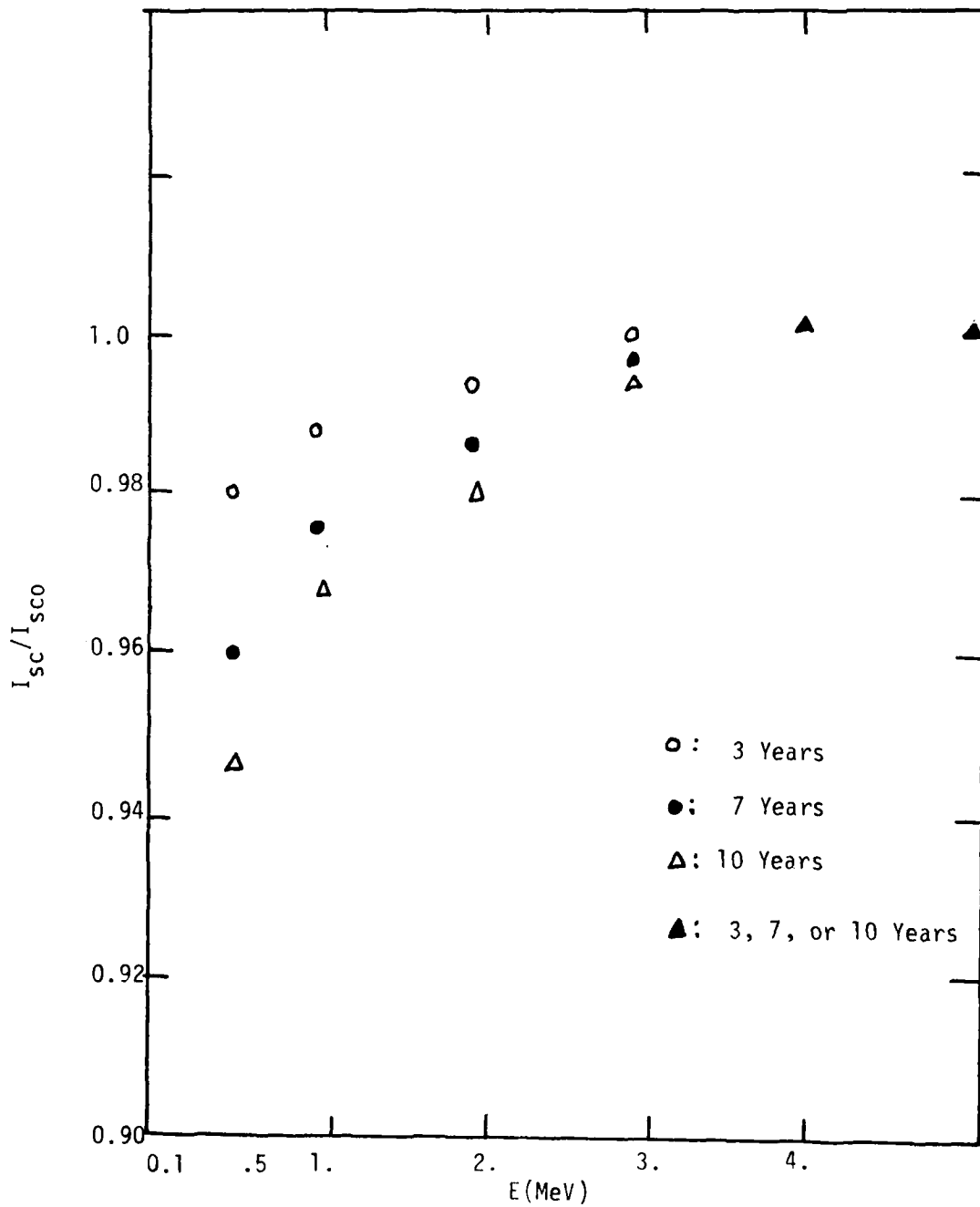for a AlGaAs/GaAs/Ge triple junction cell

57
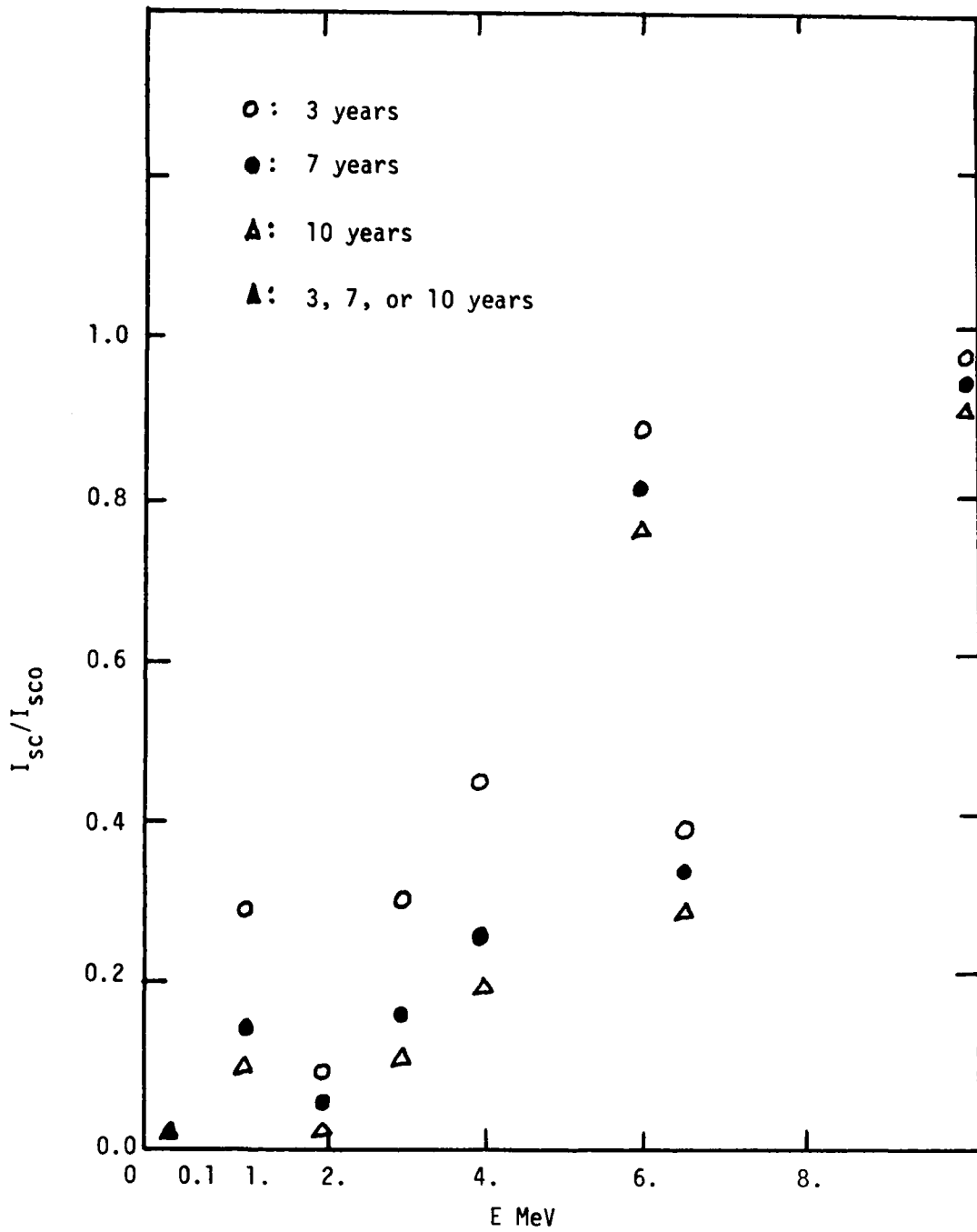
Figure 1.7.1 I_{sc} Degradation vs. Proton Fluence and Energy with 3, 7
and 10 Years Exposure for a AlGaAs in Triple Junction
Cell
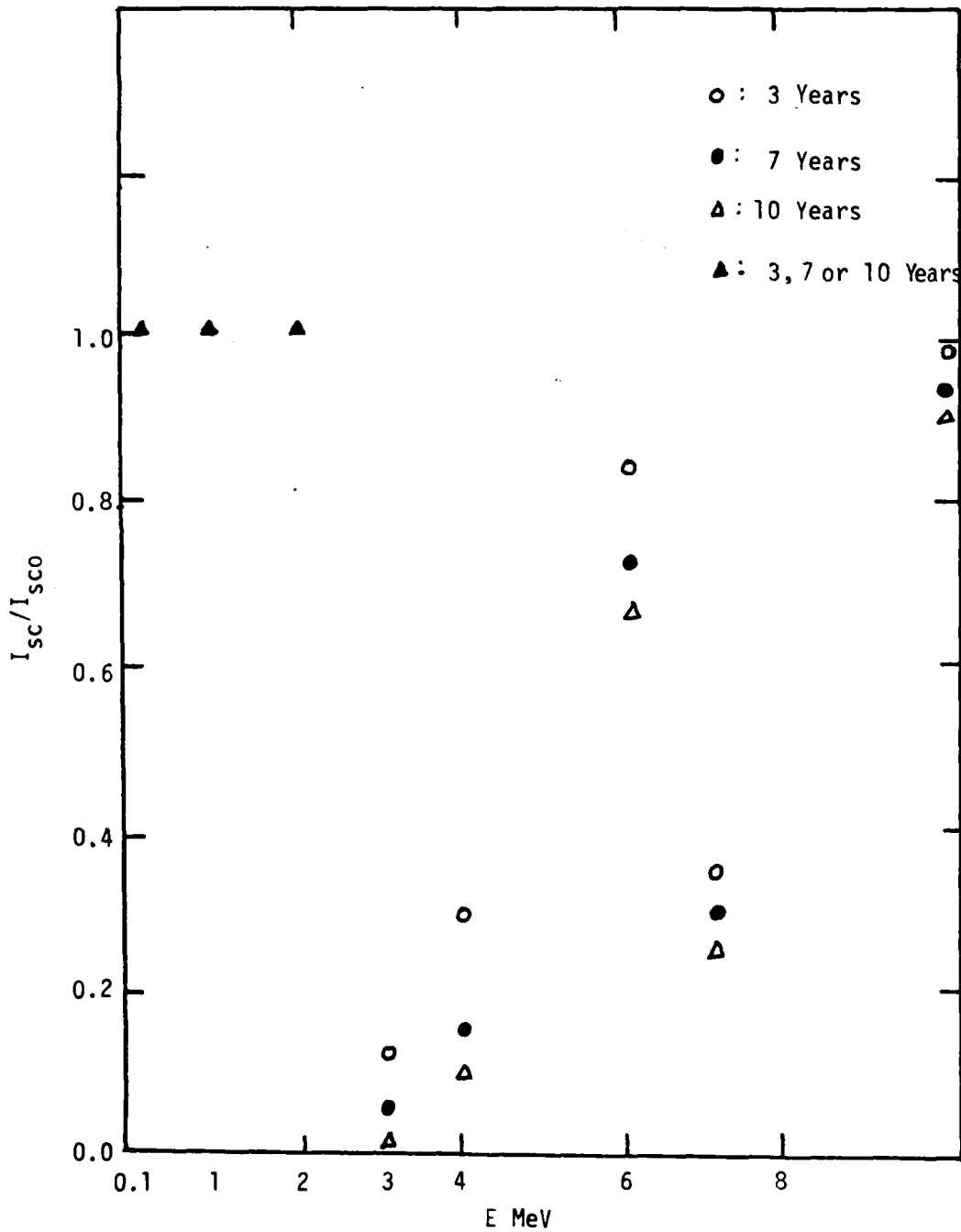
Figure 1.7.2 I_{sc} Degradation vs. Proton Fluence and Energy with 3, 7, and 10 Years Exposure for GaAs in a Triple Junction Cell
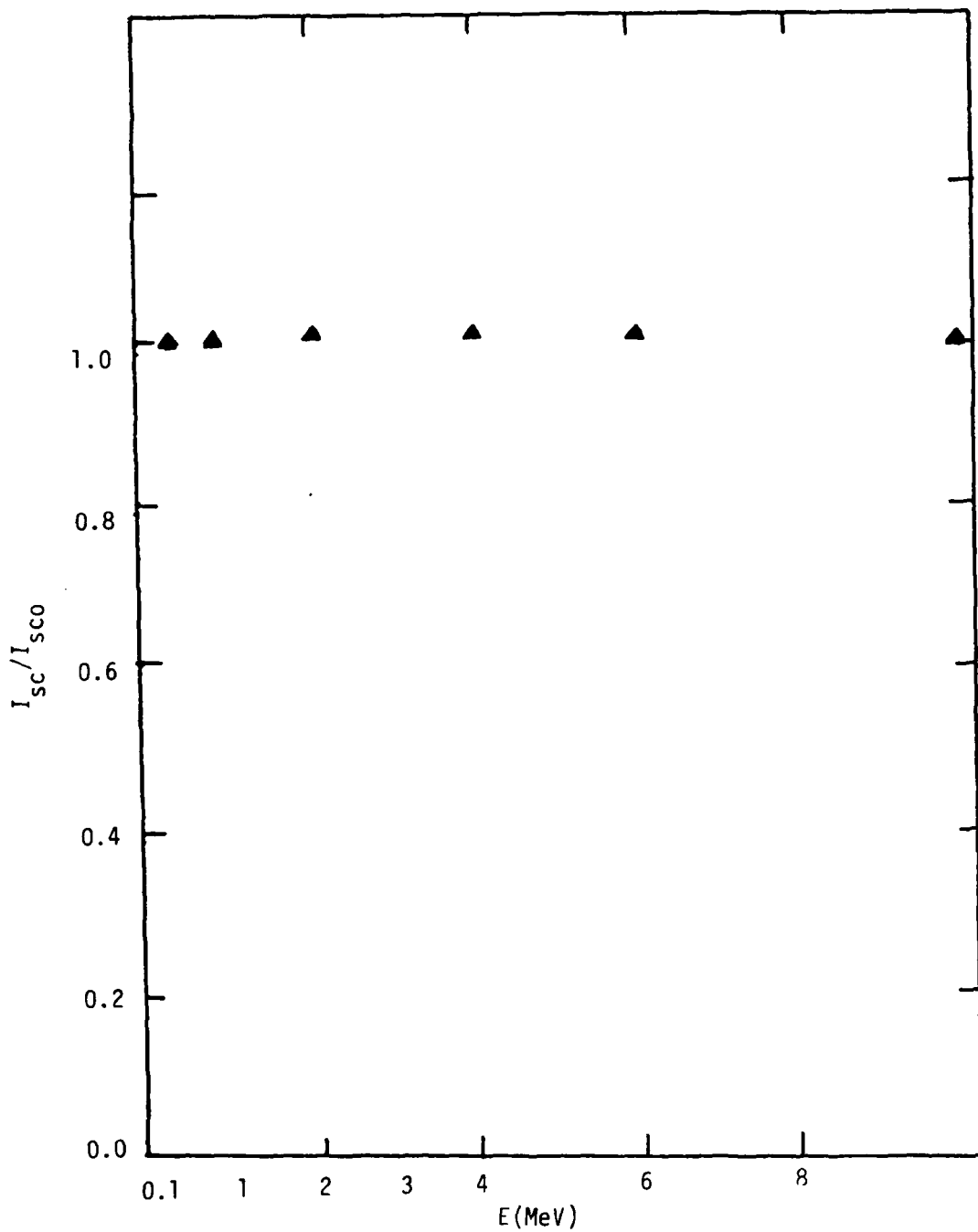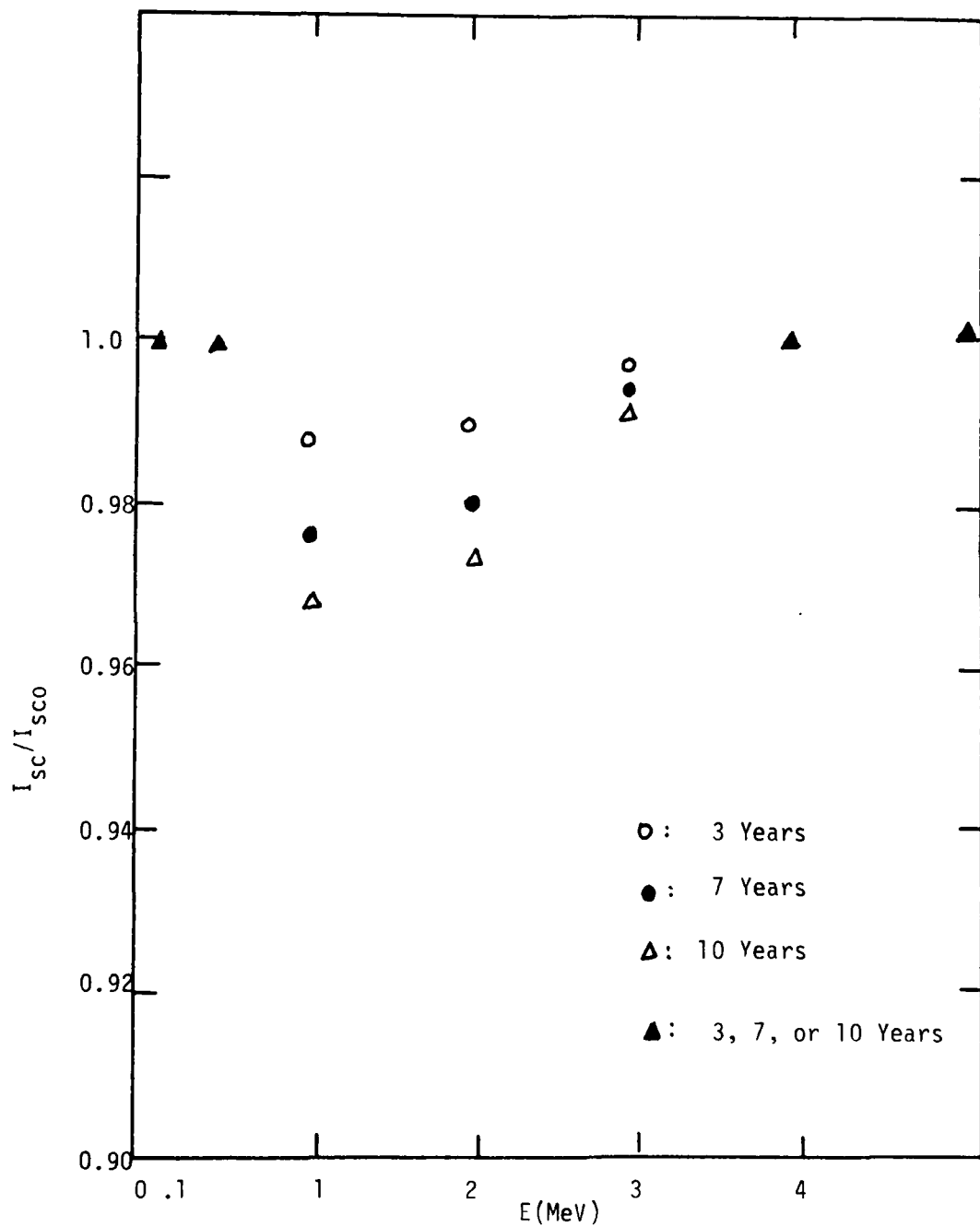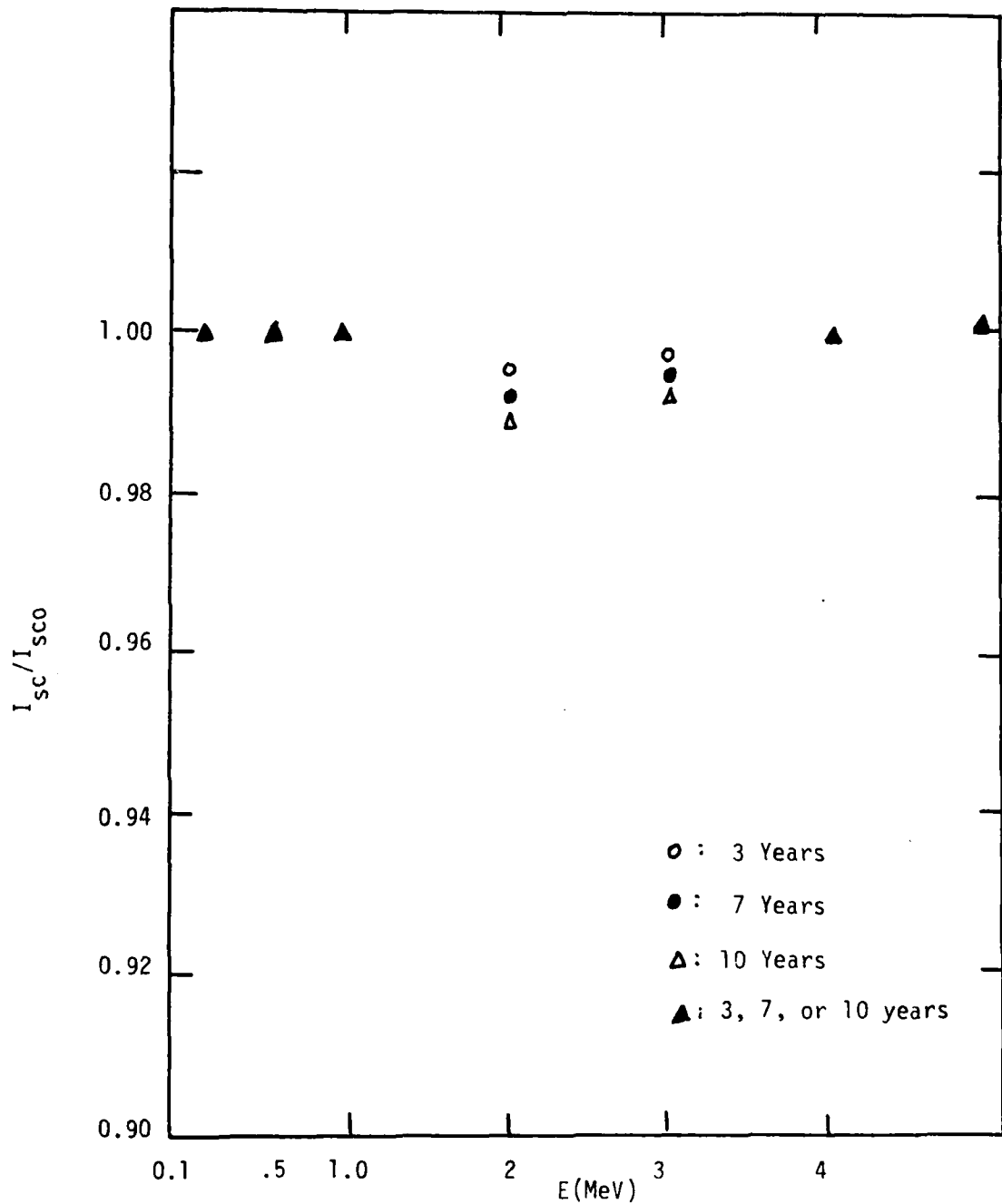
Figure 1.7.3 I_{sc} Degradation vs. Proton Fluence and Energy with 3,7 and 10 Years Exposure for InGaAs or Ge in a Triple Junction Cell
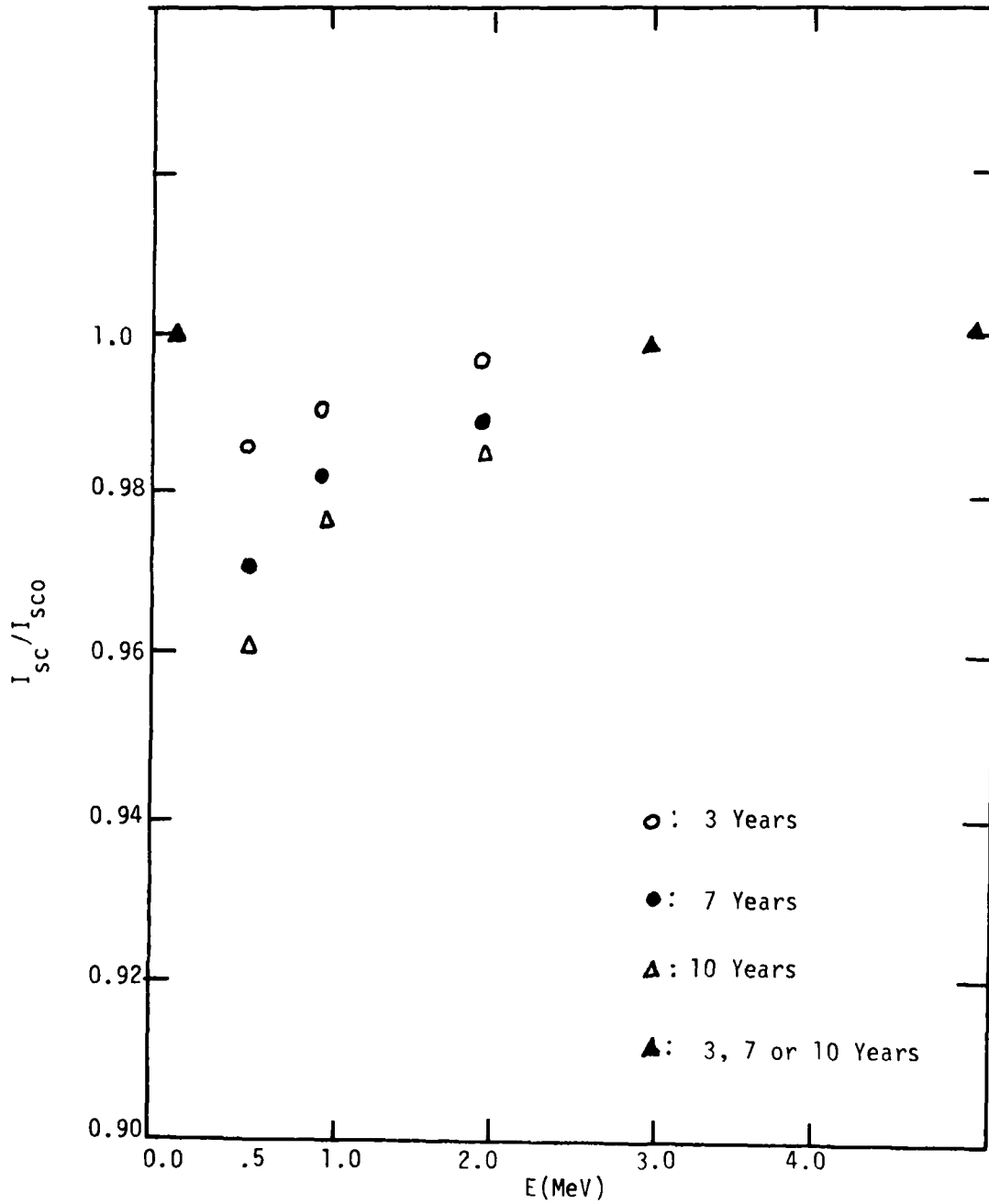
Figure 1.7.4 I_{sc} Degradation vs. Electron Fluence and Energy with 3, 7, 10 Years Exposure for AlGaAs in a Triple Junction Cell

Figure 1.7.5 I_{sc} Degradation vs. Electron Fluence and Energy
with 3, 7, and 10 Years Exposure for GaAs in a
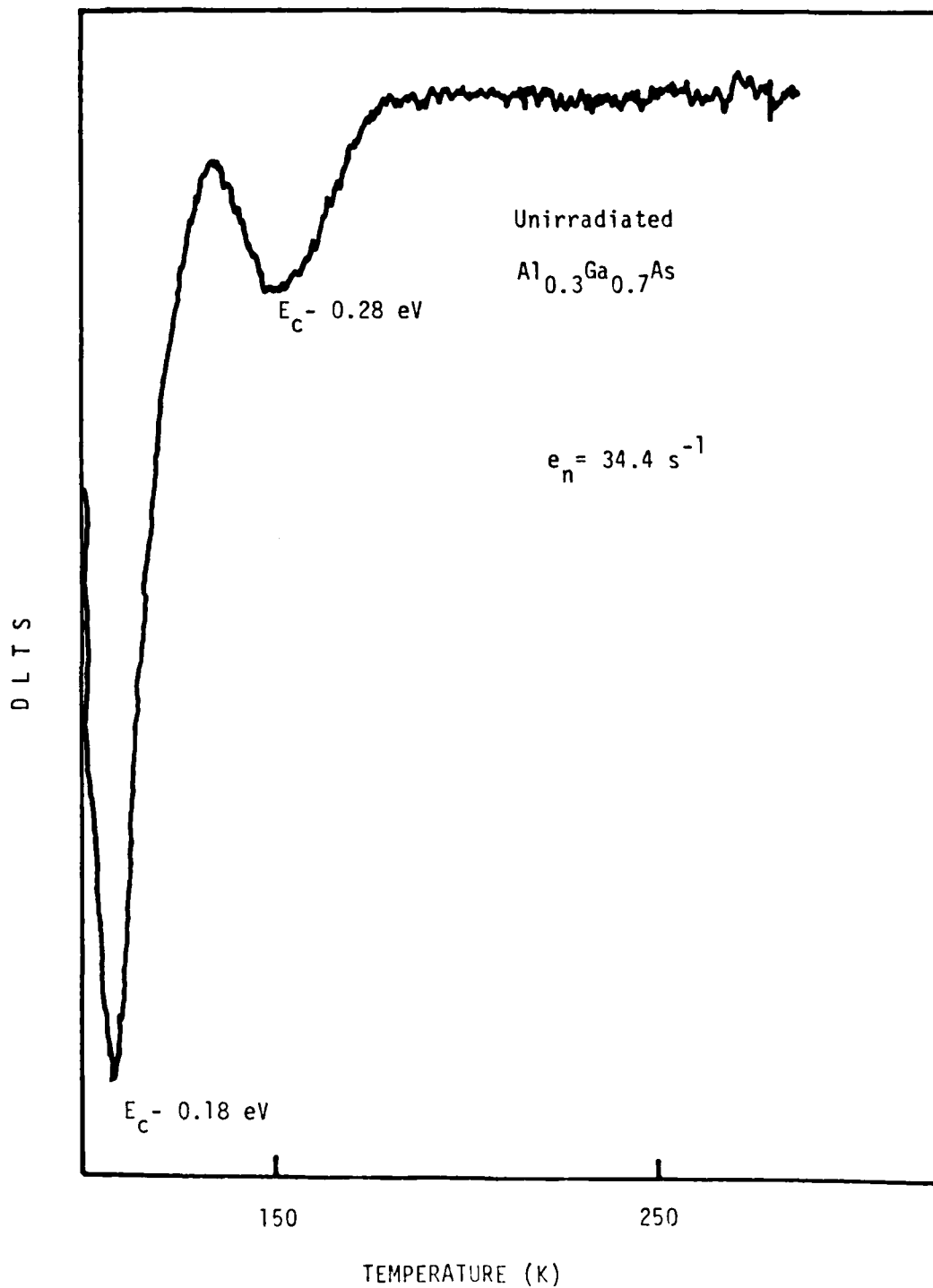Triple Junction Cell

Figure 1.7.6 I_{sc} Degradation vs. Electron Fluence and Energy with 3, 7 and 10 Years for InGaAs in a Triple Juncion Cell

Figure 1.7.7 I_{sc} Degradation vs. Electron Fluence and Energy with 3, 7, and 10 Years Exposure for Ge in a Triple Junction Cell

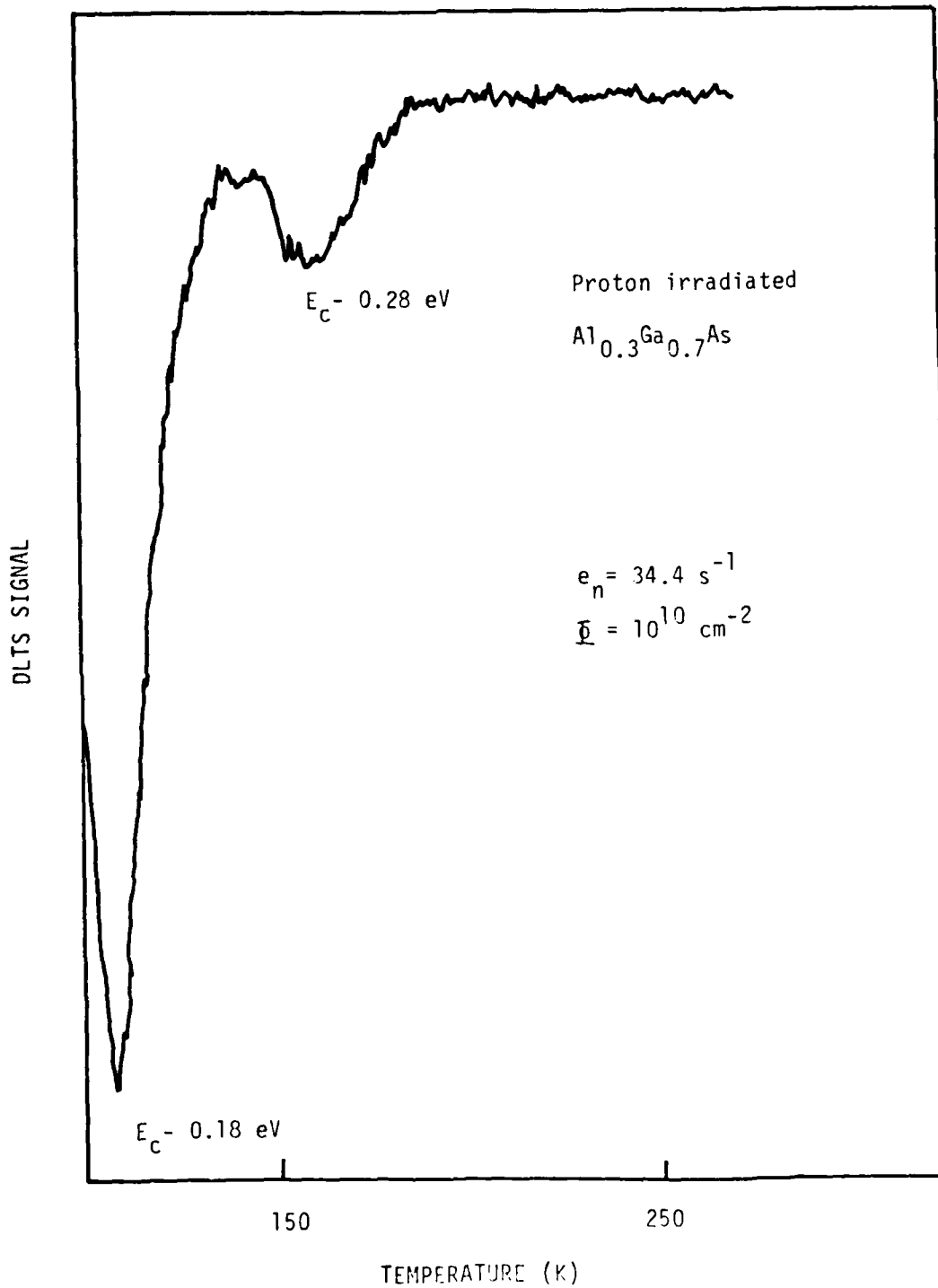Figure 2.3.1 DLTS scan of electron trap for the unirradiated $Al_{0.3}Ga_{0.7}As$ solar cell.

Figure 2.3.2 DLTS scan of electron trap for the 200 KeV proton irradiated $Al_{0.3}Ga_{0.7}As$ for the fluence of 10^{10} cm^{-2}.

66

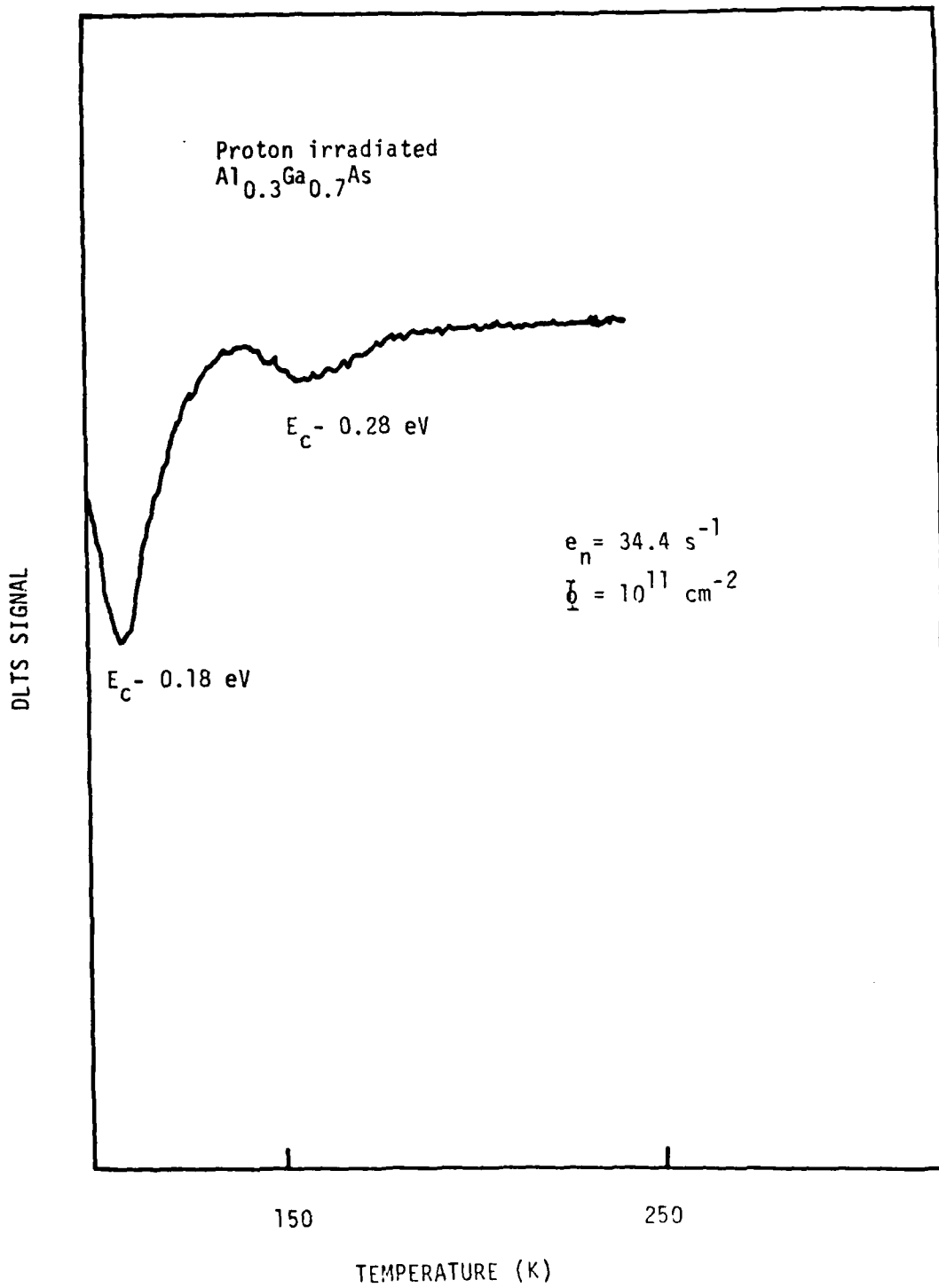Figure 2.3.3 DLTS scan of electron trap for the 200 KeV proton
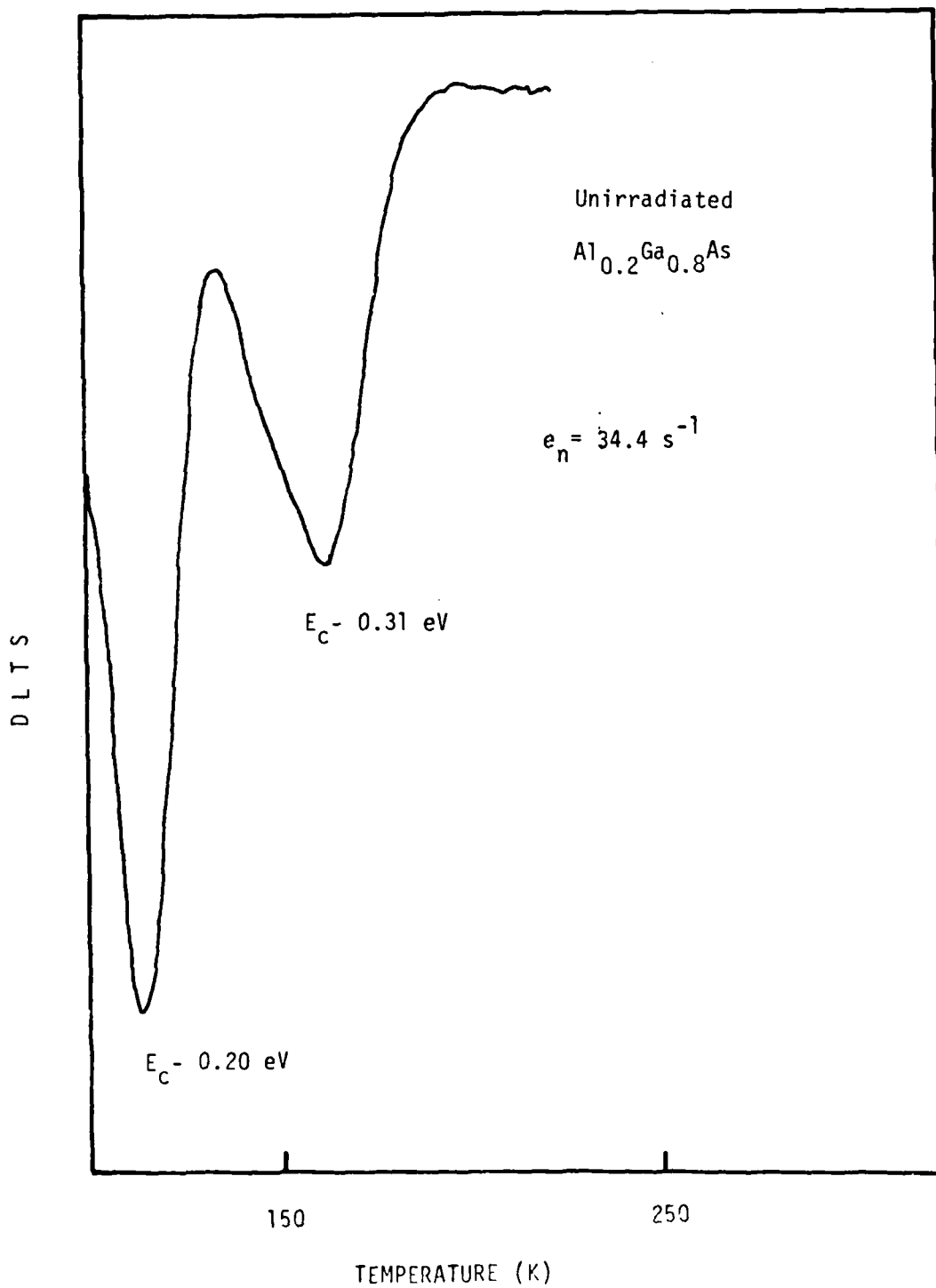irradiated $Al_{0.3}Ga_{0.7}As$ for the fluence of 10^{11} cm^{-2}.

Figure 2.3.4 DLTS scan of electron trap for the unirradiated
$Al_{0.2}Ga_{0.8}As$.

Figure 2.3.5 DLTS scan of electron trap for the 200 KeV proton irradiated $Al_{0.2}Ga_{0.8}As$ for the fluence of 10^{10} cm^{-2}.

69
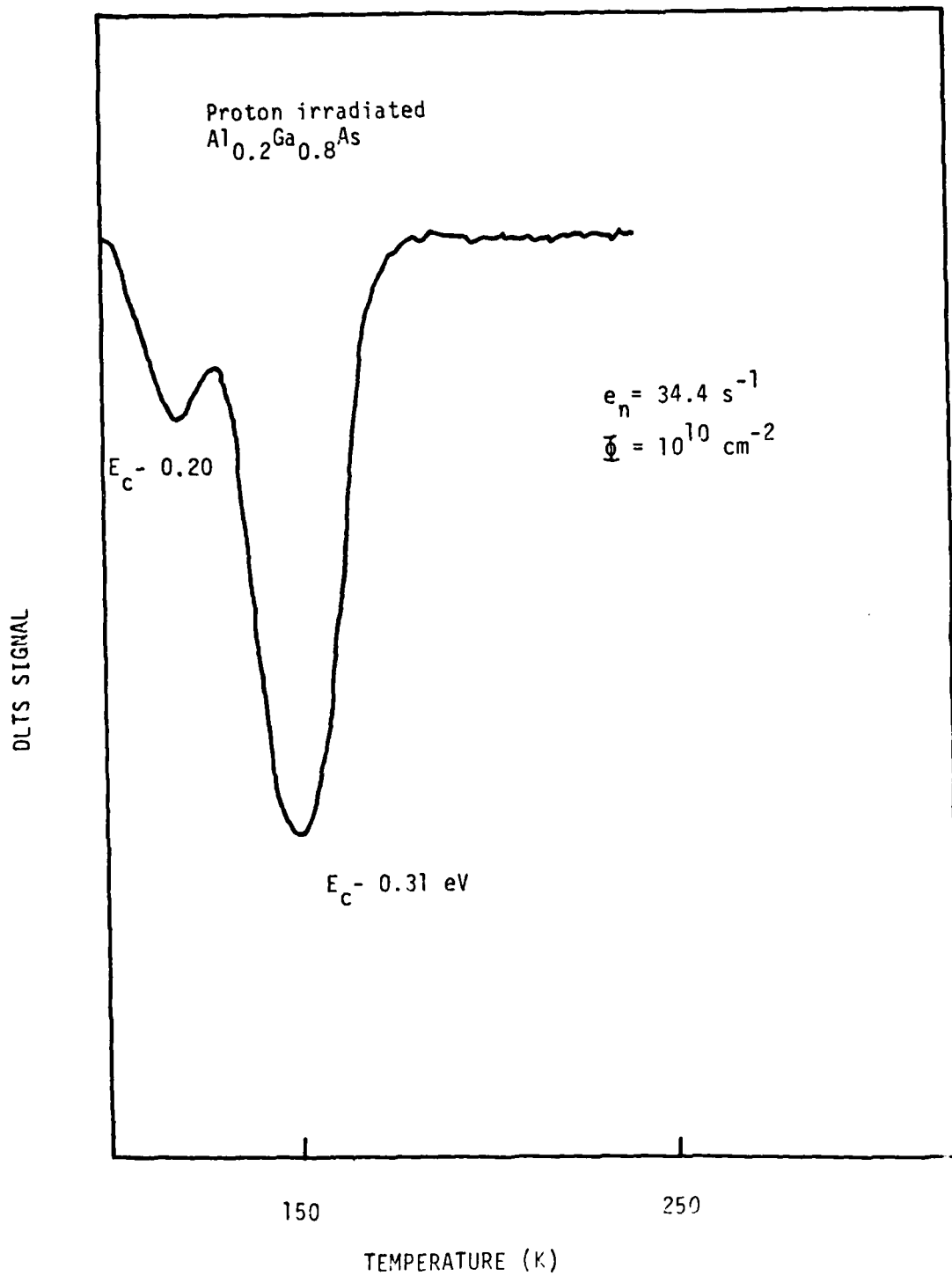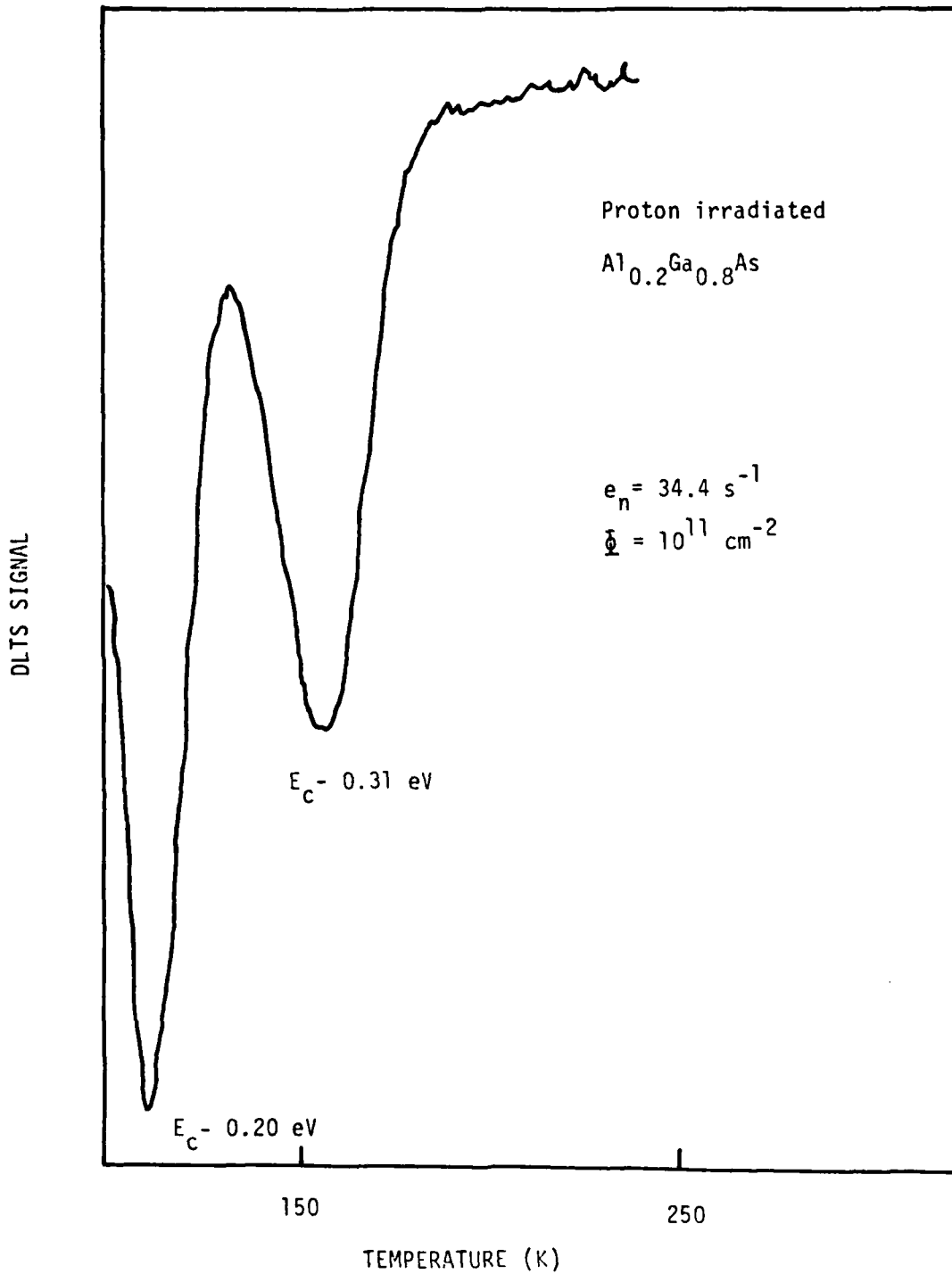
Figure 2.3.6 DLTS scan of electron trap for the 200 KeV proton irradiated $Al_{0.2}Ga_{0.8}As$ for the fluence of 10^{11} cm^{-2}.

70

Figure 2.3.7   C-V curves in $Al_{0.3}Ga_{0.7}As$ p/n junction cells irradiated by 200 KeV protons of different fluences.
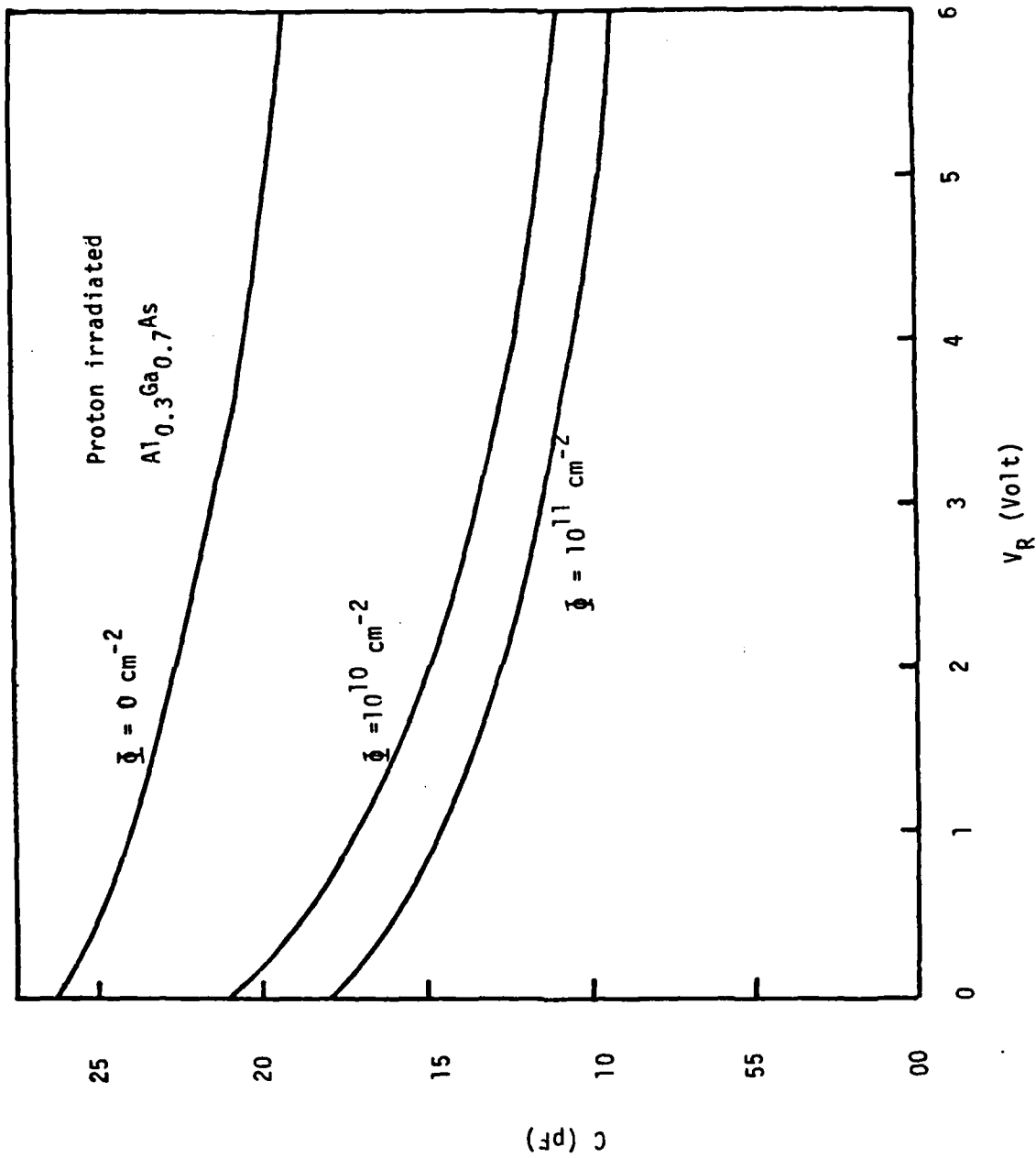
71

Figure 2.3.8   C-V curves in $Al_{0.2}Ga_{0.8}As$ p/n junction cells irradiated by 200 KeV protons of different fluences.
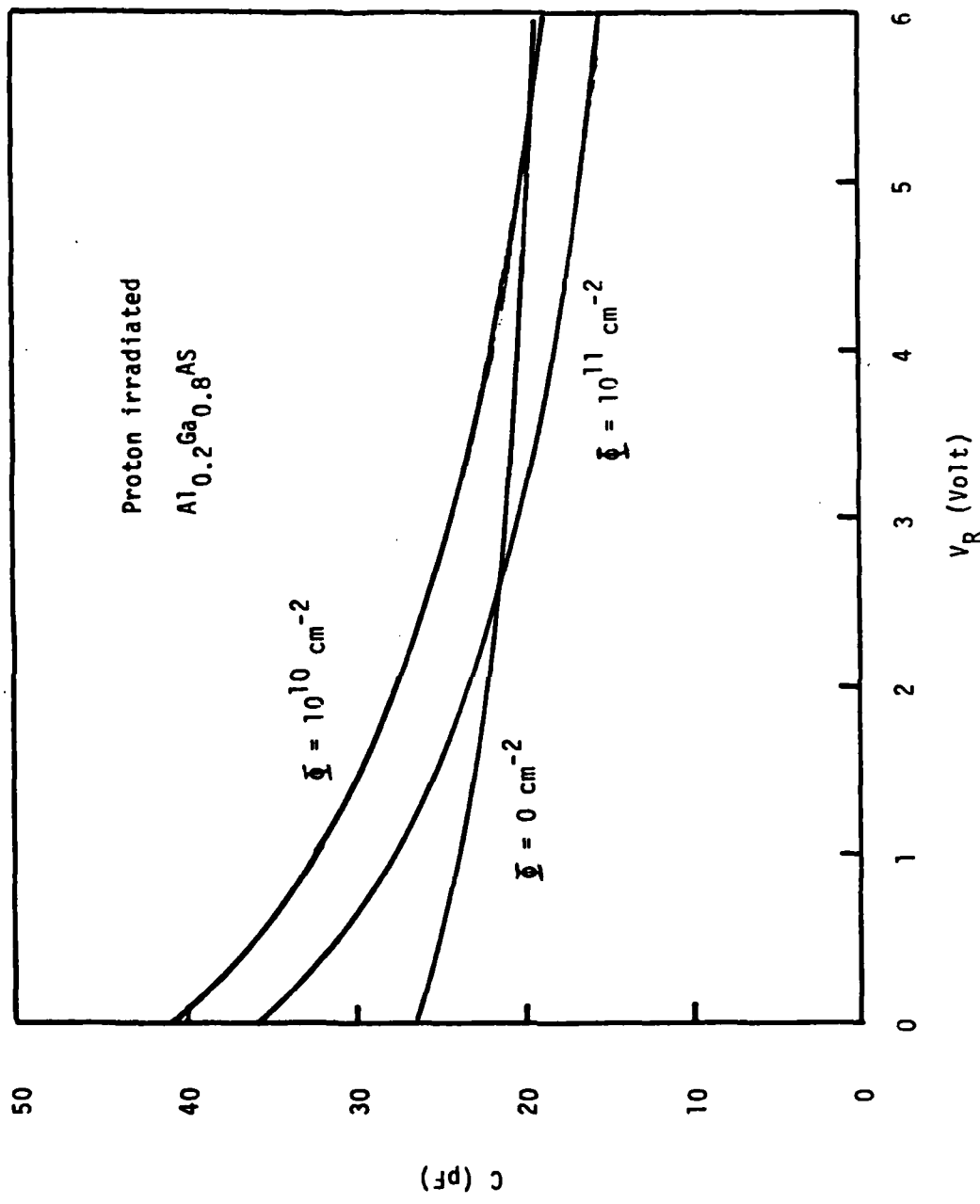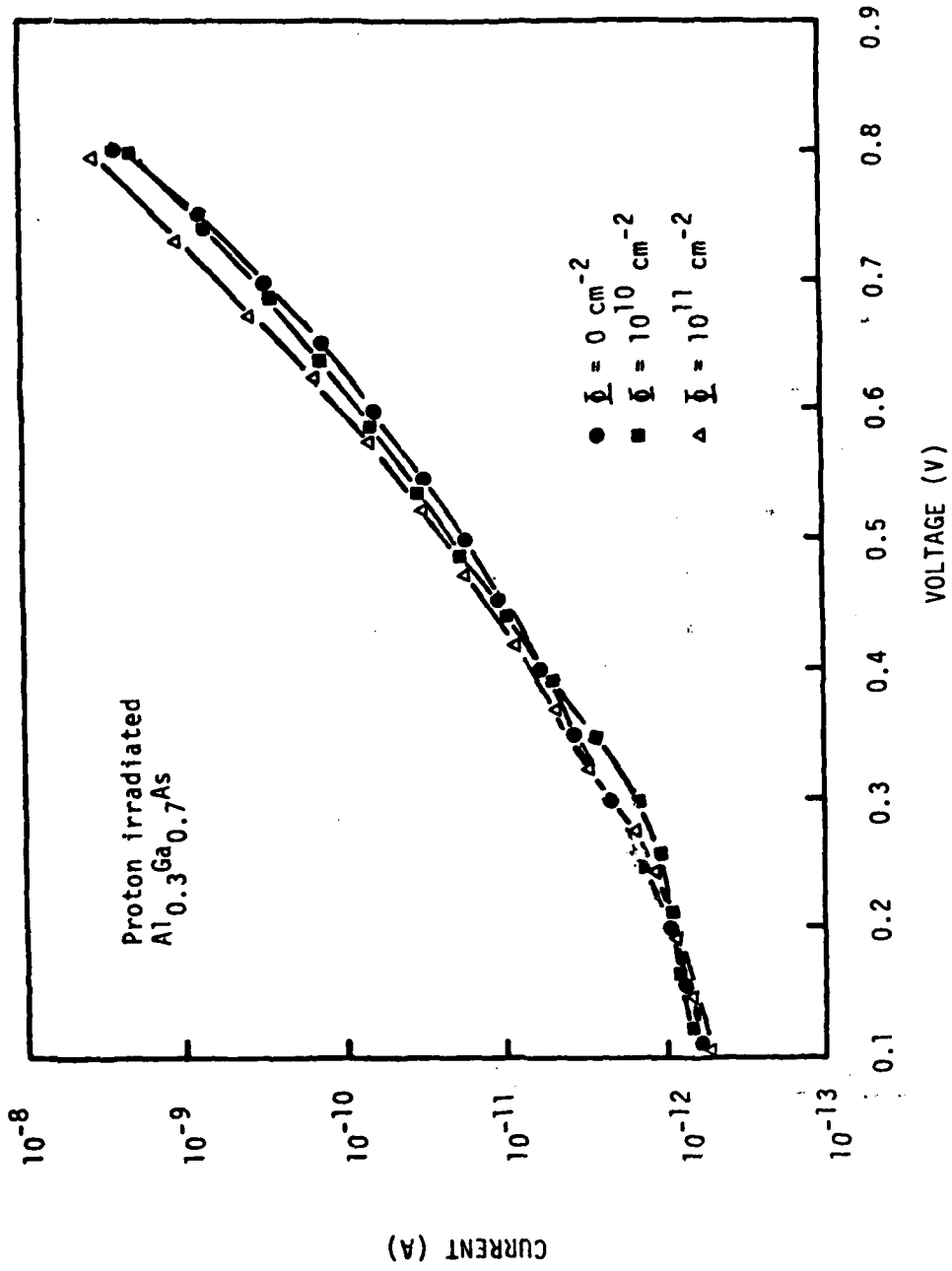
Figure 2.3.9 Forward I-V curves in $Al_{0.3}Ga_{0.7}As$ p/n junction cells irradiated by 200 KeV protons of different fluences.

73
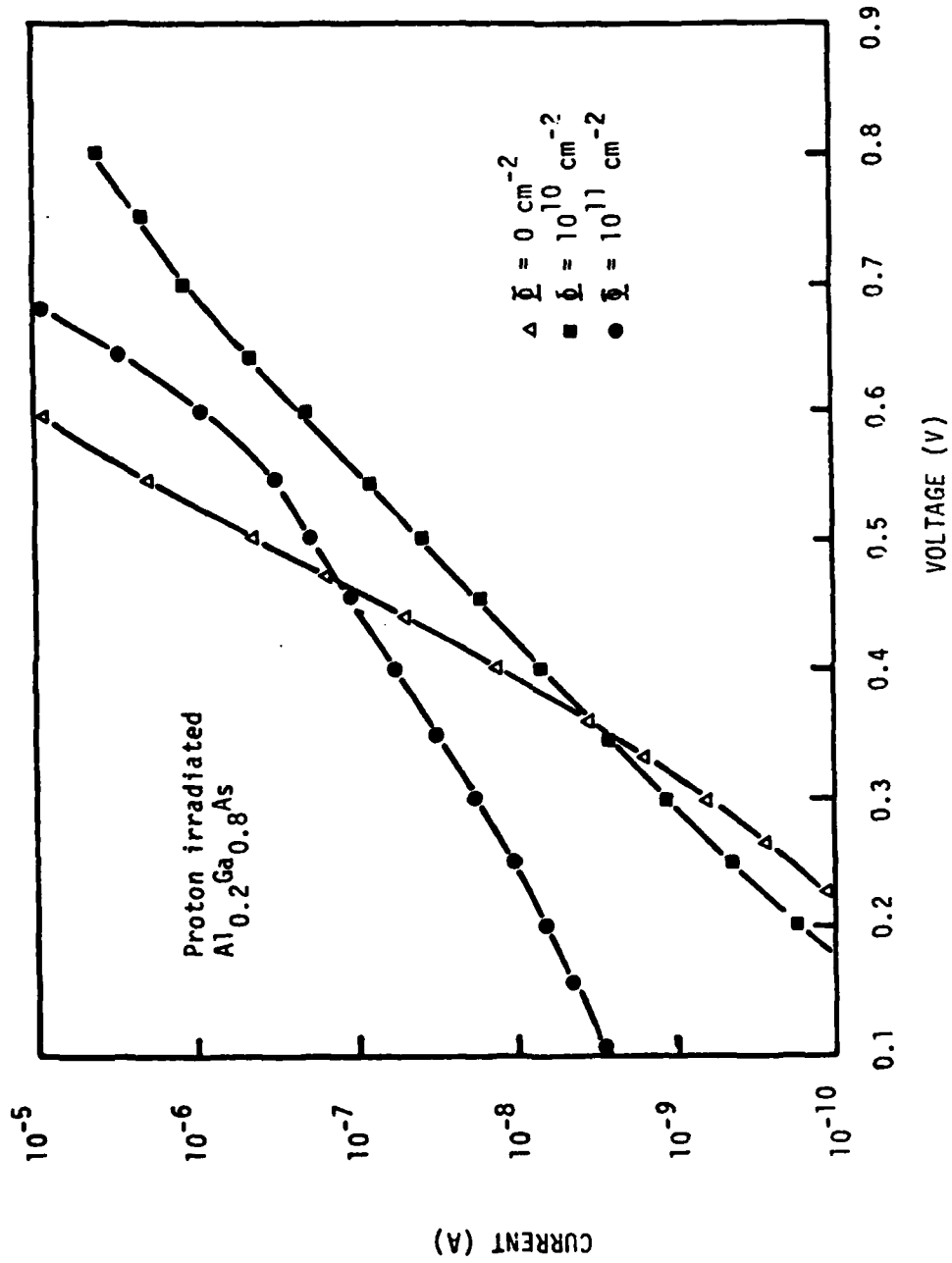
Figure 2.3.10 Forward I-V curves in $Al_{0.2}Ga_{0.8}As$ p/n junction cells irradiated by 200 KeV protons of different fluences.

74
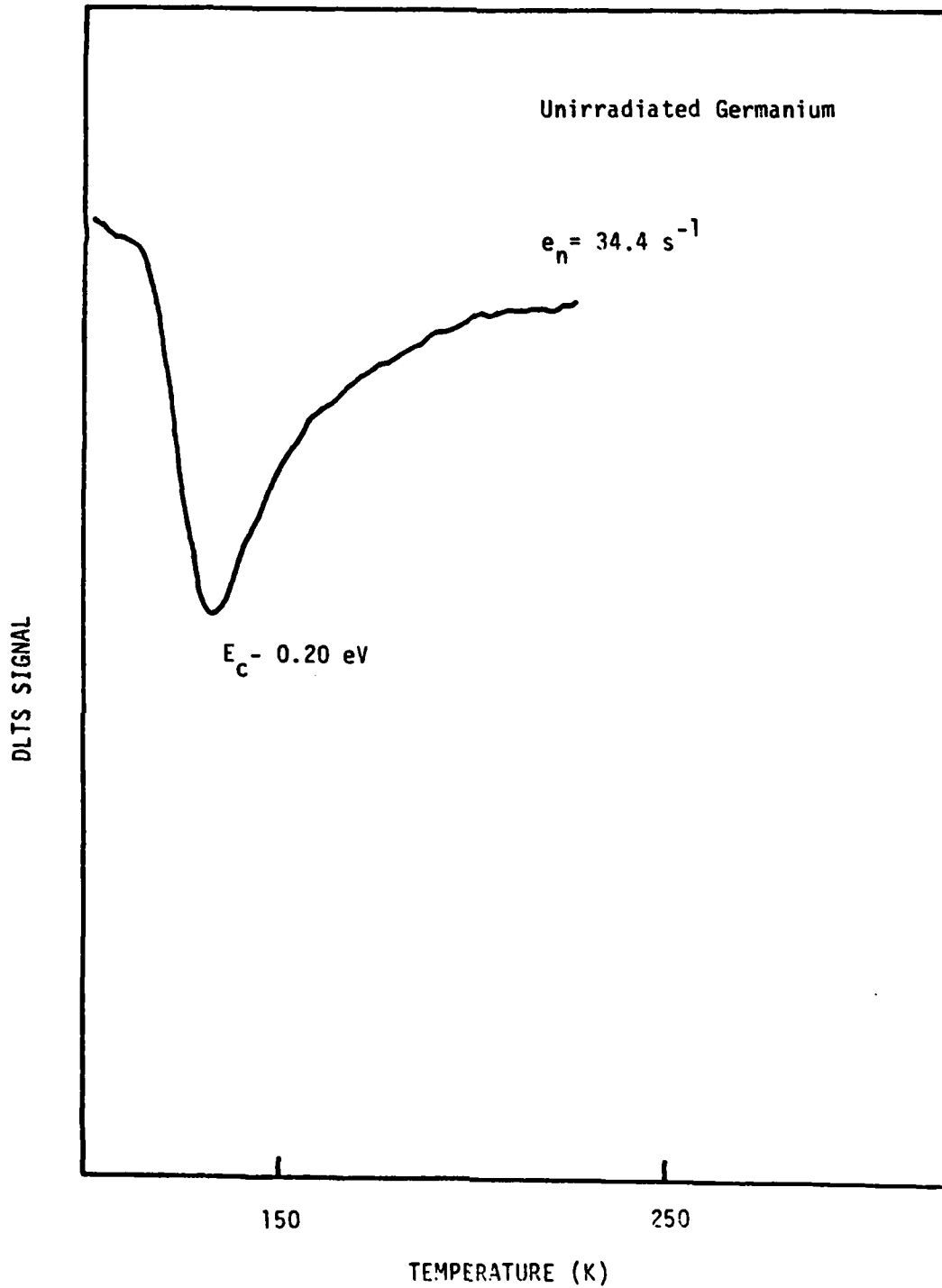
Figure 2.3.11 DLTS scan of electron trap for the unirradiated germanium cell.

Unirradiated Germanium

$e_n = 34.4 \ s^{-1}$

$E_v + 0.15 \ eV$

DLTS SIGNAL

150   250

TEMPERATURE (K)
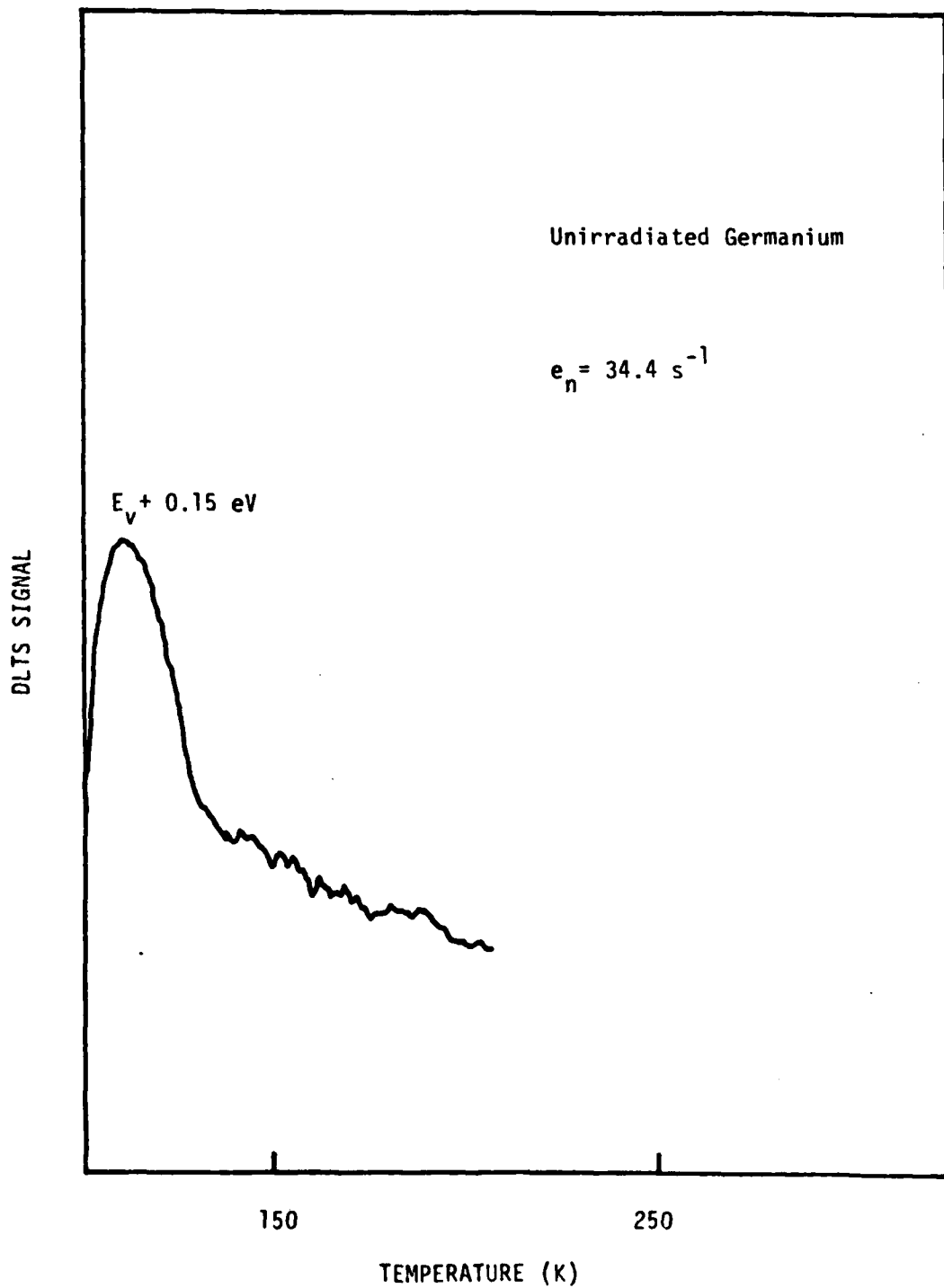
Figure 2.3.12 DLTS scan of hole trap for the unirradiated
                germanium cell.

76

Figure 2.3.13 Forward I-V curves for the unirradiated germanium cells of different doping concentrations.

77

Figure 2.3.14 C-V curves for the unirradiated germanium cells of different doping concentrations.

78

Appendix A

Empirical Formula for Pathlength and Penetration length

(i) $Al_{0.35}Ga_{0.65}As$ solar cell

For proton:

$$
\begin{aligned}
&= 0.10609 + 16.85865x - 143.7051x^2 + 640.4153x^3, && \text{for } x \leq 0.1 \text{ MeV}\\
P &= 0.24147 + 7.17523x + 3.90794x^2 - 0.089934x^3, && \text{for } x \leq 5 \text{ MeV}\\
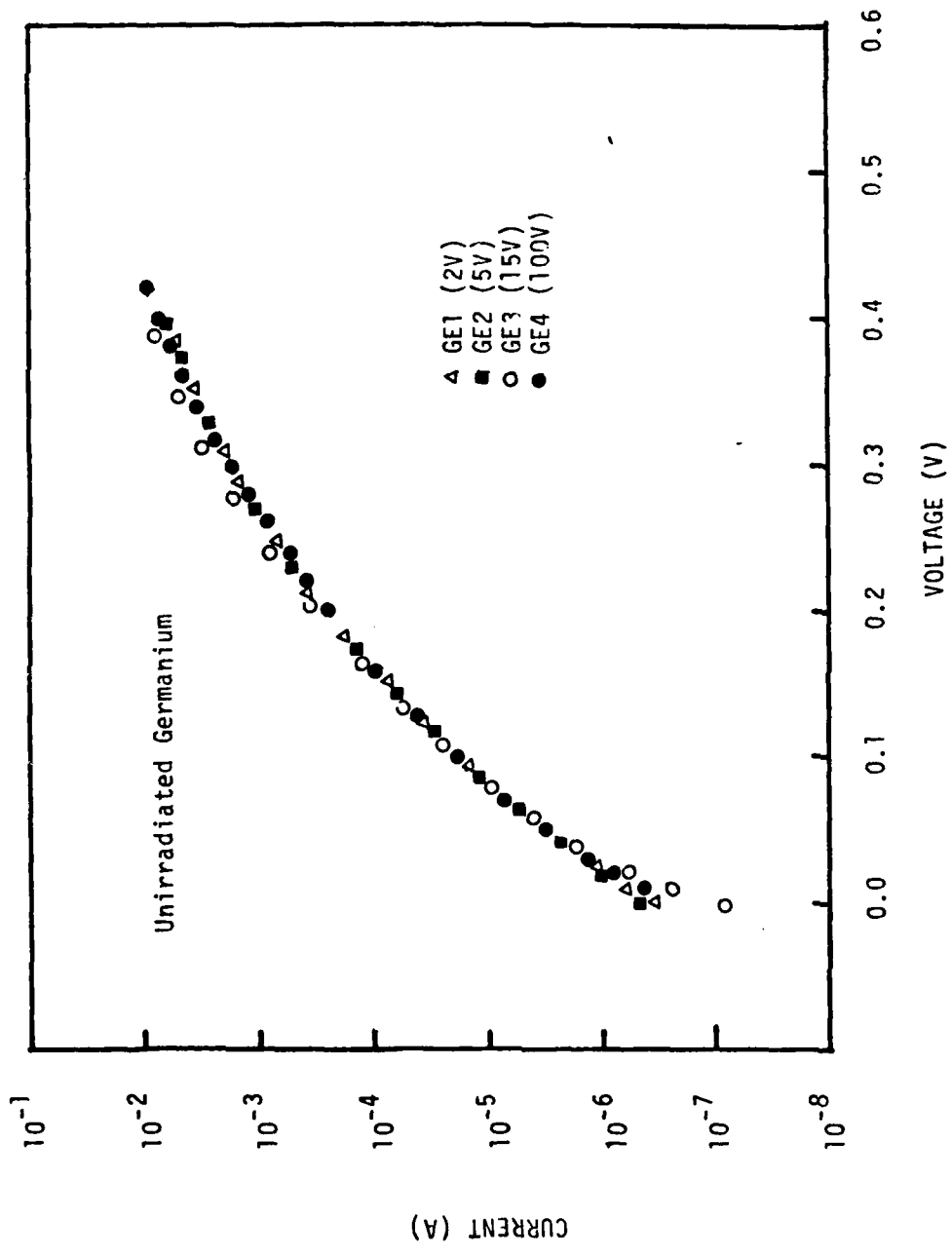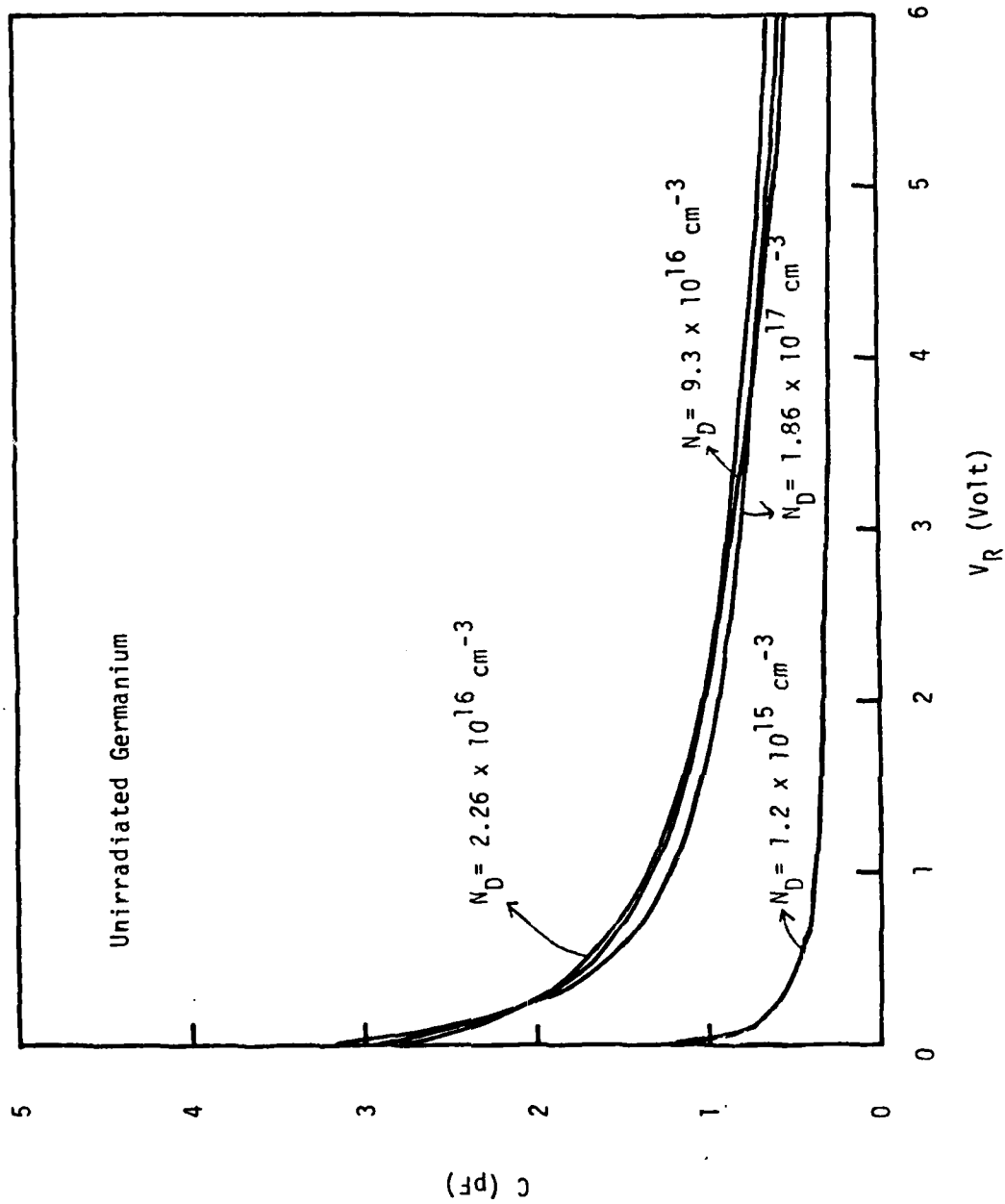&= 475.707 - 202.200X + 33.7732x^2 - 1.46734x^3, && \text{for } x \leq 10 \text{ MeV}
\end{aligned}
$$

where P is the path length (um), x is the initial energy of incident proton (MeV). Unless specify otherwise, the unit of length is in um and that of energy is in MeV.

$$
\begin{aligned}
&= 0.0076 + 9.0882x - 39.3116x^2 + 181.8816x^3, && \text{for } x \leq 0.1 \text{ MeV}\\
R &= 0.0086 + 6.7797x + 3.94880x^2 - 0.096772x^3, && \text{for } x \leq 5.0 \text{ MeV}\\
&= 470.37 - 200.227x + 33.4635x^2 - 1.45302x^3, && \text{for } x \leq 10 \text{ MeV}
\end{aligned}
$$

where R is the penetration depth. Since the small mass of electron, we only consider the penetration depth for electrons.

For electron:

$$
\begin{aligned}
&= -0.9078 + 103.524x + 3670.307x^2 - 5193.84x^3, && \text{for } x \leq 0.20 \text{ MeV}\\
R &= -50.198 + 729.989x + 825.593x^2 - 354.221 x^3, && \text{for } x \leq 1 \text{ MeV}\\
&= -261.023 + 1453.507x - 40.717x^2 + 0.84842 x^3, && \text{for } x \leq 10 \text{ MeV}
\end{aligned}
$$

(ii) GaAs solar cell

For proton:

$$
\begin{aligned}
&= 0.1068 + 17.0257x - 145.7343x^2 + 645.3220x^3, && \text{for } x \leq 0.1 \text{ MeV}\\
P &= 0.2575 + 7.03261x + 3.74480x^2 - 0.86365x^3, && \text{for } x \leq 5 \text{ MeV}\\
&= 457.39 - 194.1454x + 32.4329x^2 - 1.4079x^3, && \text{for } x \leq 10 \text{ MeV}
\end{aligned}
$$

$$
\begin{aligned}
&= 0.00688 + 8.9414x - 37.5326x^2 + 171.2658x^3, && \text{for } x \leq 0.1 \text{ MeV}\\
R &= -0.00382 + 6.6356x + 3.7874x^2 - 0.093355x^3, && \text{for } x \leq 5 \text{ MeV}\\
&= 451.244 - 192.10x + 32.1036x^2 - 1.3938x^3, && \text{for } x \leq 10 \text{ MeV}
\end{aligned}
$$

For electron:

$$
\begin{aligned}
&= -0.8763 + 100.042x + 3528.80x^2 - 4997.51x^3, && \text{for } x \leq 0.20 \text{ MeV}\\
R &= -48.067 + 700.994x + 794.971x^2 - 341.500x^3, && \text{for } x \leq 1 \text{ MeV}\\
&= -250.77 + 1397.20x - 39.4954x^2 + 0.82267x^3, && \text{for } x \leq 10 \text{ MeV}
\end{aligned}
$$

(iii) $In_{0.53}Ga_{0.47}As$ solar cell:

For proton:

$$
\begin{aligned}
&= 0.11325 + 15.8962x - 113.707x^2 + 438.5001x^3, && \text{for } x \leq 0.125 \text{ MeV}\\
P &= 0.2547 + 7.0324x + 3.9578x^2 - 0.11047x^3, && \text{for } x \leq 5 \text{ MeV}\\
&= 456.68 - 193.731x + 32.4623x^2 - 1.4114x^3, && \text{for } x \leq 10 \text{ MeV}
\end{aligned}
$$

$$= 0.00746 + 8.5463x + 32.4715x^2 + 150.7858x^3, \qquad \text{for } x \leq 0.125 \text{ MeV}$$
$$R = 0.01524 + 6.5645x + 3.99692x^2 - 0.11770x^3, \qquad \text{for } x \leq 5 \text{ MeV}$$
$$= 450.24 - 191.362x + 32.0498x^2 - 1.39383x^3, \qquad \text{for } x \leq 10 \text{ MeV}$$

For electron:

$$= -0.8649 + 99.6798x + 3378.6836x^2 - 4828.662x^3, \qquad \text{for } x \leq 0.20 \text{ MeV}$$
$$R = -46.212 + 678.5045x + 738.37x^2 - 321.266x^3, \qquad \text{for } x \leq 1 \text{ MeV}$$
$$= -230.19 + 1321.85x - 41.826x^2 + 0.9188x^3, \qquad \text{for } x \leq 10 \text{ MeV}$$

(iv) Ge solar cell:

For proton:

$$= 0.1122 + 17.8255x - 151.6034x^2 + 673.55397x^3, \qquad \text{for } x \leq 0.1 \text{ MeV}$$
$$P = 0.2708 + 7.4367x + 4.1115x^2 - 0.08929x^3, \qquad \text{for } x \leq 5 \text{ MeV}$$
$$= 504.762 - 214.870x + 35.8689x^2 - 1.55732x^3, \qquad \text{for } x \leq 10 \text{ MeV}$$

$$= 0.00838 + 9.58130x + 40.9460x^2 + 188.20789x^3, \qquad \text{for } x \leq 0.1 \text{ MeV}$$
$$R = 0.00348 + 7.0309x + 4.15505x^2 - 0.096763x^3, \qquad \text{for } x \leq 5.0 \text{ MeV}$$
$$= 500.180 - 213.002x + 35.5384x^2 - 1.543172x^3, \qquad \text{for } x \leq 10 \text{ MeV}$$

For electron:
$$= -0.96021 + 109.62x + 3864.62x^2 - 5481.251x^3, \qquad \text{for } x \leq 0.2 \text{ MeV}$$
$$R = -52.739 + 769.09x + 864.67x^2 - 372.675x^3, \qquad \text{for } x \leq 1.0 \text{ MeV}$$
$$= -269.858 + 1522.4x - 43.453x^2 + 0.9246x^3, \qquad \text{for } x \leq 10 \text{ MeV}$$

Appendix B

Empirical Formula for Reduced Energy

(i) $Al_{0.35}Ga_{0.65}As$, with multiple scattering:

$$E_{re} = \begin{cases} 1.320E-3-1.6095E-2x+1.888E-1x^2-7.5989E-2x^3, & \text{for } E_0 \leq 0.1 \text{ MeV} \\ -2.23E+2+1.2651E-1x+3.944E-3x^2+7.2113E-5x^3, & \text{for } E_0 \leq 1.75 \text{ MeV} \\ 6.32E-1+4.999E-2x-1.3749E-4x^2+1.974E-7x^3, & \text{for } E_0 \leq 10 \text{ MeV} \end{cases}$$

where E_{re} is the reduced energy in MeV; E_0 is the initial energy, x is the distance in um.

Without Multiple Scattering:

For Proton:

$$E_{re} = \begin{cases} -2.91E-4+9.402E-2x+1.3234E-1x^2-9.306E-2x^3, & \text{for } E_0 \leq 0.1 \text{ MeV} \\ 1.187E-2+1.3E-1x-4.342E-3x^2+8.412E-5x^3, & \text{for } E_0 \leq 1.75 \text{ MeV} \\ 6.596E-1+5.047E-2x-1.406E-4x^2+2.0474E-7x^3, & \text{for } E_0 \leq 10 \text{ MeV} \end{cases}$$

For Electron:

$$E_{re} = \begin{cases} 1.061E-2+36.5032x-5068.476x^2+3.38136E5x^3, & \text{for } E_0 \leq 0.1 \text{ MeV} \\ 9.002E-2+7.8972x-5.73967E-1x^2+1.4201x^3, & \text{for } E_0 \leq 10 \text{ MeV} \end{cases}$$

(ii) GaAs with multiple scattering:

$$E_{re} = \begin{cases} 1.323E-3-1.5849E-2x+1.8469E-1x^2-7.2419E-2x^3, & \text{for } E_0 \leq 0.1 \text{ MeV} \\ -2.586E-3+1.299E-2x-4.136E-3x^2+7.766E-5x^3, & \text{for } E_0 \leq 1.75 \text{ MeV} \\ 6.215E-1+5.196E-2x-1.483E-4x^2+2.213E-7x^3, & \text{for } E_0 \leq 10 \text{ MeV} \end{cases}$$

Without multiple scattering:

Proton:

$$E_{re} = \begin{cases} -2.722E-4+9.692E-2x+1.2835E-1x^2-8.972E-2x^3, & \text{for } E_0 \leq 0.1 \text{ MeV} \\ 1.049E-2+1.3669E-1x-4.577E-3x^2+9.136E-5x^3, & \text{for } E_0 \leq 1.75 \text{ MeV} \\ 6.508E-1+5.2471E-2x-1.518E-4x^2+2.297E-7x^3, & \text{for } E_0 \leq 10 \text{ MeV} \end{cases}$$

Electron:

$$E_{re} = \begin{cases} 1.061E-2+37.9136x-5465.826x^2+3.78864x^3, & \text{for } E_0 \leq 0.1 \text{ MeV} \\ 8.9865E-2+8.2195x-0.6236x^2+1.6267x^3, & \text{for } E_0 \leq 10 \text{ MeV} \end{cases}$$

(iii) $In_{0.53}Ga_{0.47}As$:

Proton:

$$E_{re} = \begin{cases} 1.219E-3-1.5049E-2+1.8258E-1x^2-7.2149E-2x^3, & \text{for } E_0 \leq 0.1 \text{ MeV} \\ -2.604E-2-1.2918E-1x-4.117E-3x^2+7.558E-5x^3, & \text{for } E_0 \leq 1.75 \text{ MeV} \\ 6.0845E-2+5.112E-2x-1.435E-4x^2+2.121E-7x^3, & \text{for } E_0 \leq 10 \text{ MeV} \end{cases}$$

<u>Without multiple scattering</u>

Proton:

$$= -4.35E-4+1.0362E-1x+1.2076E-1x^2-8.830E-2x^3, \quad \text{for } E_0 \leq 0.1 \text{ MeV}$$
$$E_{re}=1.1675E-2+1.3386E-1x-4.638E-3x^2+9.124E-5x^3, \quad \text{for } E_0 \leq 1.75 \text{ MeV}$$
$$= 6.4040E-1+5.178E-2x-1.4786E-4x^2+2.222E-7x^3, \quad \text{for } E_0 \leq 10 \text{ MeV}$$

Electron:

$$= 1.050E-2+39.1671x-5817.240x^2+4.1789E5x^3, \quad \text{for } E_0 \leq 0.15 \text{ MeV}$$
$$E_{re}=8.761E-2+8.69064x-0.57944x^2+2.21893x^3, \quad \text{for } E_0 \leq 10 \text{ MeV}$$

<u>(iv) Ge with multiple scattering:</u>

$$E_{re}=1.294E-3-1.492E-2x+1.6796E-1x^2-6.3664E-2x^3, \quad \text{for } E_0 \leq 0.1 \text{ MeV}$$
$$=-2.387E-2+1.213E-1x-3.6352E-3x^2+6.3742E-5x^3, \quad \text{for } E_0 \leq 1.75 \text{MeV}$$
$$E_{re}=6.466E-1+4.729E-2x-1.2326E-4x^2+1.6727E-7x^3, \quad \text{for } E_0 \leq 10 \text{ MeV}$$

<u>Without multiple scattering:</u>

Proton:

$$=-3.255E-4+8.924E-2x+1.1751E-1x^2-7.7981E-2x^3, \quad \text{for } E_0 \leq 0.1\text{MeV}$$
$$E_{re}=1.088E-2+1.245E-1x-3.9866E-3x^2+7.3885E-5x^3, \quad \text{for } E_0 \leq 1.75\text{MeV}$$
$$=6.737E-1+4.775E-2x-1.2611E-4x^2+1.7543E-7x^3, \quad \text{for } E_0 \leq 10 \text{ MeV}$$

Electron:

$$=1.059E-2+34.6163x-4556.1716x^2+2.8841E+5x^3, \quad \text{for } E_0 \leq 0.15 \text{ MeV}$$
$$E_{re}=8.951E-2+7.52318x-4.7343E-1x^2+1.23405x^3, \quad \text{for } E_0 \leq 10 \text{ MeV}$$

82

Appendix C

Total Number of Displacement

(i) $Al_{0.35}GaAs_{0.65}As$ cell:

Proton:

$$D_{cx} \begin{array}{ll} \qquad \qquad & \text{for } x \leq 0.00032 \text{MeV} \\ = -5.7668 + 1.5337E4x - 3.284372E6x^2 + 3.16018E8x^3, & \text{for } x \leq 0.004 \text{ MeV} \\ = 31.119 + 822.902x - 6.4357E3x^2 + 1.7539E4x^3, & \text{for } x \leq 0.2 \text{ MeV} \\ = 77.465 + 19.003x - 0.8047x^2 + 0.033244x^3, & \text{for } x \leq 10 \text{ MeV} \end{array}$$

where x is the initial energy in MeV.

Electron:

$$D_{cx} \begin{array}{ll} = 0 & \text{for } x < 0.30 \text{ MeV} \\ = 0.03857 - 0.43231x + 1.14292x^2 - 0.35809x^3, & \text{for } x < 1.1 \text{ MeV} \\ = -0.78798 + 0.7259x + 0.44538x^2 - 0.037336x^3, & \text{for } x \leq 5 \text{ MeV} \end{array}$$

(ii) GaAs solar cell:

Proton:

$$D_{cx} \begin{array}{ll} = 0 & \text{for } x \leq 0.00032 \text{ MeV} \\ = -4.7003 + 1.9340E4x - 4.159460E6x^2 + 4.00880E8x^3, & \text{for } x \leq 0.004 \text{ MeV} \\ = 39.116 + 1.030E3x - 8.0870E3x^2 + 2.2034E4x^3, & \text{for } x \leq 0.2 \text{ MeV} \\ = 96.674 + 22.294x - 0.9332x^2 + 0.039118x^3, & \text{for } x \leq 10 \text{ MeV} \end{array}$$

Electron:

$$D_{cx} \begin{array}{ll} = 0 & \text{for } x < 0.30 \text{ MeV} \\ = 0.0466 - 0.52535x + 1.3945x^2 - 0.43876x^3, & \text{for } x < 1.1 \text{ MeV} \\ = -0.97400 + 0.9147x + 0.52926x^2 - 0.04475x^3, & \text{for } x \leq 5 \text{ MeV} \end{array}$$

(iii) $In_{0.53}Ga_{0.47}As$ solar cell:

Proton:

$$D_{cx} \begin{array}{ll} = 0 & \text{for } x \leq 0.00032 \text{ MeV} \\ = -5.63716 + 2.2414E4x - 4.741112E6x^2 + 4.53575E8x^3, & \text{for } x \leq 0.004 \text{MeV} \\ = 45.234 + 1.313E3x - 1.0286E4x^2 + 2.7847E4x^3, & \text{for } x \leq 0.2 \text{ MeV} \\ = 117.71 + 30.862x - 1.4795x^2 + 0.062118x^3, & \text{for } x \leq 10 \text{ MeV} \end{array}$$

Electron:

$$D_{cx} \begin{array}{ll} = 0 & \text{for } x < 0.32 \text{ MeV} \\ = 0.07027 - 0.7030x + 1.7493x^2 - 0.55049x^3, & \text{for } x < 1.1 \text{MeV} \\ = -1.1404 + 1.0277x + 0.66216x^2 - 0.057361x^3, & \text{for } x \leq 5 \text{ MeV} \end{array}$$

(iv) Ge solar cell:

Proton:

$$D_{cx}= 0 \qquad \qquad \qquad \text{for } x \leq 0.00096 \text{ MeV}$$
$$= -1.3800 +1.8865E3x+7.399319E4x^2-3.16944E7x^3, \qquad \text{for } x \leq 0.004 \text{ MeV}$$
$$= 7.4836+3.020E2x-2.2730E3x^2+5.5966E3x^3, \qquad \text{for } x \leq 0.2 \text{MeV}$$
$$= 25.334+10.060x-0.6903x^2+0.032903x^3, \qquad \text{for } x \leq 10 \text{ MeV}$$

Electron:

$$= 0 \qquad \qquad \qquad \text{for } x < 0.60 \text{ MeV}$$
$$D_{cx}= 0.07911-0.2661x +0.2598x^2- 0.03838x^3, \qquad \text{for } x < 2.2 \text{ MeV}$$
$$= 0.1524 - 0.4971x + 0.32364x^2 - 0.025145x^3, \qquad \text{for } x \leq 5 \text{ MeV}$$

END
FILMED

6-86

DTIC